ANALYSIS OF IRON OXIDATION IN GARNETS

ERICA A. EMERSON
MOUNT HOLYOKE COLLEGE

ADVISORS:
DR. M. DARBY DYAR
MOUNT HOLYOKE COLLEGE
DEPARTMENT OF ASTRONOMY

DR. KURT HOLLOCHER
UNION COLLEGE
DEPARTMENT OF GEOLOGY

THESIS SUBMITTED TO THE DEPARTMENT OF GEOLOGY AND GEOGRAPHY OF MOUNT HOLYOKE COLLEGE IN PARTIAL FULFILLMENT OF THE REQUIREMENTS FOR THE DEGREE OF BACHELOR ARTS WITH HONORS

MAY 2008

Acknowledgements

- Thank you to my advisor Darby Dyar for all of her support and encouragement over the past 4 years. She has given me an amazing opportunity working in the Mössbauer laboratory.

- A special thank you to my reviewers, Michelle Markley and Esther Castro-Cuenca. Michelle, thank you for being understanding and always listening when I needed to talk. Esther, thank you for your encouragement and help.

- Thank you to Elizabeth Sklute! She taught me how to use the Mössbauer programs and spent hours helping me to understand difficult concepts.

- Thank you to Kurt Hollocher at Union College for his guidance during my Keck Geology Consortium study in the Adirondacks of New York.

- Thank you to the staff at Brookhaven National Laboratory for allowing me to access their Synchrotron Light Source facilities.

- I thank Jerry Marchand for his excellent sample preparations and time spent with me at the scanning electron microscope.

- I would like to thank my friends Grace Bauer, Cassie Cushman, Patrice Cobin, Sarah Beth Cadieux, Vicki Finn, Shannon Graham, Madison Barkley, Catherine Nissen, Griffan Randall, Stephanie Robinson, Nicola Price, Adrienne McCallister, Cameron Phillips, Victoria Baranow, Emma Duff, and Carrie Duffield for being amazing friends and support teams!

- Thank you to Katie Stack and Alden Denny for their debates about garnets, movie nights and geology spirit during our Keck study!

- Thank you to the Geology Department at Mount Holyoke College for allowing me to do this study and for making the past 4 years a fun and enjoyable learning experience.

- Finally, a big thank you to my family Mom, Dad, Ashley, Ryan, Kytalin and my cats. I would not be the person I am without you. Thank you for your love and support in everything that I do!

THANK YOU!

Table of Contents

List of Tables and Figures

Abstract

The oxidation state of iron indicates the amount of oxygen present when a mineral is formed. If the environment was abundant in oxygen, many of the minerals in the assemblage will contain oxidized iron, Fe^{3+}. If the environment is more reducing, there is likely to be more Fe^{2+}. The amount of oxygen present influences the elements that interact in a magma, as well as which minerals form; this is known as oxygen fugacity (f_{O_2}). The fundamental f_{O_2} directly describes the potential for multivalent cations to occur in one of its valence states and is therefore a direct measurement of the oxidation state. Iron is one of the most common multivalent rock-forming cations. Due to their differences in both size and charge, Fe^{2+} and Fe^{3+}, can occupy different sites in a mineral structure.

Given that oxidation state is important, it is then important to have ways of measuring the oxidation state. In the late 1960s, Mössbauer spectroscopy was first used to determine Fe^{2+} and Fe^{3+}. Mössbauer, however, is a bulk technique that requires a large, homogenous sample. Accurate and precise Mössbauer measurements also require knowledge of the recoil-free fractions (f) for Fe^{2+} and Fe^{3+} in specific sites for each mineral group, but these correction factors had not been determined for garnets. The first goal of this project was to measure f for both Fe^{2+} and Fe^{3+} in garnet, in order to improve the accuracy of Mössbauer measurements of Fe3+/∑Fe in garnets. The resultant values for f at 295K and 80K were 0.60 and 0.88 for Fe^{3+}, 0.84 and 0.93 for Fe^{2+}, respectively.

It would be desirable to have a method of measuring samples at microanalytical scale, such as XANES spectroscopy. For the second part of my project, I compared corrected Mössbauer results to XANES measurements on a suite of 20garnet samples with varying amounts of Fe^{2+} and Fe^{3+}.Many of the samples are from Gore Mountain, Barton Mine in New York, but due to the lack ofsignificant Fe^{3+} content of the Gore Mountain garnets, a wider range of samples was chosen.The percentage of Fe^{3+} determined by Mössbauer was compared to the area, intensity, and energy of the pre-edge peaks in the XANES data to test how well the XANES technique can determine Fe^{2+} and Fe^{3+}.

Mössbauer spectroscopy and XANES results complement each other. Mössbauer and XANES data measure approximately the same percentage of Fe^{3+} content. The percentages of Fe^{3+} and Fe^{2+} according to Mössbauer and XANES, revealing that both techniques agree well within ± 8%, with the exception of 2 samples out of 20. This conclusion suggests that XANES studies of anisotropic minerals might be successful if, as in the case for this study, the optical orientation of the crystals is the same as the optical orientation of the standards. The combination of Mössbauer spectroscopy and XANES provides a promising outlook for microanalytical techniques in the near future.

Chapter 1

Introduction

The goal of this study is to compare and contrast Fe^{2+} and Fe^{3+} contents of garnets as measured by Mössbauer spectroscopy (a bulk technique) and XANES (a microscale method). This study will determine if the XANES technique is a viable alternative to conventional Mössbauer analyses.

My interest in this subject originated during the summer of 2007, when I participated in the Keck Geology Consortium study on the growth history and origin of the Gore Mountain Garnets. The project advisor was Dr. Kurt Hollocher in the Department of Geology at Union College in Schenectady, New York. I worked in the field and laboratory with Dr. Hollocher and two other students, Katie Stack from Williams College and Alden Denny from Western Washington University. After returning from New York, I began Mössbauer research under the advisement of Dr. Melinda Darby Dyar at Mount Holyoke College. She first introduced me to the concepts of Mössbauer and X-ray near-edge spectroscopy that I will explore in my research.

The cations of iron, Fe^{2+} and Fe^{3+}, are different in both size and charge, and so they can occupy different sites in a mineral structure, making iron one of the most common multivalent rock-forming cations. This research is important because understanding how much Fe^{2+} and Fe^{3+} are present in a mineral indicates the amount of oxygen present when a mineral is formed. If the environment was

abundant in oxygen during formation, many of the minerals in the assemblage will contain oxidized iron, Fe^{3+}. If the environment is more reducing, there is likely to be more Fe^{2+}. This is important because the amount of oxygen present, known as oxygen fugacity (f_{O_2}). The fundamental f_{O_2} directly measures oxidation state because f_{O_2} is the measure of the amount of free or uncombined oxygen available in an environment (Planetary Science Research Discoveries, 2008).

Given the importance of the oxidation state, it is then critical to have methods of measuring it. Historically, this measurement was done by wet chemistry, where large and homogeneous samples (gram quantity) were necessary. In the late 1960s, Mössbauer spectroscopy was first used to determine Fe^{2+} and Fe^{3+}, but because Mössbauer is a bulk technique, heterogeneity on a microscopic scale can never be detected.To acquire data, that might shed light on the possibility of heterogeneity, XANES spectroscopy is being developed to measure samples at a microanalytical scale.

Although Mössbauer spectroscopy provides information about the relative amounts of Fe^{2+} and Fe^{3+}, the areas of thedoublets used to fit the data do not correlate directly to the amounts of Fe^{2+} and Fe^{3+} present in the minerals because the two cations have different recoil-free fractions, f (the fraction of gamma rays that are emitted or absorbed without a significant loss of energy). My first goal, therefore, was to acquire a series of spectra at16 different temperatures in order to determine f for Fe^{2+} and Fe^{3+} in garnet.These data make it possible to calculate "correction factors" that relate the areas of Fe^{2+} and Fe^{3+} doublets in Mössbauer

spectra of garnets to the true population of Fe^{2+} and Fe^{3+} present in those samples. Use of the correction factors will greatly improve the accuracy of Mössbauer measurements of Fe^{2+} and Fe^{3+} in garnets.

The XANES technique is also in need of further development in order to obtain accurate values of Fe^{2+} and Fe^{3+}. In 1994, Bajt *et al.* reported a correlation between the energy of the pre-edge peak and the amount of Fe^{2+} and Fe^{3+}in the sample; the pre-edge peak energies are different for Fe^{2+} and Fe^{3+}. The correlation appeared to give useful results to a first order, and hundreds of samples were run. Further work eventually showed that the Bajt *et al.* (1994) calibration line was overly simplistic (Dyar *et al.* 2002). The problem occurred for two reasons: 1) the Si(III) monochromator in use from 1993-2004 was fairly low resolution, such that pre-edge peaks appeared to be singlets despite their multiplet structure, and 2) the crystallographic orientation of anisotropic minerals affected the pre-edge energy. Therefore, my second objective was to demonstrate that differences in orientation alone cause this inconsistency by using a mineral for which the orientation does not matter, such as garnet. Garnet is isotropic, meaning that the optical properties are the same in all directions. As a result, light passes through them in the same way, and with the same velocity, no matter which direction the light is traveling.

The purpose of this thesis is to analyze and compare Mössbauer data to XANES data. In the process, we hope to understand how XANES results for the amounts of Fe^{2+} and Fe^{3+} correspond to Mössbauer results for the same minerals. In this study, 20 garnet samples with varying amounts of Fe^{2+} and Fe^{3+}, including

pure end-members such as almandine (Fe^{2+})and andradite (Fe^{3+}), have been analyzed to determine the percentage of Fe^{3+} shown by the Mössbauer results versus the percentage of Fe^{3+} shown by XANES. This study supplements the current data available from Mössbauer analysis, providing a more accurate measure of iron in the sample. It also demonstrates that XANES results are comparable to Mössbauer results for isotropic minerals, in this case, garnet. This raises the hope that development of careful analytical protocols to measure standards and unknowns of anisotropic minerals at the same optical orientation may eventually make routine microanalysis of Fe^{2+} and Fe^{3+} minerals possible.

Chapter 2

Background

Garnet

Garnet is a mineral group that has been used as gemstones and abrasives since as early as the Bronze Age. The name "garnet" came from "granatus" in Latin, meaning "grain", referring to the similarity in shape, size and color of pomegranate seeds (USGS, 2002). Garnet is most commonly known today as the birthstone for January and for its first industrial use, as the coating for sandpaper, by Henry Hudson Barton (founder of Barton Mines Corp.) in 1878 manufactured in New York, United States (USGS, 2002).

Garnets are known for the six common species recognized for their chemical composition; pyrope, almandine, andradite, grossular, spessartine, and uvarovite. They are most often seen as red, but form in a multitude of colors including red, orange, yellow, green, blue, purple, brown, black, pink, and colorless. One garnet, found in Bekily, Madagascar in the late 1990s and later in the United States, formed in a rare blue color as a result of containing high amounts of vanadium. Color-changing garnets exist due to exposure to incandescent light.

Chemical Composition and Structure

Garnets are neosilicates withthe general formula $X_3Y_2(SiO_4)_3$. The X site is usually occupied by divalent cations (Ca^{2+}, Mg^{2+}, Fe^{2+}) and the Y site by trivalent cations (Al^{3+}, Fe^{3+}, Cr^{3+}) in an octahedral/tetrahedral framework with $[SiO_4]^{4-}$ providing the tetrahedra (Fig. 2.1). Garnets are most often found in the dodecahedral crystal habit, but are also commonly found in the trapezohedral habit. They crystallize in an isometric system, meaning they have three axes all of equal length and perpendicular to each other. Because they lack cleavage, garnets break into sharp, concoidal pieces when they fracture underhigh stress.

As shown in Table 2.1, many of the garnet group minerals contain two valence states, Fe^{2+} and Fe^{3+}, or a mixture of the two states. Fe^{3+} is a smaller cation, with an ionic radius of 0.49-0.65 Å, and prefers to be surrounded by four oxygen atoms, known as a 4-fold site. Fe^{2+}, which has an ionic radius of 0.78 Å, prefers a 6-fold site (Fe^{2+} surrounded by six oxygens) because there is more room (Dyar and Gunter, 2007).

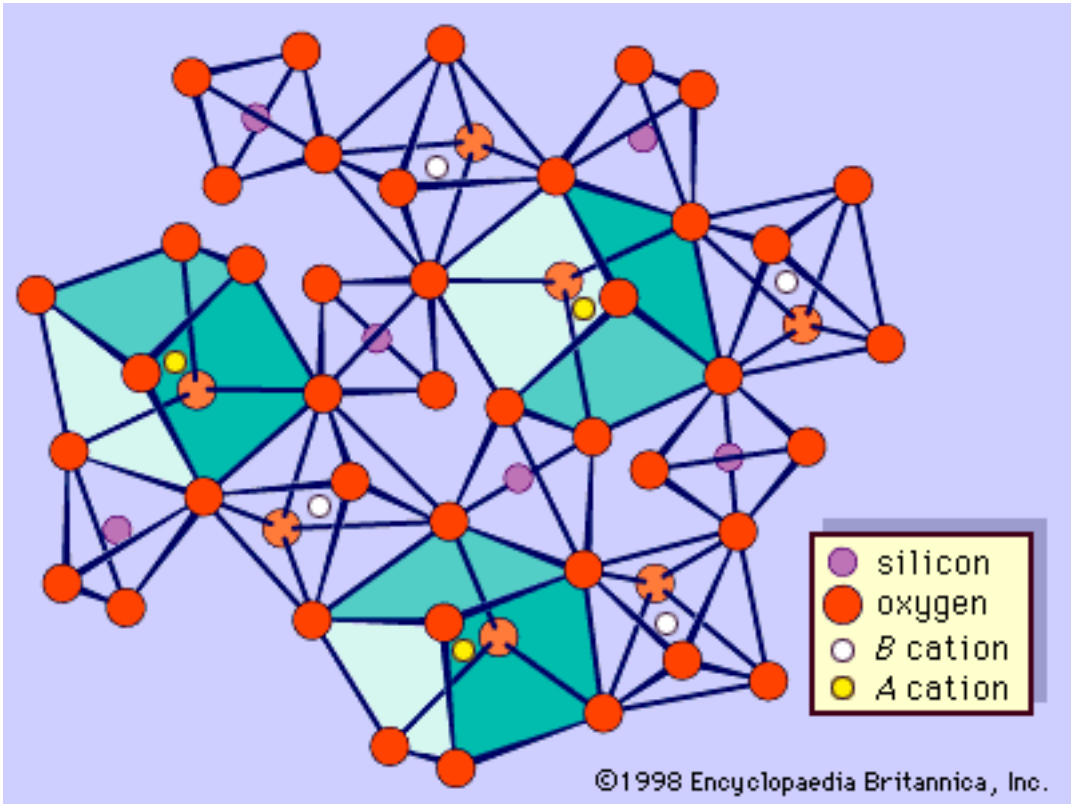

Figure 2.1:The crystal structure of garnet is composed of a framework of Si and O ions. Between them, the *Y* site (here labeled *B*) contains Al^{3+}, Fe^{3+}, or Cr^{3+}, and the *X* site(here labeled *A*) can contain Ca^{2+}, Mg^{2+}, or Fe^{2+}.(Figure from Encyclopedia Britannica).

Because the chemical composition of garnet varies, the atomic bonding in some species is stronger than others. The mineral group therefore, ranges from a scale of 6.5 to 7.5 on the Mohs scale of hardness.

This variation in chemical composition was a major factor that led to this study. This project seeks to quantify the number of Fe^{2+} and Fe^{3+} cations in varying compositions of garnet. The three main garnet species examined in this study will be almandine, containing ferrous iron, Fe^{2+}, andradite, containing Fe^{3+}, and grossular, containing a mixture of Fe^{2+} and Fe^{3+}.

Almandine

Almandine is usually red in color, but can also be orange, purple, black and brown. It can be found in a dodecahedral or trapezohedral crystal habit. It usually tends to occur in contactor regionally-metamorphosed rocks over a range of temperatures and pressures, particularly medium-temperature metamorphism, usually with schists, gneisses, granites and pegmatites. Almandine contains $Fe^{2+}$and has the chemical composition of$Fe_3Al_2(SiO_4)_3$ (Dyar and Gunter, 2007).

Andradite

Andradite, which can also be red in color if it contains sufficient Fe^{2+}, is generally green, yellow-green, brown, or black. It can be found in a dodecahedral or trapezohedral habit, but tends to be granular or massive. Andradite tends to be found in rocks that have undergone contact metamorphism, usually limestones, skarns, chlorite schists, and serpentinites. Andradite contains Fe^{3+} and has the chemical composition $Ca_3Fe_2(SiO_4)_3$ (Dyar and Gunter, 2007).

Grossular

Grossular garnets have a full range of colors, including cinnamon (red-brown), green, yellow, colorless, white, gray, pink and orange. Similar to andradite, grossular can be found as a dodecahedral or trapezohedral habit, but tends to be compact, granular or massive. It is usually found in Ca-rich rocks that have undergone contact or regional metamorphism, such as schists and

serpentinites. Both Fe^{2+} and Fe^{3+} can be substituted into the chemical composition of grossular garnet, $Ca_3Al_2(SiO_4)_3$, where the Ca^{2+} can be replaced by Fe^{2+} and the Al^{3+} with Fe^{3+} (Dyar and Gunter, 2007).

Sample Localities

The samples originally chosen for this study were primarily from the Keck Geology Consortium Gore Mountain Study. Because the Fe^{2+} and Fe^{3+}contents did not vary, additional samples were selected from various localities containing a range of Fe^{2+}/Fe^{3+}values to supplement the Keck samples (Table 2.1).

The Fort Wrangell almandine used is from the MIT Teaching collection. Two of the grossular garnets studied and the Val Malenco andradite are from the Harvard Mineralogical Museum. The Fort Wrangell almandine, typically found inbiotite schist at the Garnet Ledge near the mouth of the Stikine River Fort Wrangell, Alaska (Stowell, 2006) and the Val Malencoandradite, from Val Malenco, Italy, are close to pure end-member standards used for Mössbauer studies comparing purely Fe^{2+} (almandine) and Fe^{3+} (andradite) garnets. The two grossular samples were provided by Anne Hofmeister. The two garnet peridotites are from the Jagersfontein Mine, South Africa. The rare melanite sample, courtesy of Erick Bestland, is from Kenya, Africa.

The rest of the samples used in this studyare garnets from the Adirondacks in New York collected as part of the Keck Geology Consortium supported work. The Adirondacks are part of the southern extension of the Grenville orogenic belt

that is a continuation of the Frontenac area in Quebec (Heumann *et al.* 2006). The Grenville Province rocks are approximately 1100 Ma and represent multiple geological events that occurred during this time. These rocks have been highly deformed by folding, shearing by ductile deformation, and crushed by brittle deformation (Bartolomé, 1960).

Heumann *et al.*(2006) best describe the topography of the Grenville Province:

> The Grenville Province is divided topographically into the highlands, consisting of granulite facies orthogneisses and anorthosite massifs and the lowlands, composed of mostly of amphibolite facies metasedimentary rocks. […] A northeast-trending northwest-dipping fault is located between the highlands and lowlands, known as the Cathage-Colton mylonite zone.

Other major faults are located through the Grenville Province and the best-known fault runs between garnet-rich rocks of Gore Mountain and a meta-syenite body (Bartolomé, 1960).

The garnets at Gore Mountain in the Adirondacks are large porphyroblasts in metamorphosed metagabbros. They are generally 5-15 cm in length and occur in the upper amphibolite to lower granulite facies (Hollocher, 2007). The garnets at Gore Mountain are noted fortheir size and bright almandine-red color. The original mine was used between 1878-1983.Ruby Mine at Gore Mountain is still open for mining, however, the other mines are currently used as a tourist attraction. The garnets were used for industrial abrasive purposes (Hollocher, 2007).

Hollocher (2007) describes the main garnet body at Gore Mountain:

> The main garnet body is a coarse-grained amphibolite, occurs at the boundary between a metamorphosed olivine gabbro to the north and a pyroxene syenite to the south. The pyroxene syenite is more or less undeformed. The gabbro contains what is known as a 'corona' texture, which is a complex, layered reaction rim that formed under fluid-absent conditions during metamorphism.

Samples AK-97-2a and AK-97-2b are from Gore Mountain at Barton Mine. Sample AK-97-2a is from Pit #1 from a garnet amphibolite from a hydrated shear zone, and is notable forthe coronas present in the amphibolite (Keck, 1997). Coronas represent changing mineral compatibilities. The sample had approximately 5-10% garnet, 35% plagioclase, 55% hornblende and 5-10% biotite. The amphibolite was coarse-grained and contained foliated biotite with distinctly lineated hornblende (Keck, 1997). AK-97-2b is from a metagabbro at Pit #2 and contains coronas that present recrystallization due to changing metamorphic conditions. The metagabbro consists of approximately 3% garnet, 5% biotite, 70% pyroxene, 20% olivine, less than 1% of oxides (illmenite) and plagioclase (located in the garnet rims). The metagabbro has a corona formation of garnets rimmed by plagioclase followed by hornblende (Keck, 1997).

Sample AK-97-10c is from Woolen Mill, west of Elizabethtown. The anorthosite contains less than 5% garnet, 85% plagioclase, 13% orthopyroxene and clinopyroxene, and traces of biotite and hornblende, and has reaction rims as a result of changing pressure and temperature (Keck, 1997). This change alters orthopyroxene and causes it to becomea form ofclinopyroxene that is

incompatible with plagioclase, forming reaction rims. The plagioclase occurs in large porphyroblasts (1cm) and is often rimmed by garnet, hornblende, or biotite (Keck, 1997).

Sample AK97-29 is an almandine from the Treadway Mountain Formation, NY. The paragneiss containing approximately 5-10% garnet, 20% biotite, 65% plagioclase, quartz and feldspar, less than 2% illmenite and 5% sillmanite (and possibly tourmaline and sulfides) is medium to coarse grained and banded. The rock was suggested to have had a sedimentary protolith because of its high Al content.

Sample HE-1 is also from the Keck Consortium samples from Gore Mountain but is of an unknown exact location. The samples AK97-9b, HRM-1 and A-32-W are from Willsboro, NY. Samples AK97-8a and AK97-23 are also from the Keck Consortium Adirondack field trip and are of an unknown provenance. Sample provenance is summarized in Table 2.1.

Table 2.1 - Sample Identification and Locality Information

Sample	Sample Description	Garnet Subgroup	Locality
alm	Fort Wrangell	almandine	Fort Wrangell, AK
ah-un	AH-UN, Anne Hofmeister	grossular	Unknown provenance
g17	HMM 123017	grossular	Unknown provenance
g89	HMM 103089	grossular	Phippsburg, ME
and	HMM 87373 Val Malenko	andradite	Valmalenco, Italy
10c	Keck Garnets AK97-10c	anorthosite	Woolen Mill, NY
12-9	Kb-12-9	Garnet peridotite	Jagersfontein Mine, South Africa
bbkg	Kenya melanite, BBKG	melanite	Kenya, Africa
g5183	BPM 27, Anne Hofmeister grossular	Grossular	Los Angeles Museum, Bishop, Inyo County, CA
2a	Keck Garnets AK97-2a	amphibolite	Gore Mountain, NY Pit #1
2b	Keck Garnets AK97-2b	metagabbro	Gore Mountain, NY Pit #2
12-51	Kb-12-51	garnet peridotite xenolith	Jagersfontein Mine, South Africa
ak9723	Keck Garnets AK97-23	grossular	Adirondacks, NY
8a	Keck Garnets AK97-8a	almandine	Adirondacks, NY
9b	Keck Garnets AK97-9b	grossular	Willsboro, NY
ak9729	Keck Garnets AK97-29	Paragnesiss - almandine	Treadway Mountain Formation, NY
he1	Keck Garnets HE-1	almandine	Gore Mountain, NY
a32w	Keck Garnets A-32-W	grossular	Willsboro, NY

Sample	Sample Description	Garnet Subgroup	Locality
hrm1	Keck Garnets HRM-1	grossular	Willsboro, NY

Application of Mössbauer and XANES Technology to this Study

The goal of this study is to determine oxidation states of Fe^{2+} and Fe^{3+} in garnets. Both the XANES microprobe and Mössbauer spectrometer techniques provide this information based on nuclear or atomic transitions (Mössbauer spectroscopy) and information on chemical bonding and structural order (XANES).

Mössbauer Effect

One of the two methods to be used in this study to determine Fe^{2+} and Fe^{3+} is Mössbauer spectroscopy. Rudolf Mössbauer was born in Munich, Germany on January 31, 1929. He began studying physics in 1949 and developed the theory for Recoilless Nuclear Resonance (Resonant Gamma-ray Spectroscopy, later termed the Mössbauer Effect) during his graduate work in 1957. He later proved his theory in 1958.

The Mössbauer effect relies on theories ofradioactive decay, which can occur by alpha, beta and gamma decay. The Mössbauer Effect relies on beta decay, in which a beta particle (electron or positron) is emitted. In this particular study,we rely on the beta decay of ^{57}Co into ^{57}Fe.

Atomic Resonance

In the Mössbauerspectrometer,^{57}Co begins its decay with energy transfer occurring within the atom. In moving from an unstable state to a stable state, the ^{57}Co emits the excess energy availablein the form of a photon or gamma ray (Fig. 2.2).

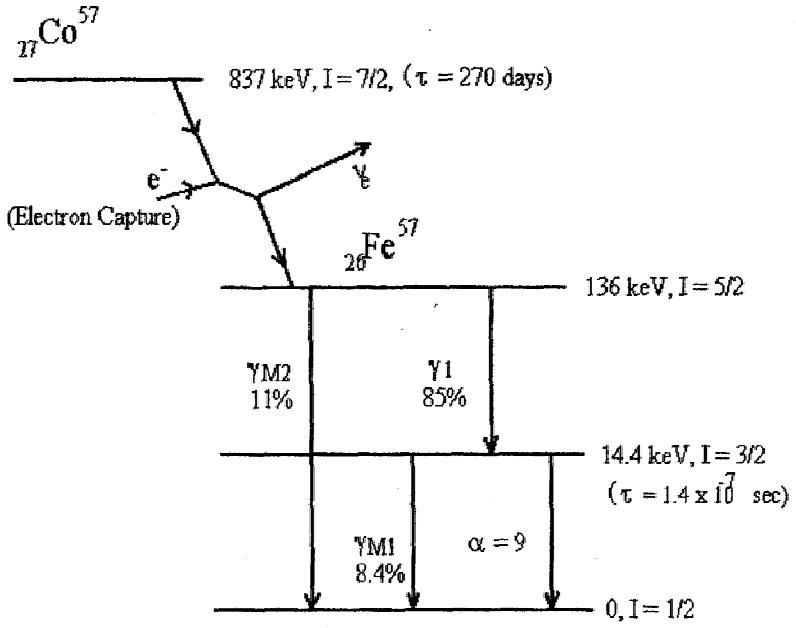

Figure 2.2: Energy scheme of ^{57}Fe. As ^{57}Co decays, it emits three energies of gamma-rays as it decays from an excited state to its ground state. The energy of 14.4 keV is the gamma-ray used for Mössbauer spectroscopy. The energy given is in percent of decays. (Sklute, 2006)

The gamma rays emitted during radioactive decay can then excite nuclear transitions in other atoms if their energies are appropriate. In a Mössbauer experiment, the gamma ray emitted by ^{57}Co is absorbed by ^{57}Fe. The atom that absorbs the emitted photon is then excited.

In a Mössbauer experiment, the involved transitions are occurring within the nucleus. However, it is easiest to understand then by drawing an analogy with electronic transitions (that occur outside the nucleus). When energy is supplied or absorbed, electrons within the sample are excited and move into a higher energy state, usually causing an electron transition to an empty or half-empty orbital in the atom.If an electron is excited while in a full or nearly full orbital, a different electron is then forced to drop into a lower state and a photon is emitted because of the excess energy. The simple process of electron transference, beginning with an initial emitted photon from the source and sample emitting a photon in response, is known as atomic resonance (Fig. 2.3) (Blackwell, 2000). The electron transition is represented in a curve, centered at the average transition energy, E_0, and varies in width depending on the composition of the atom (Fig. 2.4). An analogous process can happen in the nucleus of an atom when a gamma-ray excites transitions between the nuclear energy levels.

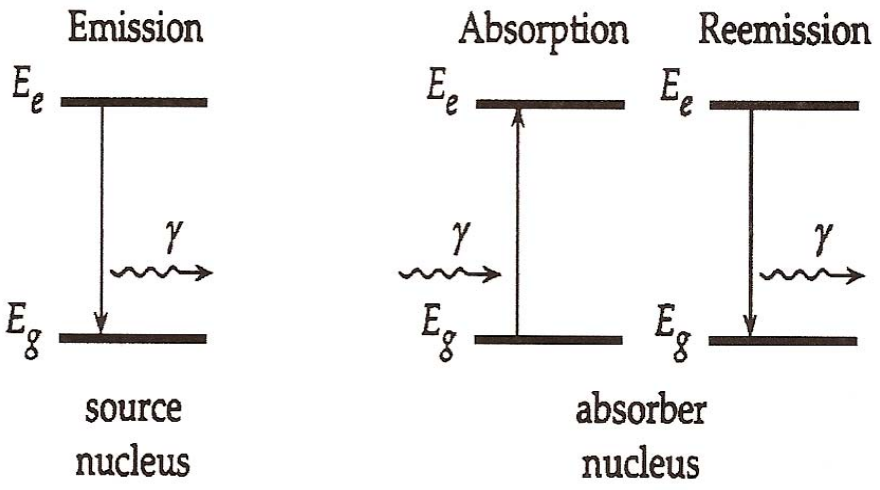

Figure 2.3: Schematic representation of atomic resonance. (Grant, 1995)

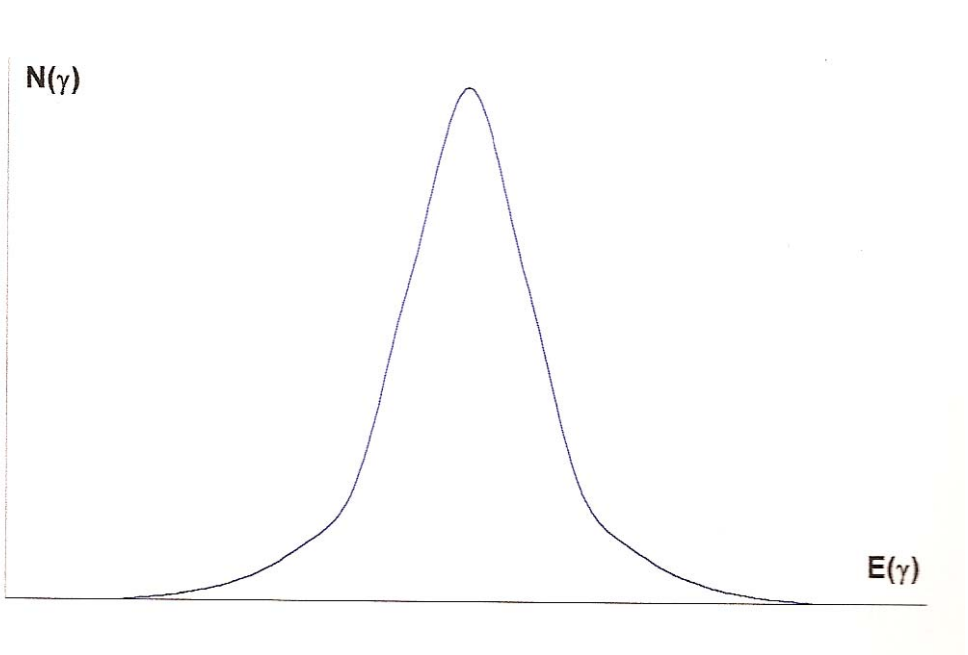

Figure 2.4: The natural line width is a curve reflecting the energies required for the transition of energy for an electron to transfer from one state to another (Blackwell, 2000).

Momentum Transfer and Recoil

When the nucleus of an atom emits radiation in the form of a gamma-ray (electron transfer from high to low energy), it resultsin photon emission at a certain energy, E, and momentum. The atom then moves slightly in the opposite direction from the force of emitting a photon(Fig. 2.5).

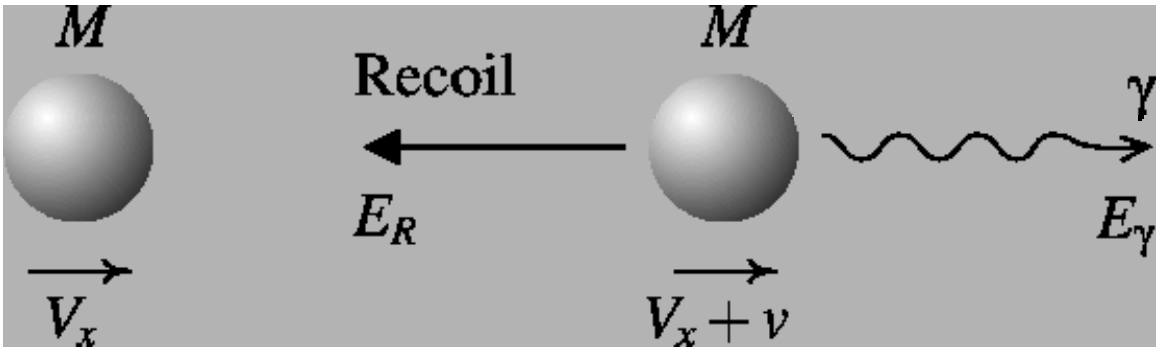

Figure 2.5: Graphic representation of an atom experiencing recoil. The atom, M, is releasing a gamma-ray, γ, and is being forced to move in the opposite direction of the velocity of the gamma-ray. (www.cmp.liv.ac.uk/frink/thesis/thesis/node10.html)

Therefore, it must "recoil" with equal and opposite momentum during emission, such that

$$E_{\gamma\text{-ray emission}} = E_{transition} - E_{recoil.} \text{ (Equation 2.1)}$$

If the nucleus of the sample atom (atom receiving the electron emitted from the source atom) absorbs radiation, the γ-ray must have enough energy to excite the nucleus and surmount the recoil energy, which is summed up in the expression:

$$E_{\gamma\text{-ray emission}} = E_{transition} + E_{recoil.} \text{ (Equation 2.2)}$$

In other words, energy is lost when a photon from the source atom is emitted. The energy from the emitted photon is less than the difference of the energy used to emit the photon and the momentum of the photon. This is due to the conservation of momentum caused by the movement of the atom in the opposite direction of the path of the emitted photon. This movement is referred to as recoil.

This recoil is significant because of the energy and momentum caused by the release of the photon. Because of the atomic recoil and the resulting loss of energy, the emitted photon cannot be reabsorbed into another atom; it no longer has enough energy to stimulate the very same transition that caused it to emit it in the first place,and cannot reenter the nucleus it came from. The source atom releasing the photon has an E_γ (photon energy) of approximately 1eV, while the kinetic energy is on the order of 10^{-10} eV in the atomic range and has little effect on the absorption and emission energies (Fig. 2.6) (Blackwell, 2000). Therefore, if the recoil does not have an effect on emission and absorption energies, atomic resonance is unable to occur (Fig. 2.7).

Emission and Absorption Spectra

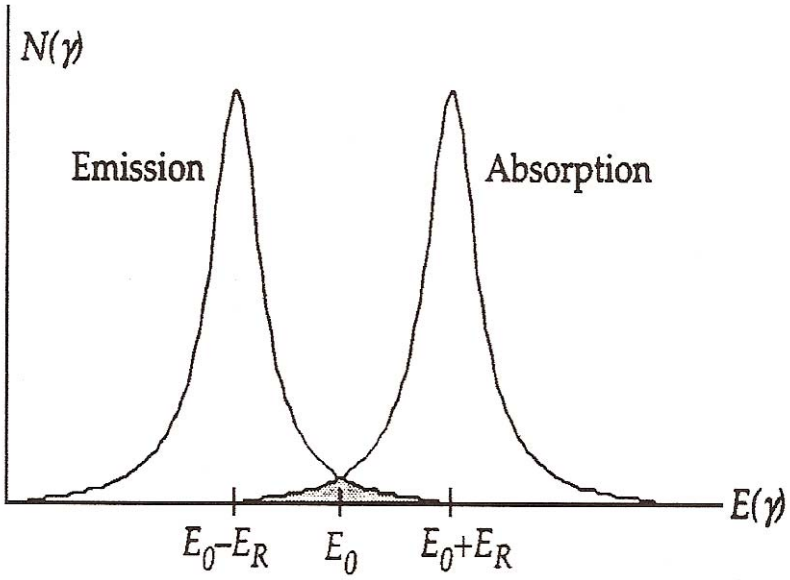

Figure 2.6: The emission and absorption spectra representing atomic transitions (Grant, 1995). $E_\gamma$is the photon energy (x-axis) versus N_γ, the number of transitions. E_0 is the transition energy and E_R is the energy lost to recoil (Blackwell, 2000).

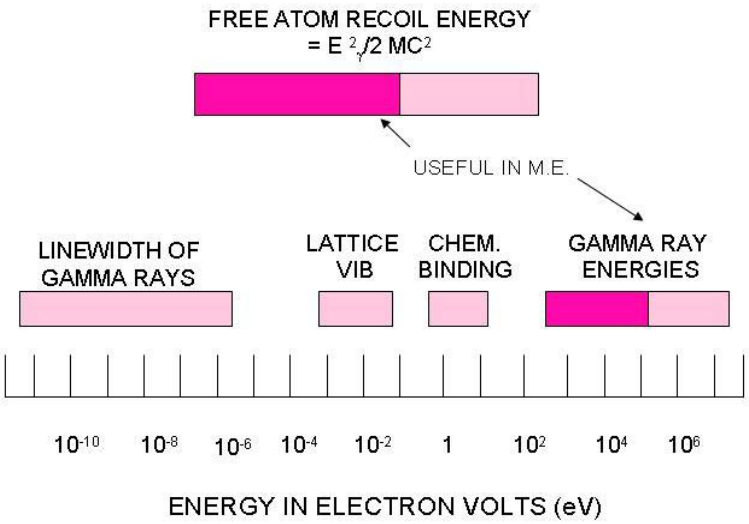

Figure 2.7: Free atom recoil energy scale shows the nuclear and atomic events important to the Mössbauer effect.

Mössbauer Effect

Rudolf Mössbauer was able to prove in 1957 that recoil could be eliminated and resonance absorption (process of a photon emission and absorption occurring at the same energy) could be achieved (Blackwell, 2000). Two methods were used to decrease the energy loss to recoil: 1) the absorbing samplewas embedded in a crystalline structure where the bonds are strong and do not allow structural movement; the mass of the recoiling object for some transitions was therefore effectively increased from the mass of the atom to the entire mass of the

crystal, enough to cause the overlap between the absorption and emission energies for gamma-rays. 2) The absorbing sample can be cooled, reducing the energy loss due to recoil (Blackwell, 2000).

Although these two methods highly reduced the amount of energy loss due to recoil, the remaining difference between emission and absorption energies needed to be solved using the Doppler effect.The Doppler effect results from a change in wavelengths—which reflect a change in energy—from a source that is moved relative to the absorbing sample (if the source is moved toward the sample the wavelengths become shortened (blue shift) and if the source is moved away from the sample the wavelengths become lengthened(red shift)) (Blackwell, 2000). Mössbauer decided to move his source in relation to his sample, and decreased the loss of energy to recoil (Fig. 2.8).

Doppler Velocity

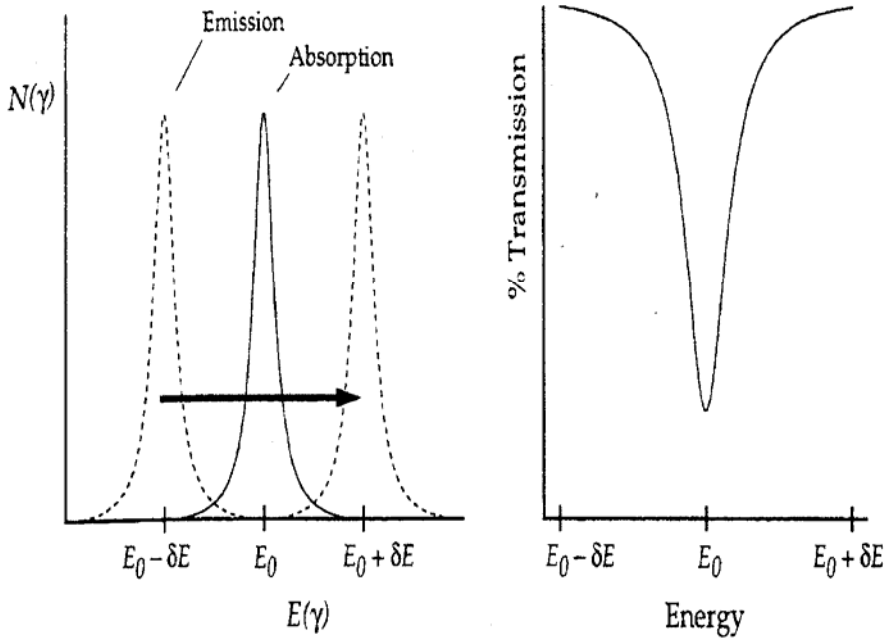

Figure 2.8: The Doppler velocity is added to the source in order to obtain an energy distribution range for the sample. The spectra on the left are the energy distributions for energy and absorption and the spectrum on theright is transmission. (Figure from Sklute, 2006).

"The combination of these techniques, are very accurate foranatom experiencing recoil within the atomic structure,which is Mössbauer spectroscopy. The amount of recoil that occurs is dependent upon two factors, 1) the structure of the site where the Fe atom is located, and 2) the electrical interactions between the surrounding atoms" (Blackwell, 2000). "This is different in gases and liquids, with the possible exception of viscous liquids, but this case is focused on recoil in solids" (Grant, 1995)."Mössbauer discovered that under suitable conditions, a

certain fraction of nuclei, which are bound to crystals, do not recoil. Instead, the entire massive crystal takes up the recoil momentum and this results in a negligible energy loss by gamma-rays" (Lustig, 1961). When the entire crystal system absorbs the energy, this is known as a recoilless energy transfer for the absorbing atom (Blackwell, 2000).

To measure the number of gamma-rays and the energies at which they are absorbed, a detector is placed behind the sample. The detector absorbs the gamma-rays that are not absorbed by the Fe atoms in the sample. This process makes it possible "to determine the energies of the photons absorbed into the sample because the source location, the number of photons not absorbed by the Fe atoms, the areas of the peaks and corresponding to particular energies are known" (Figs. 2.9, 2.10) (Blackwell, 2000).

Mössbauer Spectrometer Setup

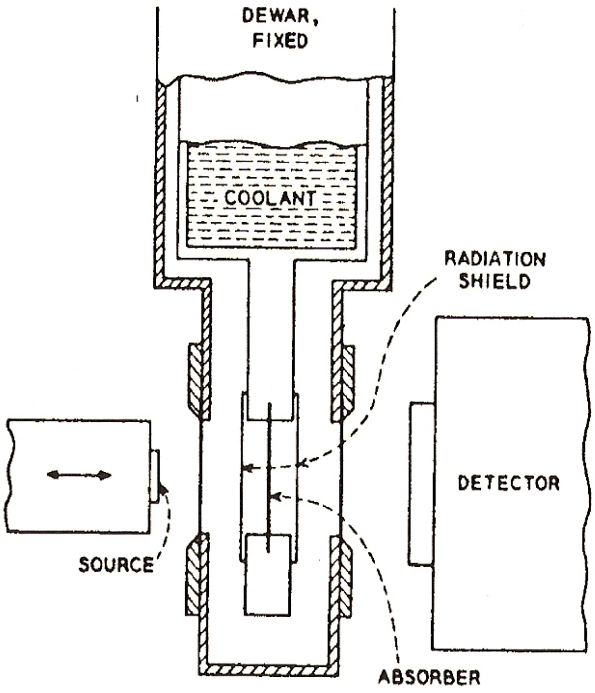

Figure 2.9: The source, oscillating because of the Doppler effect added to it, emits gamma-rays through the absorber. The detector, located behind the absorber, observes the amount of gamma-rays absorbed by the sample. (Sklute, 2006).

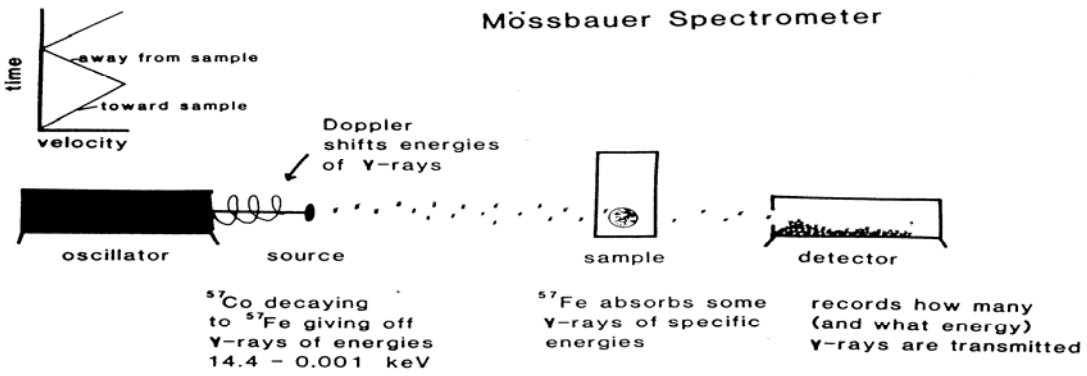

Figure 2.10: The Mössbauer spectrometer depicting the monochromatic line of emission of gamma-rays through or absorbed by the sample and the detector behind the sample. (Dyar, 1984)

Although there are ways to reduce recoil, there is alsoonly a small fraction of samples that are not affected by recoil. The gamma-rays emitted from a source that can be absorbed without recoil represent the recoil-free fraction. Although weak bonds in crystals allow more movement to occur from recoil, stronger bonds do not guarantee that recoil will not occur for all transitions, but there is a fraction that occur without recoil.

This small percentage of recoil-free transitions allowsfor inaccuracies in the measurements of Mössbauer samples and needs to be accounted for. Each valence site is different over a range of temperatures.By conducting a temperature series, it is possible to calculate this fraction, f, for each Fe valence site.

Mössbauer Parameters

Isomer Shift

The isomer shift is a result of atomic interaction between the charge of the distribution in the nucleus and the electrons around the nucleus. This interaction does not cause nuclear energy levelsto split, but allows for a shift in their energies because the photonis absorbed. When a photon is emitted from a source and absorbed bythe sample, the nucleus of the sample changes in size as a result of the additional photon and transitions from low to higher energy.As the size of the atom changes, its energy also changes, and the absorption line of the atom shifts.

Up until this point, we have assumed thatthe source and absorber are identical in the amount of energy required for electronictransition. If this is true, this point is marked as zero on the velocity spectrum whentheDoppler velocity does not need to be added to the source. However, in most cases, the source and absorber are different. Therefore, the isomer shift is thedifference between the point of absorption and the zero position, characterized by the amount of iron in the absorber. This shift is known as the isomer shift (IS or δ) and is recorded in mm/s (Fig. 2.11).

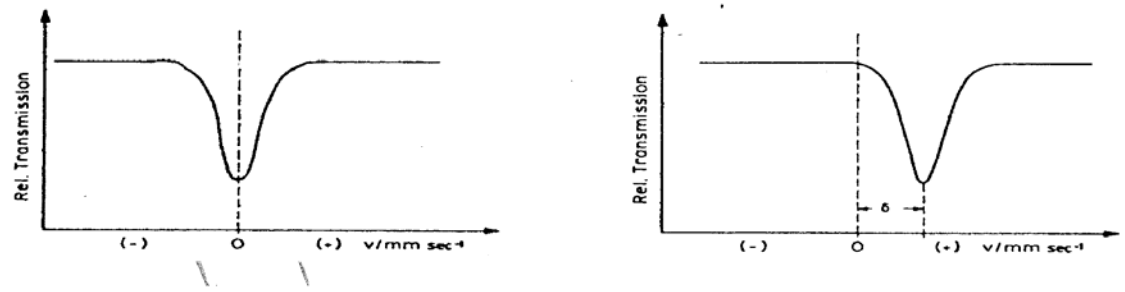

Figure 2.11: The isomer shift is a shift in the Mössbauer energy levels. The photon, emitted from a source and absorbed by the sample, causes the change in size of the nucleus of the absorbing sample because of the additional photon and transition from low to higher energy. The greater change in energy is a result of the size change of the atom and therefore the absorption line of the atom shifts as the energy changes.

Quadrupole Splitting

The electrons within the nucleus of an atom each have a particular spin. This spin causes the magnetic field around the nucleus to be asymmetrical and the nucleus becomes an oval shape. This asymmetry results in what is known as a quadrupole moment. The shape of the atom has become disturbed with a change from spherical, where the dimensions are symmetrical, to oval and asymmetrical. Two different energies are therefore needed to stimulate transitions in the nucleus. The spherical shape of the nucleus requires only one energy level to stimulate a transition within the atom because the axes were equal. With a change or distortion in shape, the atom has two different energy levels, causing the nuclear energy level to splitin an eventknown as quadrupole splitting (QS, Δ or ΔE_Q). This result produces two peaks in the Mössbauer spectrum, known as a doublet.

The quadrupole splitting is the distance between two peaks, corresponding to the difference between the split states (Fig. 2.12).

Quadrupole Splitting

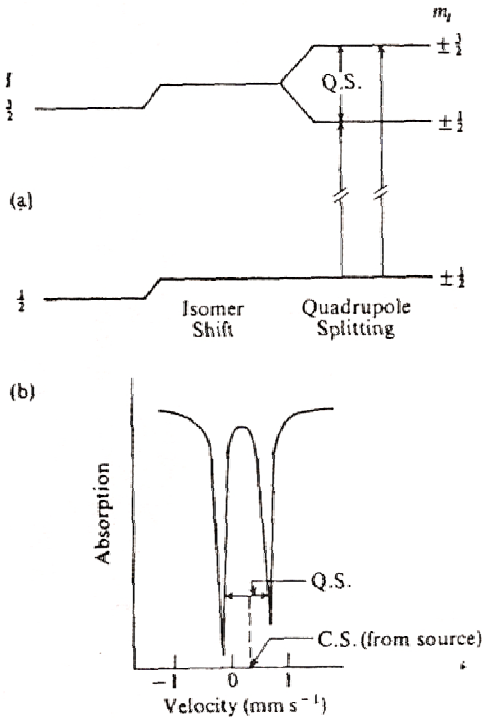

Figure 2.12: Quadrupole splitting is a change or distortion in shape of the nucleus of an atom requiring two different energy levels andcausing the nuclear energy level to split (QS, Δ or ΔE_Q). The bottom photo depicts the two peaks in the Mössbauer spectrum produced by the splitting of the nuclear energy level, known as a doublet. The quadrupole splitting is the distance between two peaks; measuring the energy difference between the two split states.

Line Width

The line width is the range of energies ΔE or Γ, which can be absorbed into an atom in order to cause a transition from a low to a high energystate. The line width is also related to the length of time the atom is in an excited state. In Fe spectra, the natural line width is approximately 0.19 mm/s.

Recoil-free Fraction Calculation

Recoil-free fractions were calculated using the program ISOMER, developed by Eddy De Grave and Toon van Alboom (Sklute, 2006). The program takes input values of temperature and isomer shift from the multi-temperature fits and calculates the recoil-free fraction across available temperature range, usually from 4-12 K and up to 600-800 K at 10-50° increments, using the equation 2.3 (Sklute, 2006).

$$f(T) = \exp\left[-\frac{3}{2}\frac{E_R}{k_B\theta_D} + \left[1 + 4\left(\frac{T}{\theta_D}\right)^2 \int_0^{\theta_D/T} \frac{x\,dx}{e^x - 1}\right]\right]$$ (Equation 2.3)

The recoil is calculated where, E_R is the recoil energy, related to the transition energy, $E\gamma$, by $E_R = E_\gamma^2/2Mc^2$ (De Grave *et al.*, 1991). This method also calculates the characteristic Mössbauer temperature, Θ_M, an approximation of the Debeye temperature, which is used for the lattice vibrational modes of a solid (Eeckhout *et al.*, 2003).

However, it should be noted that the Debeye model for the vibrational modes of a lattice is not best because of it is unrealistic and simplistic for describing a complex lattice system (Eeckhout *et al.,* 2003). The Debeye approximation is commonly used and the comparison of values are still relevant because they may offer valuable information about the tightness of binding (Eeckhout *et al.,* 2003). Plans have been made to begin work on an empirical method of calculating relative peak areas without the use of recoil-free fractions or the Debeye approximation (Sklute, 2006).

Mössbauer Peaks and Parameters

Mössbauer spectroscopy is a leading method for determining Fe^{3+}/Fe^{2+} ratios in minerals because the characteristics of peaks arising from Fe^{3+} and Fe^{2+} are quite distinct. However, there are challenges with interpreting the spectra. For example, there can be more than one possible best fit for any given spectrum. There are cases where spectra have multiple doublets, or mixtures of doublets and sextets that overlap between peaks (Sklute, 2006). This overlapleads to errors and similarity in the parameters. Sklute (2006) also warns us that:

> "The range of Fe^{3+} and Fe^{2+} isomer shifts and quadrupole splitting values is not that large (especially for Fe^{2+} isomer shifts), meaning that many samples containing Fe^{2+} iron have very similar isomer shift and quadrupole splitting values. This does limit the uses of Mössbauer spectroscopy as the self-sufficient instrument for mineral and site identification".

However, there is little overlap of peaks in the Fe^{3+} and Fe^{2+} doublets of garnet, making it possible to distinguish those features very well.

Mössbauer Parameters for Garnet

Scientists have conductedMössbauer studies of garnet since the late 1960s. Since then, many studies have focused on the different species of garnet,on different ranges of temperatures, even on synthetic garnets. Appendix A contains tables of Mössbauer parameters of summarizing past garnet studies, excluding synthetic garnets.

XANES

The second method for Fe^{2+} and Fe^{3+} determination to be used in this study is XANES spectroscopy. The first x-ray absorption beamlines began to emerge in April 1981. Among these beamlines of the 1980s, EXAFS (Extended X-ray Absorption Fine Spectroscopy) presented itself mainlyfor chemical and biological studies including, but not limited to metals, glasses, calcium and platinum-based anti-cancer drugs. XANES (X-ray Near Edge Structure) was mainly used in chemical studies for “stereochemistry, state of order, energetics and relative stabilities, reaction mechanisms, conditions of formation and structure-property relationships and to help predict physical and chemical properties of formation under various pressure-temperature conditions” (Calas *et al.*, 1987). XANES was first used to interpret data from multiple scattering

resonances for a study by Antonio Bianconi at the Stanford Synchrotron Radiation Laboratory (SSRL) (Bianconi, 1980).

Theory and Application

XANES spectroscopy relies on electron transitions in atoms. After the sample has been set in place and the beam is activated, a synchrotron light[1] or conventional X-ray bremsstrahlung[2] that has been monochromatized to direct light at a sample in order to measure the reflected or transmitted light, transmits photons or X-rays into the samples (Calas et al., 1987). The photon energy then excites electrons within the sample, resulting in low-probability, localized transitions of the *K*-level, 1*s*, to partially-filled or lowest-energy, empty, bound, excited states (Calas *et al.* 1987 and Dyar *et al*. 2002). This is the pre-edge of a XANES spectrum and precedes the "electronic transitions in a high-probability, core level to unoccupied bound or continuum states, known as the main-edge spectra" (Dyar *et al*. 2002).

XANES Main-edge Spectra

The main-edge spectra of XANES, the "region representing multiple scattering interactions of the photoelectron and reflections of long-range and

---

[1] Synchrotron light is light that has been put through a particle accelerator where a magnetic field and electric field, rotates and accelerates particles.
[2] A conventional X-ray bremsstrahlung is electromagnetic radiation that has been decelerated by the charge of a particle by the deflection of another charged particle.

short-ranger order, begins at 2-3 eV above the pre-edge and continues until approximately 50 eV above it, and was impossible to interpret until recently (Figs. 2.13, 2.14). The features represented by the scatterings were difficult to translate and access, until a detailedstudy contrasting compositions of key features in micas, minerals with a monoclinic crystal system, was conducted by Mottana *et al.* in 2002. For example, another work by Mottana *et al*. (1997) stated that Al *K* edges showed features that corresponded to octahedrally and tetrahedrally coordinated Al, and could be distinguished in XANES spectra", implying that orientation has an impact on the energy and intensity in micas and other anisotropic minerals (Dyar *et al*. 2002). Interpretation of main-edge (EXAFS) spectra is complicated, and thus was not included as part of this thesis.

XANES Main-edge and Pre-edge Peaks

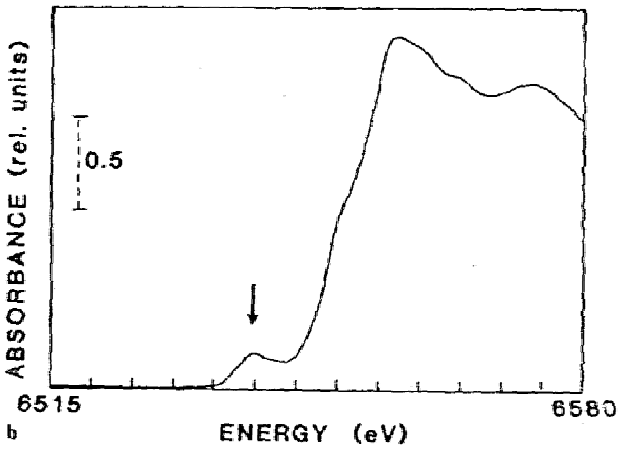

Figure 2.13: A XANES spectra depicting the main-edge structure and the pre-edge peak indicated by the arrow (Calas *et al*., 1987).

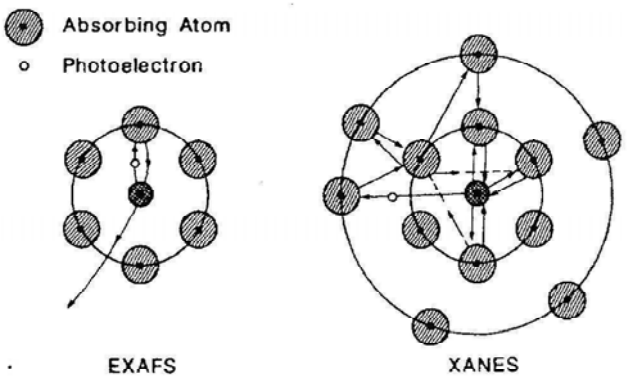

Figure 2.14: The picture on the left depicts the single scattering electron effect in the EXAFS region and the multiple scattering electron effects in the XANES region(Calas *et al*., 1987).

XANES Pre-edge Spectra

Many factors contribute to the intensity and peak energy of the pre-edge peak region in XANES spectra, such as spin state, oxidation state, site geometry, and site symmetry (Dyar *et al*. 2002). Within the sample, the "transitions between the 1*s*→ n*d* states in the pre-edge region are formally spin-forbidden, but have non-zero transition probabilities owing to extremely weak electric quadrupole splitting. Cases where the cation occupies a noncentrosymmetric site, most of the *intensity* of the pre-edge features results from fundamentally intense electric dipole coupling between 3*d* and 4*p* states. The amount of 4*p* mixing into Fe 3*d* orbitals is consistently larger for Fe^{3+} than for Fe^{2+} pre-edges. This difference was attributed by Westre *et al*. (1997) to the fact that bond lengths are shorter around Fe^{3+}, and deviations from centrosymmetry are therefore emphasized" (Dyar *et al*. 2002). Similarly, symmetrical octahedral sites display electric dipole coupling, but as site asymmetry increases, so does the 4*p* mixing into Fe 3*d* orbitals.

Octahedral to tetrahedral distortions increase the mixing as well,implying that pre-edge intensity reflects site symmetry.Orbital transitions and the Fe^{3+} -bearing minerals intensities are greater because there are more transitions of 4*p* mixing into Fe 3*d* orbitals because of the amount of space available in the *d* orbital of Fe^{3+}(Dyar *et al*. 2002).

Minerals with "simple systems can have the pre-edge spectra modeled on the basis of molecular orbital calculations predicting the intensity and energy of component peaks, but most rock-forming minerals are anisotropic. The effects of X-ray pleochrosim (as when studying mineral grains in thin section) must be considered. In a study by Dräger *et al.* (1988), it was confirmed that isotropic minerals, such as a garnet, showed identical spectra when the polarization direction is either parallel or perpendicular to an oriented crystal". Spectra of anisotropic minerals need to be acquired with the beam polarized parallel to the *X*, *Y*, and *Z* axes showing the pre-edge peaks according to each optical direction to correct for the orientation problem (Dyar *et al*. 2002).

XANES Pre-edge Peak as Quantitative Measure for Oxidation State

The technique of Bajt *et al.*, (1994), uses the pre-edge peak energy to determine oxidation states in mixed valence samples. The technique was the "derivation of an oxidation state versus a pre-edge peak energy calibration using the standards fayalite (Fe_2SiO_4), magnetite (Fe_3O_4), and hematite (Fe_2O_3), yielding a linear regression line with a correlation coefficient of 0.99" (Bajt *et al.*,

1994) (Fig. 2.15). Bajt *et al.* (1994) stated that the "data suggest that the coordination differences in the minerals used had little influence on the energy shifts that were observed and therefore, the technique could be used as the basis for measurements of oxidation state in minerals with comparable coordination sites to Fe".

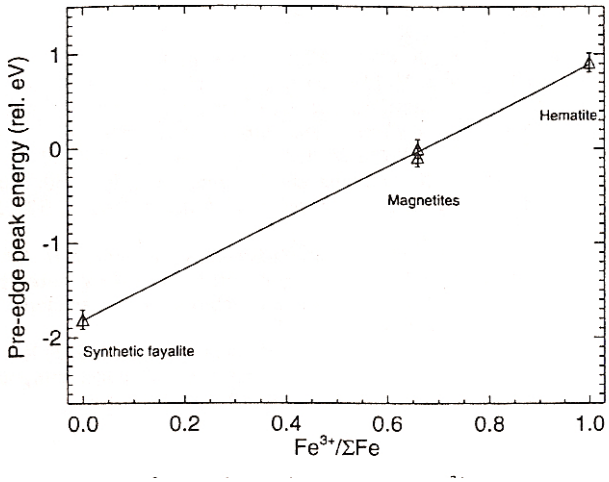

Figure 2.15: Linear calibration curve of pre-edge peak energy and oxidation state for the standards hematite (100% Fe^{3+}), magnetite (66.7%Fe^{3+}) and fayalite (100% Fe^{2+}).

This method was a good first attempt to use the pre-edge peak energy to determine proportions of various oxidation states in a mixed valence sample, but failed to recognize the optical anisotropy of minerals. Therefore, when a sample was rotated on the stage at X26A, BNL (Brookhaven National Laboratory), the pre-edge peak energies were different due to the orientations of the *X*, *Y*, and *Z* axes of anisotropic minerals. A 2002 paper noted the need for the correction of optical orientations (Dyar *et al.*), where each crystal in a sample needed to be "oriented morphologically using a spindle stage, an intense focused x-ray beam,

and methods to orient single-crystal samples optically or by x-ray diffraction" (Dyar *et al.*, 2002).

The goal of this study is to continue to analyze the oxidations states and their relation to the pre-edge peak energies of Fe by using garnet as means to side step the issues faced by Fe *K*-XANES spectra of anisotropic minerals. Garnet, as mentioned previously, is an isotropic mineral and is thereforenot dependent upon optical orientation because the *X*, *Y*, and *Z* axes in a garnet are identical. Samples of pure Fe^{2+} and Fe^{3+} will be used along with samples of varying amounts and mixturesof Fe^{2+} and Fe^{3+}, in hopes that the result will be an accuratecalibration curve of oxidation states versus pre-edge peak energies for garnet.

Chapter 3

Methods

Sample Selection

Rocks were crushed into small grain sizes and garnets were handpicked under a binocular light microscope to be as inclusion-free as possible. The sample amounts varied between 20-40 mg, and an occasional 100 mg sample, depending on the availability of the sample. A few grains of each sample were reserved for XANES analysis and the remainder was used for Mössbauer.

Mössbauer Sample Preparation

Garnets of varying species, localities and chemical composition were first selected. Between 20-40 mg of each sample were then ground using an iron-free diamonite^{TM} mortar and pestle with acetone to prevent oxidation. Sugar was then mixed and ground with the sample and acetone and to thin the sample to obtain the best range of data to be fit.

Mössbauer Spectroscopy of Samples

Each of the spectra was acquired at 300K. For one sample, the garnet standard mix, a temperature series, consisting of 17 different temperatures from 4-295K was collected, under low He gas pressure. A source of 100-70 mCi ^{57}Co in Rh was used on a WEB Research Co. model W100 spectrometer equipped with a

Janus closed-cycle He refrigerator. The time each sample ran ranged from 8-12 hours and the results were calibrated against α-Fe foil. The typical count rates were between 500,000 and 900,000 non-resonant counts/hour.

Fitting Procedures

The garnets were first fit using Mexfieldd, a set of programs created by Eddy De Grave and Toon van Alboom (Gent, Belgium). "Mexfieldd uses Lorentzian line shapes to fit doublets with a fixed area ratio of 1:1 for the peaks and determines single quadrupole splitting values (solving for the full Hamilitonian), isomer shift and width of the spectra. The best fits are then determined by the minimizing chi squared (χ^2) value. The fits are then run through another program known as Disd3e_dd, that uses velocity approximations instead of solving full Hamiltonians to obtain values for isomer shift and quadrupole splitting, searching for a distribution of quadrupole splitting values rather than a single value as in Mexdisdd" (Sklute, 2006). The input and output values produced by each of the programs could then be obtained and compared to work of previously run Mössbauer samples and to provide information about the ratios of ferrous and ferric iron detected by the Mössbauer spectrometer.

Mössbauer Peak Area Error

Inequalities in analysis are common. The error can be a result of inconsistencies in running time, a new radioactive source or fitting software. Lack

of constraints on peak parameters can also result in error. Dyar (1984) conducted a series of tests studying the precision and reproducibility of the Mössbauer parameters and discovered that the isomer shift, quadrupole splitting and peak width mean probable errors are approximately ± 0.02 mm/s on 4 peaks of 3 different spectra including the Fort Wrangell almandine and Val Malenco andradite used in this study. Individual peaks are within ± 1.6%. Results showed that isomer shifts are reproducible to within ± 0.012 mm/s and quadrupole splittings are usully good to ± 0.016 mm/s (Dyar, 1984). In an attempt to correct for error, all of the samples are corrected to an iron foil calibration, source corrections and universal fitting programs.

XANES Sample preparation

Gerard Marchand prepared the garnet mounts used for analysis at Brookhaven National Laboratory (BNL). The garnets were handpicked and placed into an acrylic mount. Approximately 3-10 grains, varying due to quantity and quality of the grains available were then glued into the mounts, with standard thin-section epoxy and polished for a smooth, even surface for analysis.

XANES Analysis Procedure

XANES analysis of the garnets took place at the National Synchrotron Light Source (NSLS) at Brookhaven National Laboratory. The samples were put into the hutch where the photon beam is located, mounted in a holder and put on

automated stage in front of the beam in the hutch. On each hole in the grain mount where the samples are located using a remote image from a camera within the hutch, two different crystals of each sample were then located (a and b). Two different crystals of each sample were chosen. Moving the automated stage allowed for each sample to be focused and then each position of the samples was saved. The X-ray beam was enabled to begin the accumulation of data.

The XANES spectra were collected over a range from -50 to 50 eV, -50 eV to include energies below and including the pre-edge peak and up to 50 eV to include the main-edge peak spectra of the samples. A standard magnetite sample was run at the beginning and end of each 12-hour injection. Magnetite was also run approximately every fifth sample in between because the pre-edge position of magnetite is already known (7113.25 eV) and can be thus used to correct for absolute energy position of the monochromator. The acquired spectra have an unknown pre-edge peak position, but with the use of the known magnetite pre-edge peak position, true energy could be calculated. Each energy interval was counted between 5-20 seconds, depending upon the intensity of the main-edge energy, for a total acquisition time of approximately 25 minutes. After acquisition, the pre-edge peaks of each sample were determined and Fe^{3+} and Fe^{2+} contents calculated.

Figure 3.1: XANES photon beam and garnet samples at Brookhaven National Laboratory

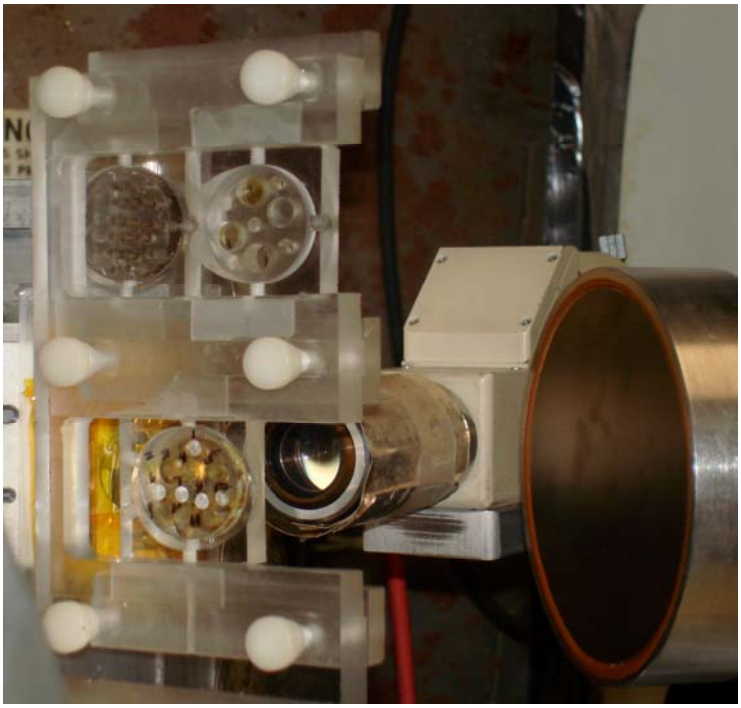

XANES Fitting Procedures

Once spectra were collected, the data were processed in program X26A Data Plotter, where the entire spectrum was displayed for fitting. The output was in the form of a file type with a PAN suffix, to be opened in the PAN: Peak Analysis program. Prior to fitting the samples in PAN, an energy correction needed to be made. To do the energy correction, magnetite spectra were fit first, using the known location of its pre-edge peak. The magnetite peak was used to calculate the amount of offset energy needed to correct the peak energy to "true" energy. It was then possible to determine where the magnetite peak would be at the time each sample was run, so we could correct all of the spectra to true wavelength (Table 3.1).

Table 3.1:XANES Energy Correction

XANES Energy Correction				
Sample	**Sample Order**	**Fit value (eV)**	**Correction factor**	**True energy (eV)**
Magnetite standard	mag.004	7114.45	-1.20	7113.25
Magnetite standard	mag.005	7114.51	-1.26	7113.25
Magnetite standard	mag.006	7112.05	1.20	7113.25
AK-97-23	ak9723.007		1.21	
Alm3	alm3.008		1.21	
And3	and3.009		1.22	
AK-97-8a	8a.010		1.23	
AK-97-29	ak9729.011		1.23	
Magnetite standard	mag.012	7112.01	1.24	7113.25
Beam Injection				
Magnetite standard	mag.013	7112.48	0.77	7113.25
Magnetite standard	mag.014	7112.30	0.95	7113.25
Magnetite standard	mag.015	7112.27	0.98	7113.25
Magnetite standard	mag.016	7112.23	1.02	7113.25
Alm1	alm1.017		1.05	
AHUN	ahun.018		1.08	
G17	g17.019		1.12	
G89	g89.020		1.15	
And1	and1.021		1.18	
Beam Injection				
Magnetite standard	mag.022	7112.03	1.22	7113.25
Magnetite standard	mag.023	7111.92	1.33	7113.25
Magnetite standard	mag.024	7111.87	1.38	7113.25
Grossular 5183	g5183.025		1.39	
BBKG	bbkg.026		1.39	
Kb-12-9	129.027		1.40	
AK-97-10c	10c.028		1.40	
Magnetite standard	mag.029	7111.84	1.41	7113.25
AK-97-2a	2a.030		1.40	
AK-97-2b	2b.031		1.39	
Kb-12-51	1251.032		1.38	
Magnetite standard	mag.033	7111.87	1.38	7113.25
Beam Injection (Dyar/Delaney samples run)				
Magnetite standard	mag.076	7111.98	1.27	7113.25
Magnetite standard	mag.077	7111.85	1.40	7113.25
Magnetite standard	mag.078	7111.80	1.45	7113.25
ak9723	ak9723.079		1.45	
AK-97-9b	9b.080		1.45	

Sample	Sample Order	Fit value (eV)	Correction factor	True energy (eV)
AK-97-9b	9bb.081		1.45	
AK-97-2b	ak972b.082		1.45	
AK-97-23	he1.083		1.44	
Magnetite standard	mag.084	7111.81	1.44	7113.25
AK-32-W	a32w.085		1.43	
HRM-1	hrm1.086		1.42	
Alm1b	alm1b.087		1.41	
AH-UNb	ahunb.088		1.40	
G17b	g17b.089		1.39	
G89b	g89b.090		1.38	
Magnetite standard	mag.091	7111.88	1.37	7113.25
And1b	and1b.092		1.36	
BBKGb	bbkgb.093		1.35	
AK-97-10cb	10cb.094		1.35	
AK-97-2bb	2bb.095		1.34	
Kb-12-51b	1251b.096		1.33	
Magnetite standard	mag.097	7111.93	1.32	7113.25
Beam Injection				
Magnetite standard	mag.098	7111.74	1.50	7113.25
Magnetite standard	mag.099	7111.73	1.52	7113.25
Magnetite standard	mag.100	7111.73	1.52	7113.25
g5183b	g5183b.101		1.51	
Kb-12-9b	129b.102		1.50	
2ab	2ab.103		1.49	
AK-97-23b	ak9723b.104		1.48	
Magnetite standard	mag.105	7111.78	1.47	7113.25
8ab	8ab.106		1.46	
HE-1b	he1b.107		1.44	
AK-97-9b	ak979b.108		1.43	
AK-32-Wb	a32wb.109		1.41	
HRM-1b	hrm1b.110		1.40	
Magnetite standard	mag.111	7111.87	1.38	7113.25

***Samples with the letter b, represent analysis of different part of a sample analyzed to provide samples from a different or unknown orientation of a garnet crystal.**

The energy-corrected outputs were opened in the PAN: Peak Analysis. PAN allows for the baseline of the pre-edge peak to be fit and removed. A Gaussian peak (fits the centroid peak) was then used to fit the select, small regions of the entire spectrum, known as the pre-edge. The PAN files were then

opened in excel and corrected for the true energy on the x-axis, and then PAN was used to fit individual component pieces.

XANES Error

Error in XANES data can be a result of the overheating of the monochromator, photon injections at the beam, incorrect orientation of crystals or inconsistent fits of peaks. Table 3.1 lists the sample order and beam injections. By recording beam injections and duration of sample analysis by the beam, visitors to the beam are able to document if samples were affected by the monochromator running too long, resulting in the beam being offset over long periods, or if a sample began analysis while an injection was still occurring.

Pre-edge peak extraction in using X26A Data Plotter resulted in the error of ± 0.03 eV. Pre-edge peaks were extracted 5 times for each spectrum including the magnetite standard, to measure inconsistency in the data. The extracted pre-edges were then corrected according to the energies in Table 3.1 and opened in PAN: Peak Analysis. The energy corrected peaks were then fit 5 times each and resulted in an error of ± 0.1 eV. The energy corrected peaks bear much more precise results than those of the uncorrected extracted pre-edges.

Chapter 4

Mössbauer Results

Mössbauer Spectroscopy Results

Mössbauer data (Appendix B) were fit using the programs described in Chapter 3. The data acquired from the fit process according to Mexfieldd is listed in Table 4.1. The data are organized from Fe^{2+}-rich to Fe^{3+}-rich with varying amounts of Fe^{2+}/Fe^{3+} in between. Samples containing only Fe^{2+} or only Fe^{3+} were fit with one doublet. Samples with mixed Fe^{2+}/Fe^{3+} contents, such as grossular garnets and samples with impurities, were fit with a range of 2-6 separate doublets.

The garnet standard mix was a combination of the Fort Wrangell almandine and Val Malenko andradite to model a garnet with intermediate Fe^{2+}/Fe^{3+} contents. Spectra of this sample were acquired over a temperature range from 4-295K in order to develop a correction for the recoil-free fractions, f, as described in Chapter 3. The isomer shifts of the doublets in these spectra were used to calculate f, for both doublets of the garnet standard mix. The purpose of this calculation was to correct for the area ratios in a mixed mineral spectrum to provide the true percentages of Fe^{2+} and Fe^{3+} in a sample. The recoil-free fraction values are given in Tables 4.2 and 4.3.

Table 4.1

Sample	chi^2	IS 1	QS 1	Width 1	Area 1(%)	IS 2	QS 2	Width 2	Area 2(%)	IS 3	QS 3	Width 3	Area 3 (%)	IS 4	QS 4	Width 4	Area 4 (%)	IS 5	QS 5	Width 5	Area 5 (%)	IS 6	QS 6	Width 6	Area 6 (%)
alm	1.66	1.29	3.528	0.30	100																				
ak9729	14.84	1.30	3.535	0.27	100																				
ak972a	4.59	1.29	3.55	0.29	100																				
8a	4.61	1.30	3.548	0.28	100																				
he1	2.97	1.30	3.557	0.30	97	0.39	0.35	0.30	3																
129	7.90	1.29	3.567	0.30	96	0.34	0.27	0.30	4																
1251	7.29	1.29	3.566	0.30	89	0.16	0.45	0.30	3	0.35	0.32	0.30	8												
Garnet Standard Mix	15.19	1.29	3.54	0.30	48	0.41	0.56	0.30	52																
9b	9.35	1.28	3.582	0.30	46	0.39	0.48	0.30	54																
ak9723	6.64	1.28	3.547	0.30	83	1.10	2.66	0.30	8	0.33	0.47	0.30	6	1.18	1.88	0.30	2								
ak972b	5.44	1.29	3.547	0.30	73	1.11	2.65	0.30	9	1.21	1.57	0.30	5	0.48	0.43	0.30	6	1.05	2.20	0.30	7				
10c	56.80	1.28	3.54	0.30	51	1.11	0.57	0.30	8	1.15	2.55	0.30	13	0.40	-0.49	0.30	17	1.76	0.74	0.30	10	0.68	1.99	0.30	1
g17	4.83	1.28	3.593	0.34	46	0.39	0.62	0.57	51	1.19	2.03	0.26	4												
g89	7.53	1.28	3.587	0.43	50	0.40	0.57	0.54	48	1.07	2.24	0.30	3												
bbkg	1.47	1.11	3.152	0.31	6	0.41	0.63	0.36	73	0.57	2.02	0.38	7	0.30	1.16	0.40	0.14								
g5183	10.26	1.28	3.572	0.30	12	0.39	0.58	0.29	90	2.24	0.12	-0.23	-1												
ak32w	6.46	1.29	3.581	0.31	19	0.39	0.59	0.34	82																
ahun	8.27	1.28	3.569	0.29	6	0.40	0.58	0.27	94																
hrm1	10.53	1.27	3.555	0.26	4	0.40	0.58	0.29	96																
and	6.63	0.41	0.557	0.29	100																				

Table 4.2: Recoil-free Fraction Values for Fe^{2+}

Recoil-free Fraction (*f*) Values for Fe^{2+}	
Temperature (K)	***f* Values**
18	0.883
28	0.879
38	0.874
48	0.866
58	0.858
68	0.848
78	0.838
88	0.827
98	0.816
108	0.804
118	0.792
128	0.781
138	0.769
148	0.757
158	0.745
168	0.733
178	0.722
188	0.710
198	0.699
208	0.687
218	0.676
228	0.665
238	0.654
248	0.643
258	0.633
268	0.622
278	0.612
288	0.602

Table 4.3: Recoil-free Fraction Values for Fe^{3+}

Recoil-free Fraction (*f*) Values for Fe^{3+}	
Temperature (K)	***f* Values**
18	0.932
28	0.931
38	0.930
48	0.929
58	0.927
68	0.924
78	0.922
88	0.919
98	0.916
108	0.913
118	0.909
128	0.906
138	0.902
148	0.898
158	0.894
168	0.889
178	0.885
188	0.881
198	0.877
208	0.873
218	0.868
228	0.864
238	0.859
248	0.855
258	0.852
268	0.846
278	0.843
288	0.837

The recoil-free fraction calculation also determines the intrinsic isomer shift and related Mössbauer temperature (Tables 4.4, 4.5, 4.6 and 4.7). Figures 4.1and 4.2 show graphical representations of the garnet standard mix data for the curve to calculate f, intrinsic isomer shift, and Mössbauer temperature.

Table 4.4: Experimentally-Determined Isomer Shift Values for Fe^{2+}

Temperature Series Isomer Shift Fe^{2+}	
Temperature (K)	**Isomer Shift (mm/s)**
18	1.44
24	1.44
30	1.44
45	1.44
60	1.44
80	1.43
100	1.42
125	1.41
175	1.38
200	1.36
225	1.34
250	1.33
275	1.31

Table 4.5:Experimentally-Determined Isomer Shift Values for Fe^{3+}

Temperature Series Isomer Shift Fe^{3+}	
Temperature (K)	**Isomer Shift (mm/s)**
18	0.52
24	0.52
30	0.52
45	0.52
60	0.51
80	0.51
100	0.51
125	0.50
175	0.48
200	0.46
225	0.45
250	0.44
275	0.42

Table 4.6: Isomer Shifts for Fe^{2+} at Various Temperatures Based on Equation 2.2

Predicted Isomer Shift for Fe^{2+}	
Temperature (K)	**Isomer Shift (mm/s)**
18	1.44
28	1.44
38	1.44
48	1.44
58	1.44
68	1.43
78	1.43
88	1.43
98	1.42
108	1.42
118	1.41
128	1.40
138	1.40
148	1.39
158	1.39
168	1.38
178	1.37
188	1.37
198	1.36
208	1.35
218	1.35
228	1.34
238	1.33
248	1.33
258	1.32
268	1.31
278	1.31

Table 4.7:Isomer Shifts for Fe^{3+}at Various Temperatures Based on Equation 2.2

Predicted Isomer Shift forFe^{2+}	
Temperature (K)	**Isomer Shift (mm/s)**
18	0.52
28	0.52
38	0.52
48	0.52
58	0.52
68	0.51
78	0.51
88	0.51
98	0.51
108	0.51
118	0.50
128	0.50
138	0.49
148	0.49
158	0.49
168	0.48
178	0.48
188	0.47
198	0.47
208	0.46
218	0.45
228	0.45
238	0.44
248	0.44
258	0.43
268	0.42
278	0.42
288	0.41

Figure 4.1: Predicted Isomer Shift versus the Actual Isomer Shift (mm/s) at Temperatures of 18-295K of Fe^{2+}.

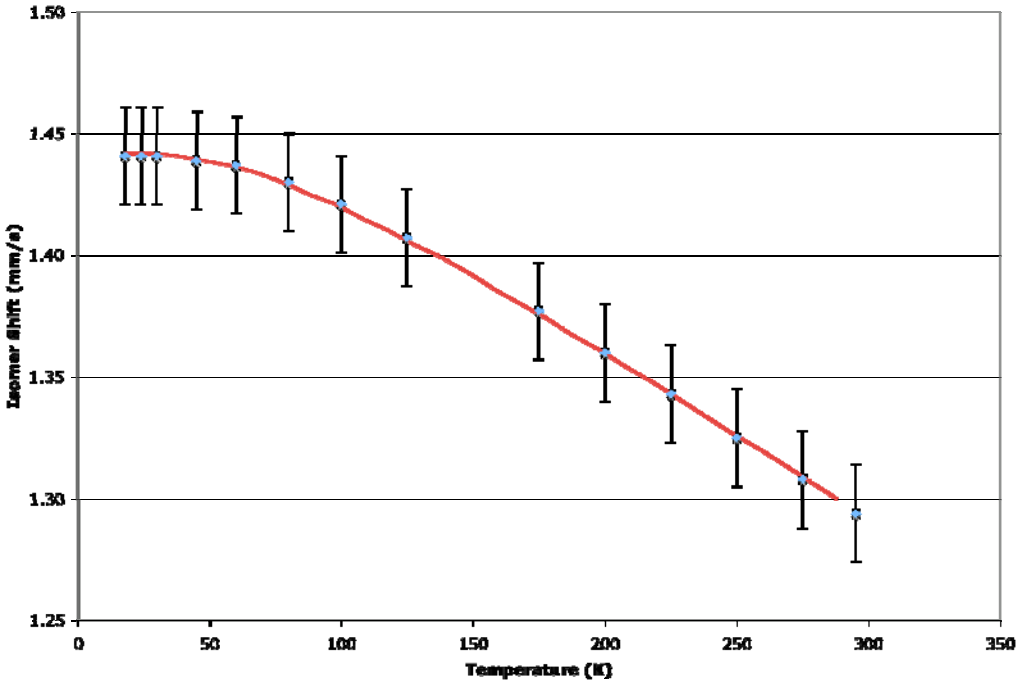

Error bars are at ± 1 for temperature (K) and ±0.02 for isomer shift (mm/s).

Figure 4.2: Predicted Isomer Shift versus the Actual Isomer Shift (mm/s) at Temperatures of 18-295K of Fe^{3+}.

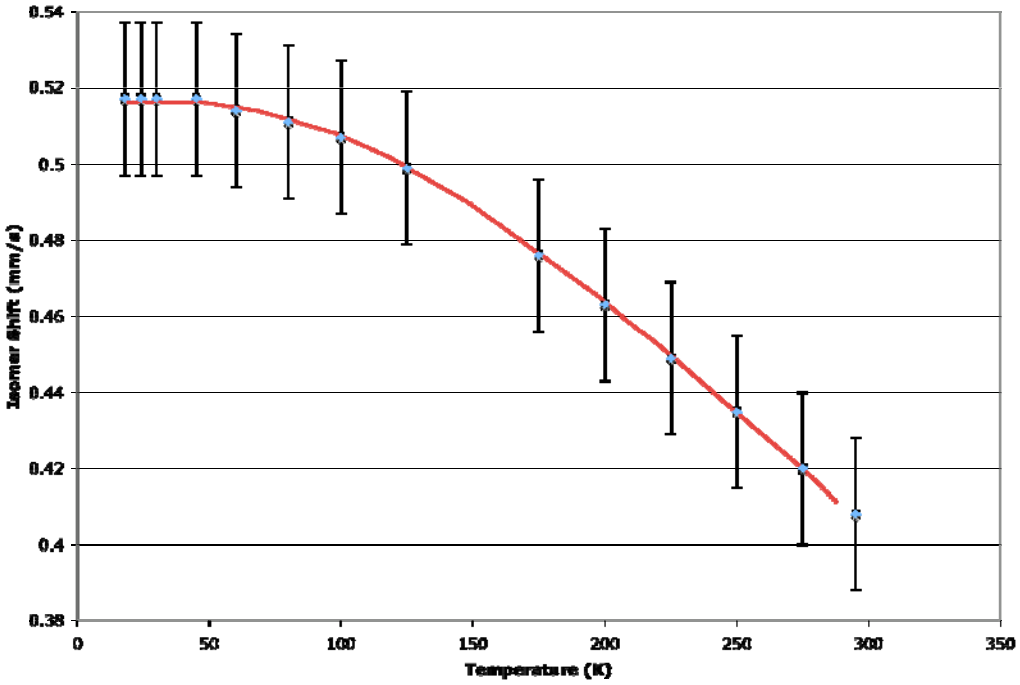

Error bars are at ± 1 for temperature (K) and ±0.02 for isomer shift (mm/s).

To determine the cations of Fe^{2+}andFe^{3+} per formula unit, the final Mössbauer peak areas were corrected to account for differential recoil-free fractions of Fe^{2+}andFe^{3+} (Dyar *et al*., 2007) using the following equation:

$$N^{Fe^{3+}} = \frac{100 \times A^{Fe^{3+}}}{A^{Fe^{3+}} + \left(C \times \left(100 - A^{Fe^{3+}} \right) \right)}$$

where $C = \frac{f^{3+}}{f^{2+}}$.

A is the doublet area of Fe^{2+}orFe^{3+} and *N* is the "true" amount of each species present (Dyar *et al.*, 2007). True Fe^{3+} is calculated from the area of Fe^{3+}. This equation comes from Dyar *et al.* (2007) and it relates the doublet areas to the true abundance of each species. The "true" areas of Fe^{3+} and Fe^{2+} have been corrected for and the results are listed in Table 4.8.

Table 4.8: Mössbauer peak areas corrected using *f* values from Tables 4.6 and 4.7

True Amount of Fe^{3+} and Fe^{2+} for Mössbauer		
Sample	**Mössbauer % Area Fe^{3+}**	**Mössbauer True % Area Fe^{3+}**
alm	0	0
ak972a	0	0
ak978a	0	0
ak9729	0	0
he1	3	2
129	4	3
1251	11	8
Garnet Standard Mix	52	44
9b	54	46
ak9723	7	5
2b	7	5
10c	18	14
g17	51	43
g89	48	40
bbkg	94	92
5183g	90	86
a32w	81	76
ahun	94	92
hrm1	96	95
and	100	100

The true Mössbauer peaks for Fe^{3+} and Fe^{2+} can now be compared to the XANES peaks. Corrected peaks are important for analysis because the correction can vary from 1-8% absolute (Table 4.8). Peaks corrected for recoil-free fraction allow for more accurate determination of valence state in a mixed sample and distinguish true Fe^{3+}/Fe^{2+}ratios.

Table 4.8 shows that many of the garnets analyzed contain a mix of Fe^{3+} and Fe^{2+}. This indicates how oxidizing the conditions were at the time the garnets crystallized. The samples from the Adirondacks, NY and more specifically

samples from Gore Mountain, contain mainly Fe^{2+}. Other samples contain small percentages of Fe^{3+}.

Chapter 5

XANES Results

XANES data (Appendix C) were fit using the programs described in Chapter 3. The peak positions acquired from the fits are listed in Table 5.1. The data are organized from Fe^{2+}-rich to Fe^{3+}-rich with varying amounts of Fe^{2+}/Fe^{3+} in between. The samples were fit with 2-4 peaks: two peaks for Fe^{2+}-rich to Fe^{3+}-rich samples and up to four peaks for those with mixed Fe^{2+}/Fe^{3+} contents.

In all of the samples, Fe^{2+}/Fe^{3+} peak areas are similar to those determined by Mössbauer spectroscopy. The exception to this is the Kenya melanite samples, with spectra names bbkg.026, bbkgb.093 and 129b.102. The parameters for Fe^{2+} peaks fit by the program PAN are 7111.50-7117.09eV and 7112.17-7113.40eV and the parameters for Fe^{3+} peaks are 7112.84-7113.45eV and 7111.98-7114.34eV. Sample bbkg.026 has peaks at 7113.26eV and 7111.06eV best matching a Fe^{2+} peak, because the peak at 7113.26 can fit in both the Fe^{2+} and Fe^{3+} parameters. With one peak already distinguished as Fe^{2+}, the best bet may appear to classify the data as being two Fe^{2+} peaks.

However, the results of bbkgb.093 should be taken into consideration as well. Sample bbkgb.093, also from the same garnet but a location on the crystal, has peaks at 7113.34eV and 7111.46eV. Again, one peak fits the Fe^{2+} parameters and one peak can be considered either Fe^{2+} or Fe^{3+} (Fig. 5.1).

Table 5.1: XANES Peak Positions and Percent Areas

XANES Peak Positions								
	Fe^{2+}				Fe^{3+}			
	Peak 1		Peak 2		Peak 3		Peak 4	
Sample	Center	Area	Center	Area	Center	Area	Center	Area
alm1.007	7111.67	3.48	7113.43	8.22				
alm1b.087	7111.66	1.05	7113.50	2.24				
alm3.008	7111.55	7.09	7113.35	2.17				
he1.083	7111.61	5.09	7113.33	7.49				
he1b.107	7111.68	6.89	7113.38	1.45				
2a.030	7111.59	8.47	7113.64	1.77				
2ab.103	7111.68	5.60	7113.33	1.20				
2b.031	7111.61	5.87	7113.39	1.26				
2bb.095	7111.57	3.87	7113.37	5.84				
8a.010	7111.50	6.81	7113.50	1.04				
8ab.106	7111.60	1.02	7113.56	2.58				
129b.102	7111.68	2.79	7113.31	8.23				
ak972b.082	7111.66	4.22	7113.27	7.56				
ak9723.007	7111.52	3.76	7113.41	6.33				
ak9723.079	7111.59	6.67	7113.38	1.18				
ak9723b.104	7111.55	7.05	7113.42	2.20				
ak9729.011	7111.54	8.37	7113.39	1.85				
ak9729b.108	7111.56	7.24	7113.39	1.48				
10c.028	7111.49	2.25			7113.39	5.69		
10cb.094	7111.56	3.76			7113.46	7.14		
bbkg.026	7111.06	4.91			7113.26	9.53		
bbkg.093	7111.46	1.90			7113.34	5.17		
9b.080	7111.65	6.94	7113.01	4.29			7114.25	3.40
9bb.081	7111.72	8.19	7113.09	4.76			7114.26	2.66
129.027	7111.64	2.53	7113.45	1.06			7115.91	1.02
1251.032	7111.60	1.26	7113.00	5.90	7113.24	7.44		
1251b.096	7111.76	1.90	7113.65	1.75			7114.64	2.02
g17.019	7111.70	1.50	7110.44	1.38	7113.10	2.25	7114.49	1.29
g17b.089	7111.57	2.07	7111.97	1.25	7112.85	2.71	7114.23	2.88
g89.020	7112.68	4.94	7113.38	2.01	7112.12	4.65	7114.33	1.68
g89.090	7111.92	6.75	7111.14	9.80	7113.09	2.37	7114.16	9.59
g5183.025	7115.03	1.97			7113.03	4.15		
g5183b.101	7114.58	3.85			7113.08	4.09		
a32w.085	7114.59	2.81			7112.85	2.27		
a32wb.109	7114.29	1.07			7112.51	2.66		
ahun.018					7113.02	1.31	7114.70	1.84
ahunb.088					7112.99	3.82	7114.71	6.90
hrm1.086					7112.96	3.13	7114.55	1.09
hrm1b.110					7113.19	4.63	7114.64	8.90
and3.009					7112.84	3.45	7114.34	1.99
and1.092					7112.86	9.89	7114.44	5.54
and1.021					7112.97	4.67	7114.49	2.69

All of the samples contain Fe^{2+}/Fe^{3+} peak parameters that allow the samples to be categorized as the same type of garnet as fit by the Mössbauer, except for the Kenya melanite samples bbkg.026, bbkgb.093 and 129b.102. The parameters for Fe^{2+} peaks fit by the program PAN are 7111.50-7117.09eV and 7112.17-7113.40eV and the parameters for Fe^{3+} peaks are 7112.84-7113.45eV and 7111.98-7114.34eV. Sample bbkg.026 has peaks at 7113.26eV and 7111.06eV best matching a Fe^{2+} peak, because the peak at 7113.26 can fit in both the Fe^{2+} and Fe^{3+} parameters. With one peak already distinguished as Fe^{2+}, the best bet may appear to classify the data as being two Fe^{2+} peaks. However, the results of bbkgb.093 should be taken into consideration as well. Sample bbkgb.093, also from the same garnet but a location on the crystal, has peaks at 7113.34eV and 7111.46eV. Again, one peak fits the Fe^{2+} parameters and one peak can be considered either Fe^{2+} or Fe^{3+} (Fig. 5.1). Two possible conclusions can be drawn: 1) the peaks are both representative of ferrous iron (Fe^{2+}) or 2) the peaks represent one peak of Fe^{2+} and one peak of Fe^{3+}.

To determine which conclusion is more plausible, the peaks can then be compared to the Mössbauer data collected. According to the Mössbauer results, sample bbkg contains Fe^{2+} andFe^{3+}. The best conclusion to make is that the results are representative of Fe^{2+} andFe^{3+}.

The other sample providing difficulty during interpretation was sample 129b.102 (Fig. 5.1). The sample 129b.102 (Fig. 5.2) only contains two Fe^{2+} peaks,

Figure 5.1: **XANES spectra for samples of pure Fe^{2+}, almandine, and pure Fe^{3+}, andradite, are displayed in comparison with samples bbkg.026 and bbkgb.093, which have been concluded to be samples containing both Fe^{2+} andFe^{3+}.**

Sample alm1.017

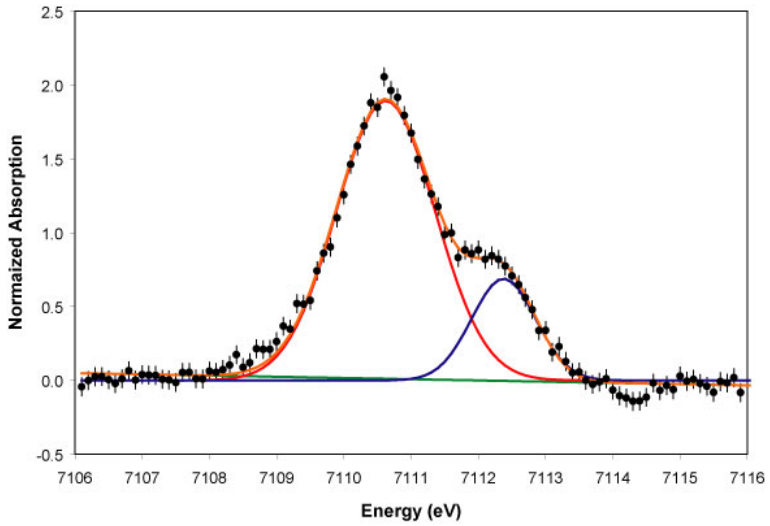

Sample and3.009

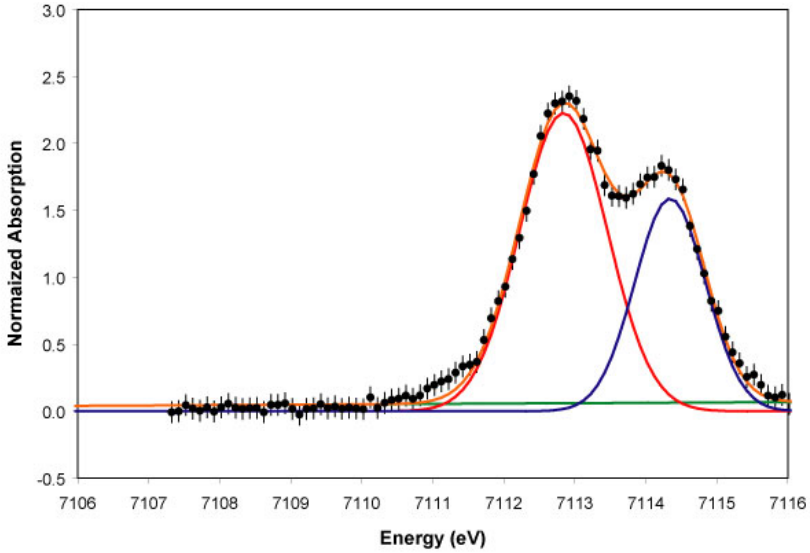

Sample bbkg.026

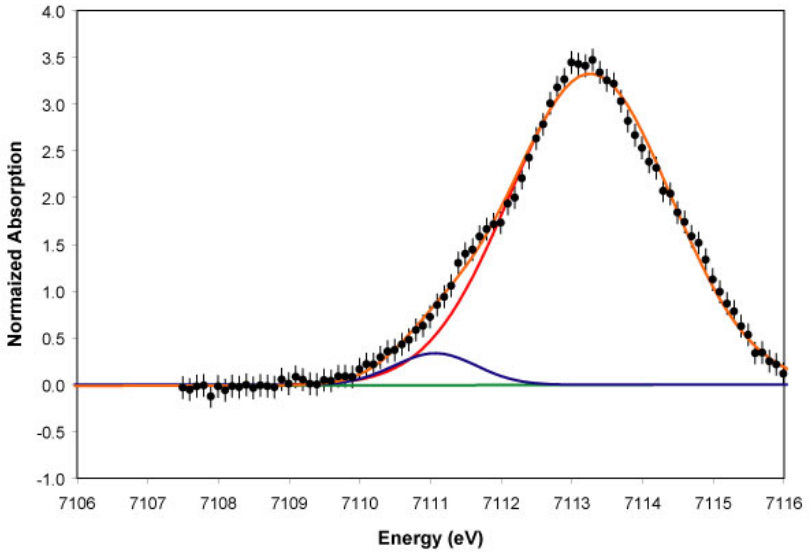

Sample bbkgb.093

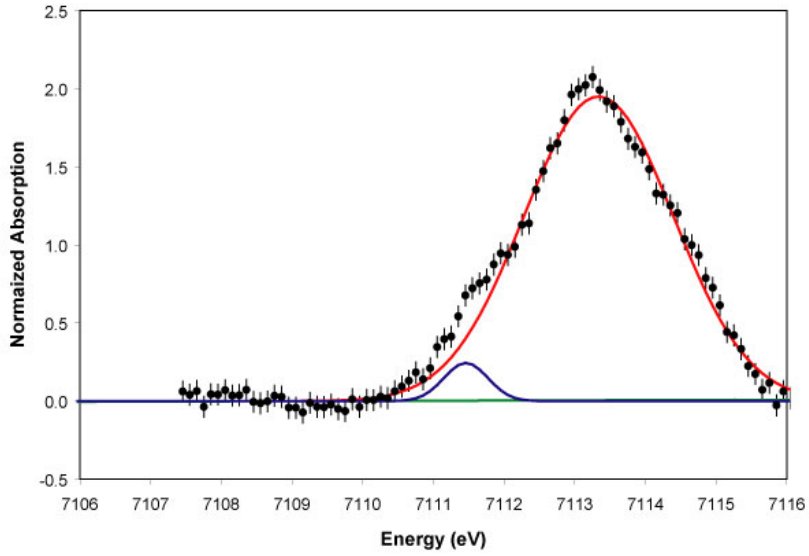

while sample 129.027 (from the same garnet) contains three peaks, two Fe^{2+} peaks and oneFe^{3+}peak. The problem associated with sample 129b.102 was a lack of recognizing a Fe^{3+} peak. The PAN program would crash for sample 129.027 if more than two peaks were used to fit the data. It is possible that 129b.102 was only Fe^{2+}, but highly unlikely if both the Mössbauer and another sample of the same garnet, 129.027, contained both Fe^{2+} andFe^{3+} peaks.

It is also plausible to conclude that sample Kb-12-9, where samples 129.027 and 129b.102 come from, is a zoned crystal. A zoned crystal means that the environment changed as a crystal grew. The center of a garnet would have one chemical composition as it grew and the next few layers to grow would be of a different composition. This can occur to due metamorphism which is quite common or from impurities added to a crystal during growth. Samples AK-97-2b, AK-97-23 and AK-97-10c contain ilmenite, a titanium oxide impurity. The parameters for a mixed sample of Fe^{2+} andFe^{3+} along with parameters for the addition of the ilmenite were used when fitting the Mössbauer data and were therefore detected early on. However, Mössbauer spectroscopy is unable to detect zoning because samples are crushed and mixed together and is not used for the indication of zoned samples. Further research (for example, traverses in a straight line across individual grains) at Brookhaven National Laboratory would be needed to conclude if this sample was in fact zoned, impure or if the spectrum was flawed prior to being fit.

Figure 5.2: Sample 129b.102

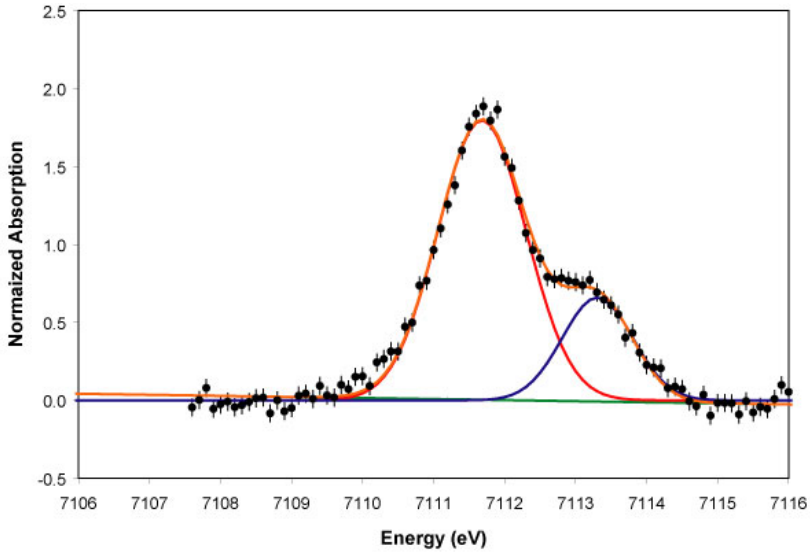

Sample 129b.102 has only two peaks of Fe^{2+} represented

Table 5.2: Fe^{3+} and Fe^{2+} in represented by XANES Spectra

Percentages of Fe^{3+} measured by XANES Spectra	
Sample	**% Fe^{3+}**
alm	0
ak972a	0
ak978a	0
ak9729	0
he1	0
ak9723	0
2b	0
10c	18
129	11
1251	7
9b	10
g17	41
g89	49
bbkg	96
5183g	93
a32w	79
ahun	100
hrm1	100
and	100

Chapter 6

Conclusions

The first part of this study was to measure recoil-free fraction for Fe^{2+} and Fe^{3+} and use those results to measure Fe^{3+} accurately on a suite of 20 garnet samples by Mössbauer spectroscopy. The second part of the study was to use XANES spectroscopy on the same samples, calculate the percentage of Fe^{3+},and compare the percentages of Fe^{2+} and Fe^{3+} represented by both Mössbauer and XANES techniques. Table 6.1 shows the percentages of Fe^{3+} according to Mössbauer and XANES, revealing that results of the two methods agree within ~8%, with the exception of sample 9b. These results are shown graphically in Figure 6.1.

The Mössbauer and XANES percentages of Fe^{3+} were then plotted against one another showing a linear regression with almost a 1:1 ratio between Mössbauer and XANES data. Compared to the 1:1 line, R^2 is 0.973, as shown in Figure 6.1, the graph of the plotted Mössbauer and XANES results. This ratio shows that the Mössbauer and XANES data agree very wellwith the exception of sample 9b, which is the only outlier in the data.

Table 6.1: True Amount of Fe^{3+} for Mössbauer and XANES Peaks

True Amount of Fe^{3+} for Mössbauer and XANES Peaks		
Samples	**Mössbauer True % Area Fe^{3+}**	**XANES % Area Fe^{3+}**
alm	0	0
ak972a	0	0
ak978a	0	0
ak9729	0	0
he1	2	0
ak9723	5	0
2b	5	0
10c	14	18
129	3	11
1251	8	7
9b	46	11
g17	43	41
g89	40	49
bbkg	92	96
5183g	86	93
a32w	76	79
ahun	92	100
hrm1	95	100
and	100	100

The percentages of Fe^{3+} andFe^{2+}were calculated for each XANES spectrum and then averaged together for the table above to be compared against the Mössbauer Fe^{3+} andFe^{2+}peaks.

Figure 6.1: Mössbauer and XANES percentages of Fe^{3+} were then plotted against one another showing a linear regression with almost a 1:1 ratio between Mössbauer and XANES data.

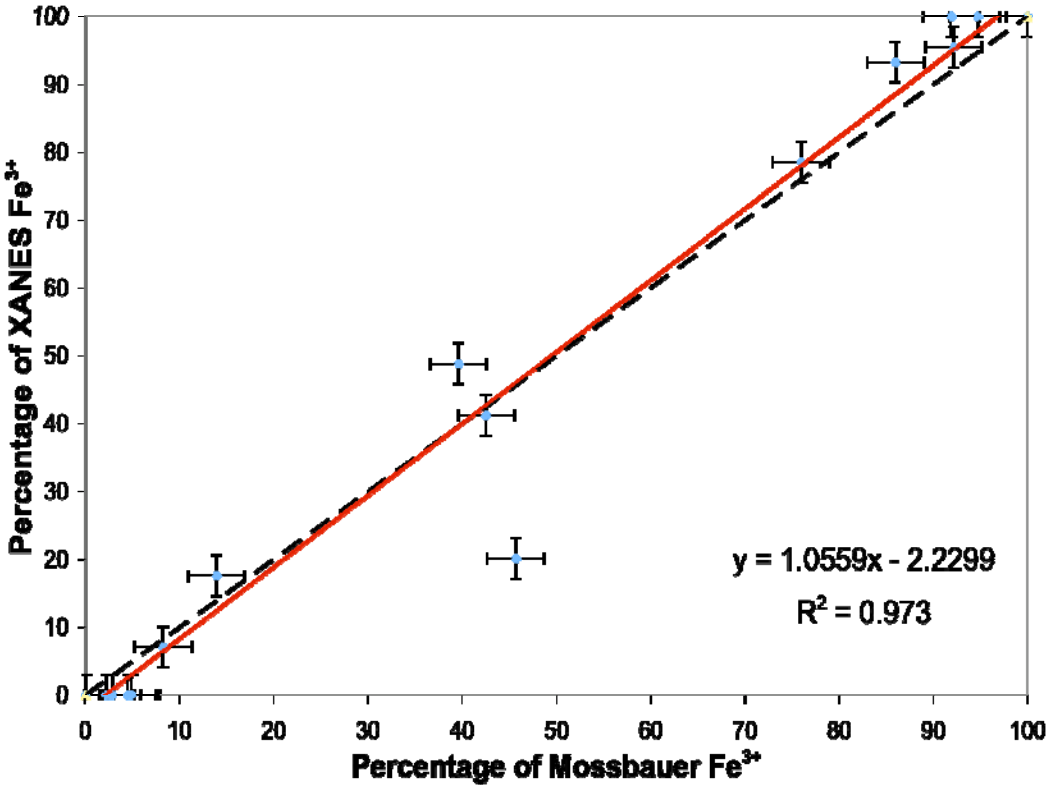

The fact that the Mössbauer and XANES results are approximately 1:1 brings me to my second conclusion that orientation is the only problem faced when measuring XANES data, with the exception of anisotropic minerals in which orientation is not a problem. If there were another problem with the XANES data, that was not orientation based, the results collected would reflect this drawback and would not be able to represent the same amounts of Fe^{3+} as Mössbauer.

Discrepancies in Results

Although the ratio is almost a 1:1 ratio between Mössbauer and XANES data, there were a few problem samples. As stated in Chapter 5, samples bbkg and 9b, have provided difficulty. The samples were studied under the SEM (scanning electron microscope) and reveal the presence of the iron titanium oxide, ilmenite ($FeTiO_3$). The content of Fe^{3+} is affected because Fe^{3+} contents vary as a function of their proximity to nearby oxides, such as ilmenite (Dyar et al.2002).

Both samples, bbkg and 9b, were run under the scanning electron microscope (SEM) in search of zoning which could have caused the discrepancies in the results from these samples. Zoning was not detected in the iron content of these samples. Because the samples were crushed prior to analysis by the SEM, it is possible that the grains analyzed did not contain zoned areas.

It has been concluded that the Kenya melanite, bbkg, contains Fe^{2+} andFe^{3+}. The comparison between the peak energies of XANES data and the

parameters obtained by fitting of the Mössbauer data collected, both reveal parameters for Fe^{2+} andFe^{3+}. In a detailed study by Earle Whipple (1973) it was noted that the melanite sample often had spectra that were more complex than low-titanium garnets because of charge transfer effects. The Fe^{2+} andFe^{3+} can be located next to each other in the garnet structure causing the sharing of electrons. This sharing of electrons results in an overlap of the peaks where an average of the parameters for Fe^{2+}/Fe^{3+} is seen.

In the future, we should take the time to single out samples containing oxides and melanites. Sample 9b could be back to Brookhaven to analyze the zoning in the sample and bbkg could be analyzed to see if XANES spectroscopy could detect the small, high velocity Fe^{2+} peaks that prove to be difficult to analyze.

Sources of Error in XANES Data

As mentioned in Chapter 3, error in XANES data can be a result of the overheating of the monochromator, photon injections at the beam, incorrect orientation of crystals or inconsistent fits of peaks. Pre-edge peak extraction in using X26A Data Plotter resulted in the error of ± 0.03 eV. Pre-edge peaks were extracted 5 times for each spectrum, to prevent any inconsistencies in the fitting of the XANES data. The extracted pre-edges were then corrected according to the energies in Table 3.1. The energy corrected peaks were then fit 5 times each, to detect inconsistencies in the fitting procedure, in PAN: Peak Analysis and resulted

in an error of ± 0.1 eV. The calibration to energy corrected peaks proves to be important and presents results that are more precise than those of the uncorrected extracted pre-edges.

Sources of Error in Mössbauer Data

As mentioned in Chapter 3, inequalities in analysis are common. The error can be a result of inconsistencies in running time, a new radioactive source or fitting software. Lack of constraints on peak parameters can also result in error. A series of tests conducted on the precision of the Mössbauer parameters resulted in the isomer shift, quadrupole splitting and peak width mean probable errors on 4 peaks of 3 different spectra including the Fort Wrangell almandine and Val Malenco andradite are approximately ± 0.02 mm/s (Dyar 1984). Individual peaks are within ± 1.6%. The standard procedure to correct for error is to correct to all samples to an iron foil calibration, to test and correct the radioactive source and use universal fitting programs.

Recoil-free Fraction

As mentioned in Chapter 4, spectra of the garnet standard mix were a acquired over a temperature range from 4-295K in order to develop a correction for the recoil-free fractions, f, as described in Chapter 3. The garnet standard mix was a combination of the Fort Wrangell almandine and Val Malenco andradite to model a garnet with intermediate Fe^{2+}/Fe^{3+} contents. The isomer shifts of the

doublets in these spectra were used to calculate f, for both doublets of the garnet standard mix. The purpose of this calculation was to correct for the area ratios in a mixed mineral spectrum to provide the true percentages of Fe^{2+} and Fe^{3+} in a sample.

These fractions were then calculated to give *C* a value using the equation,

$$C = \frac{f^{3+}}{f^{2+}}.$$

These fractions give a sense of the magnitude of correction factors and the extent to which they are important if "true" valence state and site occupancy information is desired. Table 6.2 shows the correction factors by previous workers using wet chemistry for garnet and my correction factor for Mössbauer spectroscopy. Unlike wet chemistry, the Mössbauer calculation for *C* is the same for each of the garnets in order to analyze a range of garnet compositions. These correction factors help to account for the energy lost due to recoil and provide accurate percentages of Fe^{2+} and Fe^{3+} in a sample.

Table 6.2: Correction Factors Determined by Previous Workers Using Wet Chemistry

Group	Mineral	*C* value	Reference
garnet	grossular	1.26-1.29	Whipple (1968)
	spessartine	1.31	Whipple (1968)
	andradite	1.29	Whipple (1968)
	schorl	> 15.0	Whipple (1968)
	melanite	3.8	Whipple (1968)
	garnet standard mix	1.39	Emerson (2008)

Conclusion

The goal of this study was to measure the oxidation states of garnets using the Mössbauer and XANES techniques. This conclusion suggests that XANES studies of anisotropic minerals might be successful if, as in the case for this study, the optical orientation of the crystals is the same as the optical orientation of the standards.

In conclusion, the Mössbauer spectroscopy and XANES results complement each other. Mössbauer and XANES data measure approximately the same percentage of Fe^{3+} content. These two techniques are useful for determining the iron oxidation state of minerals. The combination of Mössbauer spectroscopy and XANES provides a promising outlook for microanalytical techniques in the near future.

Appendix A: Known Mössbauer Parameters for garnets

Amthauer *et al.*, 1977										
Isomer Shifts δ of ^{57}Fe in 2 schorlomites at different temperatures										
T	Isomer Shift									
	Fe^{2+} (dod)		Fe^{2+} (oct)		Fe^{2+} (tet)		Fe^{3+} (oct)		Fe^{3+} (tet)	
K	Sample (mm/s)		Sample (mm/s)		Sample (mm/s)		Sample (mm/s)		Sample (mm/s)	
	1	2	1	2	1	2	1	2	1	2
295	1.23	1.27	1.10	1.11	0.60	0.59	0.42	0.42	0.17	0.16
240	1.26	1.31	1.14	1.17	0.70	0.70	0.45	0.45	0.20	0.21
180	1.36	1.35	1.21	1.21	0.77	0.76	0.49	0.49	0.23	0.24
140	1.39	1.40	1.23	1.24	0.83	0.81	0.50	0.50	0.25	0.25
100	1.43	1.41	1.27	1.26	0.86	0.86	0.52	0.51	0.27	0.27
77	1.44	1.43	1.28	1.26	0.88	0.88	0.53	0.52	0.28	0.27
55	1.42	1.42	1.25	1.26	0.89	0.90	0.51	0.52	0.27	0.29
30	1.41	1.44	1.23	1.27	0.90	0.93	0.50	0.53	0.26	0.29
20	1.44	1.45	1.26	1.27	0.93	0.93	0.53	0.53	0.28	0.29
17.5	1.44	--	1.26	--	0.92	--	0.53	--	0.28	--
15	1.45	--	1.27	--	0.91	--	0.53	--	0.29	--

Amthauer *et al.*, 1977										
Nuclear quadrupole splittings Δ of ^{57}Fe in 2 schorlomites at different temperatures										
	1	2	1	2	1	2	1	2	1	2
295	3.30	3.40	3.05	3.08	2.04	2.05	0.69	0.70	1.19	1.20
240	3.31	3.40	3.08	3.12	2.19	2.19	0.70	0.70	1.20	1.19
180	3.44	3.43	3.16	3.13	2.16	2.25	0.69	0.70	1.19	1.20
140	3.47	3.49	3.15	3.16	2.34	2.31	0.70	0.70	1.20	1.20
100	3.50	3.48	3.18	3.19	2.37	2.38	0.69	0.71	1.19	1.20
77	3.51	3.49	3.19	3.16	2.40	2.40	0.60	0.70	1.18	1.19
55	3.48	3.49	3.14	3.15	2.42	2.44	0.68	0.71	1.18	1.20
30	3.47	3.50	3.11	3.15	2.46	2.47	0.68	0.70	1.17	1.18
20	3.48	3.50	3.11	3.14	2.44	2.47	0.67	0.69	1.16	1.18
17.5	3.47	--	3.12	--	2.43	--	0.67	--	1.16	--
15	3.46	--	3.12	--	2.44	--	0.68	--	1.15	--

$\Delta = ½\ eQVtt\ (1 + n^{2/3)½}$

-- = not determined

Barcova *et al.,* 2002					
Results of the Mössbauer spectra fitting of Barton HP 80 U.S. sample					
Barton (all temperatures)					
Fe^{2+}	IS (mm/s)	1.53-1.54	Fe^{3+}	IS (mm/s)	0.38-0.46
	QS (mm/s)	3.52-3.54		QS (mm/s)	0.58-0.66
	FW (mm/s)	0.33-0.38		FW (mm/s)	0.66-0.83
	A (%)	89.4-95.2		A (%)	7.2-10.6

Barcova, *et al.,* 2001				
Hyperfine parameters of iron (III) oxides isolated from sample heated at 750°C for 4 hours				
	IS (mm/s)	QS (mm/s)	B (T)	A (%)
γ-Fe2O3 nanoparticles	0.36±0.02	0.92±0.02	--	73.4±0.5
ε-Fe2O3	0.37±0.02	-0.21±0.02	51.6±0.2	10.2±0.5
ε-Fe2O3 octahedral sites Fe1 and Fe2	0.38±0.02	-0.12±0.02	44.6±0.2	7.2±0.5
ε- Fe2O3 octahedral sites Fe3	0.39±0.02	-0.03±0.02	39.5±0.2	4.8±0.5
ε-Fe2O3 tetrahedral sites Fe4	0.23±0.02	-0.09±0.02	26.6±0.2	4.4±0.5

IS – Isomer Shift, QS – Quadrupole Splitting, B – Hyperfine Magnetic Field,
A – Percentage of Subspectrum Area

Belozerskii *et al.,*1969							
Mössbauer parameters of hyperfine interaction and relative bonding forces between the *a* and *d* sublattices of the garnets							
Orientation of YIG sample	Temp. K	Δ (mm/s)	Ha kGauss	Hd kGauss	Sa/Sd	εa (mm/s)	εd (mm/s)
	300	0.232±10	488±2	396±15	0.665±15	-0.14±6	-0.14±6
211	300	0.222±10	490±2	396±1.5	0.81±12	-0.16±6	-0.00±6
111	300	0.225±10	485±2	396±1.5	0.77±12	-0.12±10	-0.02±10
	80	0.240±10	555±2	474±2	0.68±4	-0.14±8	-0.02±6

Δ relative chemical shift (isomer)
ε energy of the quadrupole (quadrupole splitting)
H effective magnetic field

S area under the first and sixth lines of the NGR spectra of "a" and "d" sublattices

Belozerskii *et al.,* 1969		
Mössbauer effect in indium-gallium iron garnet		
	Temperature, °K	
	80	300
H eff, kG	541 ±3	471 ±3
H eff, kG	463 ±3	385.5 ±3.5
Δ a-d, (mm/s)	0.22 ±0.02	0.260 ±0.020
(eqQ)a, (mm/s)	-0.15 ±0.02	0.06 ±0.03
(eqQ)d, (mm/s)	-0.07 ±0.02	-0.020 ±0.020

Berry, *et al.,* 1996

^{57}Fe Mössbauer parameters obtained by fitting the spectra recorded at 298 K from compounds of composition YCa2SbFe4- GaO12 (= - 3) to one *d* and one a doublet

	Site	δ (mm/s^{-1})	Δ (mm/s^{-1})	Γ (mm/s^{-1})	Area (%)	A_{oct}/A_{tet}	x^2
$YCa_2SbFe_4O_{12}$	d	0.18(4)	1.24(2)	0.38(2)	79		
	a	0.38(4)	0.39(3)	0.30(4)	21		
						0.27	6
$YCa_2SbGaFe_3O_{12}$	d	0.18(4)	1.26(2)	0.38(2)	70		
	a	0.38(4)	0.38(3)	0.30(4)	30		
						0.43	4.7
$YCa_2SbGaFe_2O_{12}$	d	0.19(4)	1.28(2)	0.37(2)	59		
	a	0.38(4)	0.35(3)	0.32(4)	41		
						0.70	1.8
$YCa_2SbGa_3FeO_{12}$	d	0.20(4)	1.28(2)	0.39(2)	49		
	a	0.38(4)	0.32(3)	0.35(4)	51		
						1.02	1.3

Berry *et al.,* 1996

^{57}Fe Mössbauer parameters obtained by fitting the spectra recorded at 298 K from compounds of composition YCa2SbFe4- GaO12 (= - 3) to two *d* doublets and one a doublet

	Site	δ (mm/s^{-1})	Δ (mm/s^{-1})	Γ (mm/s^{-1})	Area (%)	A_{oct}/A_{tet}	x^2
$YCa_2SbFe_4O_{12}$	d	0.18(4)	1.24(2)	0.38(2)	79		
	a	0.38(4)	0.39(3)	0.30(4)	21		
						0.27	6
$YCa_2SbGaFe_3O_{12}$	d	0.18(4)	1.26(2)	0.38(2)	70		
	a	0.38(4)	0.38(3)	0.30(4)	30		
						0.43	4.7
$YCa_2SbGaFe_2O_{12}$	d	0.19(4)	1.28(2)	0.37(2)	59		

	a	0.38(4)	0.35(3)	0.32(4)	41		
						0.70	1.8
$YCa_2SbGa_3FeO_{12}$	d	0.20(4)	1.28(2)	0.39(2)	49		
	a	0.38(4)	0.32(3)	0.35(4)	51		
						1.02	1.3

Berry *et al.*, 1996							
^{57}Fe Mössbauer parameters obtained by fitting the spectra recorded at 298 K from compounds of composition YCa2SbFe4- GaO12 (= - 3) to two *d* doublets and one a doublet							
	Site	δ (mm/s^{-1})	Δ (mm/s^{-1})	Γ (mm/s^{-1})	Area (%)	A_{oct}/A_{tet}	x^2
$YCa_2SbFe_4O_{12}$	d1	0.17(3)	1.15(2)	0.32(3)	54		
	d11	0.18(3)	1.46(2)	0.28(2)	22		
						0.32	4.5
	a	0.37(3)	0.38(3)	0.30(2)	24		
$YCa_2SbGaFe_3O_{12}$	d1	0.18(3)	1.13(2)	0.29(3)	35		
	d11	0.19(3)	1.43(2)	0.30(2)	31		
						0.53	2.3
	a	0.37(3)	0.37(3)	0.32(2)	34		
$YCa_2SbGaFe_2O_{12}$	d1	0.19(3)	1.15(2)	0.30(2)	33		
	d11	0.18(3)	1.45(2)	0.28(2)	23		
						0.79	1.3
	a	0.37(3)	0.35(3)	0.33(4)	44		
$YCa_2SbGa_3FeO_{12}$	d1	0.18(3)	1.14(2)	0.37(2)	29		
	d11	0.20(3)	1.42(2)	0.28(2)	19		
						1.08	1.1
	a	0.37(3)	0.31(3)	0.36(4)	52		

Berry *et al.*, 1996								
^{57}Fe Mössbauer parameters obtained by fitting the data recorded from the compounds of composition YCa_2SbFe_4- GaO_{12} (= - 3), Y_3-$_2Ca_2SbFe_5$- O_{12} (= - 1.25, 1.5), Y_3- Ca $SnFe_{55}$-O_{12} (=12) and $NaCa_2Sb_2FeGa_2O_{12}$ to a distribution of quadrupole split absorptions for the tetrahedral (*d*) sites								
Sample	δ^a (mm/s^{-1})	Δ^a (mm/s^{-1})	Γ^a (mm/s^{-1})	Area (%)	δ^d (mm/s^{-1})	Δ^d (mm/s^{-1})	Area ^{d} (%)	x^2
$YCa_2SbFe_4O_{12}$	0.37	0.38	0.29	24	0.18	1.24	76	3.2
$YCa_2SbGaFe_3O_{12}$	0.37	0.37	0.30	33	0.18	1.26	67	2.8
$YCa_2SbGaFe_2O_{12}$	0.37	0.35	0.32	43	0.18	1.26	57	1.4
$YCa_2SbGa_3FeO_{12}$	0.37	0.31	0.35	52	0.18	1.25	48	0.9

$Y_{0.5}Ca_{2.5}Sb_{1.25}Fe_{3.75}O_{12}$	0.37	0.31	0.30	30	0.18	1.21	80	1.4
$Ca_{2\backslash 3}Sb_{1.5}Fe_{3.5}O_{12}$	0.38	0.24	0.29	16	0.19	1.16	84	2.7
$Y_2CaSnFe_4O_{12}$	0.38	0.43	0.24	19	0.17	1.09	81	2.5
$YCa_2Sn_2Fe_3O_{12}$	--	--	--	--	0.17	1.01	100	2.0
$NaCa_2FeGa_2O_{12}$	--	--	--	--	0.18	0.84	100	0.8

Berry *et al.*, 1996

Lattice and Mössbauer parameters of some iron-containing garnets at room temperature

Garnet	*a* (Å)	δ^a (mm/s^{-1})	Δ^a (mm/s^{-1})	δ^d (mm/s^{-1})	Δ^d (mm/s^{-1})	Ref.
$Y_3Fe_5O_{12}$	12.386	0.38	0.47	0.16	0.97	[15]
$Sm_3Fe_5O_{12}$		0.41	0.34	0.16	0.83	[16]
$Gd_3Fe_5O_{12}$		0.42	0.38	0.16	0.89	[16]
$Dy_3\ Fe_5O_{12}$		0.38	0.49	0.16	0.90	[16]
$Yb_3\ Fe_5O_{12}$		0.40	0.50	0.15	0.99	[16]
$Lu_3\ Fe_5O_{12}$		0.39	0.57	0.20	0.95	[16]
$Tb_3Fe_5O_{12}$		0.36	0.37	0.15	0.87	[17]
$Y_3Fe_3Ga_2O_{12}$	12.347	0.37	0.37	0.15	0.87	[8]
$Y_3Fe_{2.2}Ga_{2.8}O_{12}$	12.327	0.39	0.39	0.12	0.93	[18]
$Y_3FeGa_4O_{12}$	12.308	0.37	0.32	0.15	1.01	[8]
$Y_3Fe_3Al_2O_{12}$	12.245	0.41	0.42	0.13	0.97	[7]
$Y_3Fe_2Al_3O_{12}$	12.176	0.41	0.38	0.12	0.99	[7]
$Y_3FeAl_4O_{12}$	12.091	0.42	0.33	0.09	0.97	[7]
$Y_3FeGaAl_3O_{12}$		0.39	0.38	0.10	0.95	[18]
$Ca_3Fe_2Ti_{1.42}Si_{1.58}O_{12}$		0.40	0.75	0.20	1.15	[19]
$Y_{2.5}Ca_{0.5}Sn_{1.5}Fe_{3.5}O_{12}$		0.42	0.48	0.14	0.99	[20]
$Y_2CaSnFe_4O_{12}$		0.42	0.52	0.14	1.06	[20]
$Y_{1.5}Ca_{0.5}Sn_{1.5}Fe_{3.5}O_{12}$		0.44	0.49	0.15	1.04	[20]
$YCa2_2Sn_2Fe_3O_{12}$				0.16	1.02	[20]
$GdCa_2Sn_2Fe_2O_{12}$	12.666			0.17	0.97	[21]
$Ca_3Zr_2Fe_2SiO_{12}$	12.610			0.18	1.04	[15]
$YCa_2Zr_2Fe_2AlO_{12}$	12.618			0.17	1.09	[15, 18]
$Ca_3ZrSbFe_3O_{12}$	12.669			0.23	0.99	[3]
$Ca_3SnSbFe_3O_{12}$	12.634			0.22	0.96	[3]
$NaCa_2Sb_2Fe_3O_{12}$	12.600			0.22	0.51	[3]
$Na_3Te_2Fe_3O_{12}$	12.524			0.23	0.51	[15]

$Ca_3Fe_2Ge_3O_{12}$	12.320	0.39	0.35			[22]
$Ca_3FeAlGe_3O_{12}$	12.205		0.31			[22]
$Ca_3FeInGe_3O_{12}$	12.475		0.45			[22]
$CdFe_2Ge_3O_{12}$	12.263	0.38	0.26			[22]
$Ca_3Fe_2Si_3O_{12}$	12.070	0.41	0.59			[23]
$Mn_3Fe_2Si_3O_{12}$	11.821	0.39	0.34			[23]
$Cd_3Fe_2Si_3O_{12}$		0.38	0.57			[23]

Note. δ values are referred to metallic iron. Superscript *a* refers to octahedral sites. Superscript *d* refers to tetrahedral sites.

Berry *et al.,* 1996

^{57}Fe Mössbauer parameters obtained from the spectra recorded at 18 K from compounds of composition YCa_2SbFe_4- GaO_{12}

	Site	δ (mm/s^{-1})	Δ (mm/s^{-1})	Γ (mm/s^{-1})	H (kG)	Area (%)
$YCa_2SbFe_4O_{12}$	d1	0.31(2)	-0.17(1)	0.56(3)	392	6.5
	d2	0.31(2)	-0.09(2)	0.56(3)	417	18
	d3	0.31(2)	0.04(2)	0.56(3)	437	30
	d4	0.31(2)	-0.03(2)	0.56(3)	456	18
	d5	0.31(2)	-0.03(2)	0.56(3)	465	6.5
	a	0.31(3)	-0.05(1)	0.49(3)	514	21
$YCa_2SbGaFe_3O_{12}$	d1	0.31(2)	0.04(1)	0.71(3)	365	8
	d2	0.31(2)	-0.01(2)	0.71(3)	395	17
	d3	0.31(2)	0.00(2)	0.71(3)	417	26
	d4	0.31(2)	-0.04(2)	0.71(3)	438	20
	d5	0.31(2)	-0.04(2)	0.71(3)	448	8
	a	0.53(3)	0.02(1)	0.68(3)	484	21
$YCa_2SbGa_2Fe_2O_{12}$	d1	0.24(5)	1.15(3)	0.49(2)		38
	d11	0.24(5)	1.41(3)	0.49(2)		30
	a	0.43(5)	0.32(3)	0.40(2)		32
$YCa_2SbGa_3FeO_{12}$	d1	0.29(5)	1.11(3)	0.30(2)		25
	d11	0.31(5)	1.39(3)	0.30(2)		22
	a	0.43(5)	0.32(3)	0.35(2)		53

Note. Δ is quadrupole shift.

Berry *et al.,* 1996

^{57}Fe Mössbauer parameters obtained from the spectra recorded at 18 K from compounds of composition $Y_{3-}{}_2Ca_2SbFe_5$- O_{12} (= 1.25, 1.5)

	Site	δ (mm/s^{-1})	Δ (mm/s^{-1})	Γ (mm/s^{-1})	H (kG)	Area (%)
$Y_{0.5}Ca_{2.5}Sb_{1.25}Fe_{3.75}O_{12}$	d1	0.29(2)	-0.10(1)	0.73(3)	334	4
	d2	0.29(2)	-0.04(2)	0.73(3)	381	10
	d3	0.29(2)	-0.03(2)	0.73(3)	413	23
	d4	0.29(2)	0.07(2)	0.73(3)	438	28

	d5	0.29(2)	-0.02(2)	0.73(3)	460	22
	a	0.51(3)	-0.01(1)	0.57(3)	518	13
$Ca_3Sb_{1.5}Fe_{3.5}O_{12}$	d1	0.28(2)	0.06(1)	0.85(3)	261	8
	d2	0.28(2)	0.06(2)	0.85(3)	304	16
	d3	0.28(2)	-0.03(2)	0.85(3)	346	22
	d4	0.28(2)	0.06(2)	0.85(3)	380	30
	d5	0.28(2)	0.06(2)	0.85(3)	408	16
	a	0.44(3)	-0.12(1)	0.75(3)	439	6
	a	0.44(2)	0.24(2)	0.32(3)		2

Berry *et al.,* 1996

^{57}Fe Mössbauer parameters obtained from the spectra recorded at 18 K from compounds of composition $Y_{3-2}CaSnFe_5- O_{12}$ (= 1,2)

	Site	δ (mm/s^{-1})	Δ (mm/s^{-1})	Γ (mm/s^{-1})	H (kG)	Area (%)
$Y_2CaSnFe_4O_{12}$	d1	0.27(2)	0.03(1)	0.56(3)	408	6
	d2	0.27(2)	-0.06(1)	0.56(3)	427	20
	d3	0.27(2)	0.08(2)	0.56(3)	446	28
	d4	0.27(2)	-0.03(2)	0.56(3)	465	20
	d5	0.27(2)	-0.03(2)	0.56(3)	485	6
	a	0.52(3)	-0.02(1)	0.57(3)	522	20
$YCa_2Sn_2Fe_3O_{12}$	d1	0.27(3)	-0.40(2)	0.49(3)	364	13
	d2	0.27(3)	-0.44(5)	0.34(3)	392	31
	d3	0.27(3)	-0.40(2)	0.45(3)	411	45
	d4	0.25(3)	1.06(2)	0.46(3)		11

Geiger *et al.,* 1992

Hyperfine parameters of Fe^{2+} in almandine

T (K)	chi^2	IS (mm/s)	QS (mm/s)	HW L (mm/s)	HW H (mm/s)	AS	Ae (%)	Ah (%)	Ae/Ah
420	0.78	1.20	3.36	0.26	0.24	8.0	51.36	48.64	1.056
295	0.64	1.28	3.50	0.26	0.24	8.0	50.93	49.07	1.038
80	0.55	1.42	3.65	0.26	0.25	4.0	50.48	49.52	1.019
15	0.73	1.43	3.65	0.36	0.36	0.0	50.08	49.92	1.003

HW L = half-width of the low velocity line (± 0.01 mm/s)
HW H = half-width of high velocity line (± 0.01 mm/s)
AS = asymmetry
Ae = resonant absorption area of the low velocity line (± 0.5%) referred to the total resonant absorption area = 100%
Ah = resonant absorption area of the high velocity line (±0.5%) referred to the total resonant absorption = 100%

Geiger *et al.*, 2003								
Mössbauer parameters 298 K								
Sample	δ	ΔEq	HW[a] l	HW[a] h	DAS[b]	A[c] l	A[c] H	(A l/A h)
$Alm_{93}Pyr_{07}$	1.27	3.52	0.278	0.254	4.5	51.1	48.9	1.045
$Alm_{85}Pyr_{15}$	1.27	3.53	0.278	0.254	4.5	51.3	48.7	1.053
$Alm_{60}Pyr_{40}$	1.27	3.54	0.276	0.242	6.5	51.2	48.8	1.049
$Alm_{50}Pyr_{50}$	1.27	3.55	0.280	0.232	9.4	51.4	48.6	1.058
$Alm_{38}Pyr_{62}$	1.27	3.57	0.308	0.264	7.7	51.7	48.3	1.070
$Alm_{20}Pyr_{90}$	1.26	3.57	0.284	0.236	9.2	51.3	48.7	1.053
$Alm_{87}Spe_{13}$	1.27	3.53	0.256	0.230	5.3	51.2	48.8	1.049
$Alm_{75}Spe_{25}$	1.27	3.54	0.256	0.232	4.9	50.8	49.2	1.032
$Alm_{50}Spe_{50}$	1.28	3.55	0.266	0.234	6.4	51.6	48.4	1.040
$Alm_{25}Spe_{75}$	1.27	3.56	0.280	0.246	6.5	49.8	50.2	1.006
$Alm_{09}Spe_{91}$	1.27	3.56	0.302	0.240	11.4	51.3	48.7	1.053
Alm_{100}	1.28	3.50	0.236	0.236	5.2	50.9	49.1	1.038
$Alm_{90}Gro_{10}$	1.28	3.50	0.238	0.238	4.4	50.8	49.2	1.034
$Alm_{50}Gro_{50}$	1.27	3.53	0.236	0.236	6.9	51.6	48.4	1.068
$Alm_{10}Gro_{90}$	1.26	3.55	0.220	0.220	4.8	52.3	47.7	1.095

Geiger *et al.*, 2003								
Mössbauer parameters 77 K								
Sample	δ	ΔEq	HW[a] l	HW[a] h	DAS[b]	A[c] l	A[c] H	(A l/A h)
$Alm_{93}Pyr_{07}$	1.42	3.71	0.304	0.286	6.1	51.14	48.86	1.046
$Alm_{85}Pyr_{15}$	1.42	3.71	0.300	0.276	8.3	51.44	48.56	1.059
$Alm_{60}Pyr_{40}$	1.41	3.69	0.292	0.272	7,1	50.80	49.20	1.033
$Alm_{50}Pyr_{50}$	1.41	3.69	0.280	0.254	9.7	51.00	49.00	1.041
$Alm_{38}Pyr_{62}$	1.41	3.68	0.316	0.270	15.7	51.85	48.15	1.077
$Alm_{20}Pyr_{90}$	1.40	3.68	0.290	0.260	10.9	50.47	49.53	1.019
$Alm_{87}Spe_{13}$	1.41	3.66	0.280	0.258	8.2	51.62	48.38	1.067
$Alm_{75}Spe_{25}$	1.40	3.65	0.404	0.380	6.1	51.99	48.01	1.083
$Alm_{50}Spe_{50}$	1.40	3.64	0.294	0.264	10.8	51.90	48.10	1.079
$Alm_{25}Spe_{75}$	1.40	3.64	0.348	0.304	13.5	52.29	47.71	1.096
$Alm_{09}Spe_{91}$	1.40	3.63	0.314	0.262	22.2	51.53	48.47	1.063
Alm_{100}	1.42	3.65	0.260	0.248	4.7	50.48	49.52	1.019
$Alm_{90}Gro_{10}$	1.42	3.65	0.260	0.248	4.7	50.45	49.55	1.018

$Alm_{50}Gro_{50}$	1.41	3.64	0.264	0.244	7.9	50.76	49.24	1.031
$Alm_{10}Gro_{90}$	1.40	3.63	0.250	0.242	3.3	50.27	49.73	1.011

Luth *et al.*, 1990

^{57}Fe Mössbauer data for garnet samples at 298 K

Sample	Fe^{2+}						
	A (LV)	A (HV)	LW (LV)	LW (HV)	IS	QS	I(HV)/ I(LV)
9883	0.471	0.461	0.284	0.255	1.269	3.516	1.092
HRV 247A	0.503	0.472	0.313	0.270	1.271	3.512	1.085
FRB 838	0.476	0.451	0.336	0.272	1.273	3.519	1.171
FRB135	0.477	0.450	0.333	0.266	1.288	3.559	1.184
PHN 1917	0.478	0.456	0.338	0.262	1.288	3.559	1.232
FRB 131	0.460	0.449	0.326	0.261	1.274	3.521	1.221
FRB 1033	0.447	0.429	0.324	0.257	1.295	3.566	1.205
PHN 1611	0.437	0.421	0.320	0.268	1.285	3.544	1.151
PHN 5549	0.481	0.452	0.331	0.268	1.288	3.558	1.162
PHN 1925	0.444	0.425	0.325	0.264	1.287	3.550	1.179
PHN 5267	0.433	0.411	0.329	0.261	1.284	3.555	1.198
PHN 1503C	0.435	0.421	0.303	0.260	1.285	2.546	1.127
BD 2501	0.447	0.428	0.333	0.265	1.276	3.530	1.205
FRB 76	0.440	0.427	0.324	0.266	1.275	3.504	1.184
FRB 140	0.447	0.428	0.321	0.265	1.273	3.513	1.163
PHN 5635B	0.481	0.463	0.302	0.271	1.272	3.522	1.075
PHN 2654	0.482	0.463	0.345	0.276	1.275	3.525	1.204
PHN 2825	0.485	0.458	0.370	0.281	1.275	3.527	1.243
PHN 2635	0.474	0.454	0.293	0.264	1.301	3.613	1.063
PHN 1643E	0.489	0.474	0.313	0.264	1.309	3.625	1.148
PHN 1543U	0.491	0.466	0.328	0.261	1.306	3.617	1.191
Mo4500-24	0.499	0.473	0.318	0.269	1.303	3.605	1.119
Vi313-3	0.486	0.471	0.302	0.250	1.291	3.576	1.170
Vi313-4	0.493	0.472	0.303	0.253	1.295	3.579	1.150
Vi313-5	0.488	0.471	0.300	0.248	1.291	3.578	1.167
Vi313-6	0.498	0.462	0.303	0.243	1.289	3.571	1.158
Vi313-8	0.482	0.466	0.300	0.246	1.290	3.570	1.182
Vi313-54	0.484	0.469	0.302	0.244	1.286	3.559	1.199

A(LV) =Area of low velocity Fe^{2+} peak (% of total absorbance)
A(HV) =Area of high velocity Fe^{2+} peak (% of total absorbance)
LW(LV) = Full width at half height of low velocity Fe^{2+} peak (mm/s)
LW(HV) = Full width at half height of high velocity Fe^{2+} peak (mm/s)
IS = Isomer shift (mm/s) with reference to Fe metal at 198 K
QS = Quadrupole splitting (mm/s)

I(HV)/(LV) = (Intensity of high velocity Fe^{2+} peak)/(Intensity of low velocity Fe^{2+} peak)
LW = Full width at half height of both Fe^{3+} peaks (mm/s)
A = Area (Fe^{3+})/(Area(Fe^{2+})+Area(Fe^{3+}))
M = MISFIT (Ruby 1973)
ΔM = Uncertainty of MISFIT (Ruby 1973)
Yo = Off-resonance (baseline) counts

Luth *et al.*, 1990								
^{57}Fe Mössbauer data for garnet samples at 298 K								
Sample	Fe^{3+}			A	x^2	M $x10^2$	ΔM $x10^2$	Yo $x10^{-6}$
	LW	IS	QS					
9883	0.490	0.299	0.364	0.068	253	2.77	1.33	1.02
HRV 247A	0.309	0.407	0.213	0.025	330	4.68	1.44	1.22
FRB 838	0.482	0.286	0.274	0.074	280	5.38	1.54	0.94
FRB135	0.462	0.321	0.279	0.073	279	2.30	1.65	1.25
PHN 1917	0.369	0.288	0.310	0.066	284	5.65	3.50	0.93
FRB 131	0.560	0.350	0.261	0.091	303	4.56	1.93	1.83
FRB 1033	0.329	0.342	0.272	0.124	329	7.07	2.20	2.87
PHN 1611	0.410	0.341	0.258	0.142	285	4.45	1.10	1.29
PHN 5549	0.410	0.353	0.265	0.067	255	2.84	0.99	1.10
PHN 1925	0.415	0.343	0.251	0.131	296	4.41	2.14	1.14
PHN 5267	0.382	0.333	0.272	0.156	286	3.25	1.48	0.92
PHN 1503C	0.350	0.344	0.280	0.144	333	6.74	1.81	0.96
BD 2501	0.336	0.337	0.281	0.125	283	1.82	1.20	1.38
FRB 76	0.289	0.330	0.281	0.134	243	4.36	1.20	1.37
FRB 140	0.438	0.312	0.272	0.125	332	5.70	1.72	1.11
PHN 5635B	0.516	0.335	0.249	0.056	350	5.01	1.20	1.53
PHN 2654	0.363	0.329	0.250	0.056	263	1.87	1.52	1.88
PHN 2825	0.395	0.238	0.250	0.057	246	4.60	3.32	1.77
PHN 2635	0.495	0.373	0.344	0.072	364	4.27	1.02	1.66
PHN 1643E	0.361	0.339	0.150	0.037	315	5.79	2.10	1.15
PHN 1543U	0.328	0.316	0.250	0.043	296	4.59	2.22	1.48
Mo4500-24	0.318	0.358	0.250	0.029	300	2.38	0.76	1.21
Vi313-3	0.447	0.384	0.335	0.043	248	2.49	2.70	1.05
Vi313-4	0.363	0.370	0.232	0.036	537	8.27	1.07	5.02
Vi313-5	0.402	0.332	0.196	0.041	249	2.49	2.99	1.01
Vi313-6	0.303	0.335	0.250	0.040	259	7.92	4.26	0.99
Vi313-8	0.430	0.338	0.337	0.052	251	3.90	3.33	1.09
Vi313-54	0.325	0.349	0.250	0.047	302	16.45	6.00	1.09

Luth *et al.*, 1990							
^{57}Fe Mössbauer data for garnet at 77 K							
Sample	Fe^{2+}						
	A (LV)	A (HV)	LW (LV)	LW (HV)	IS	QS	I(HV)/I(LV)
9883	0.500	0.477	0.393	0.357	1.439	3.693	1.052
HRV 247A	0.510	0.476	0.411	0.369	1.447	3.713	1.040
FRB 838	0.501	0.466	0.448	0.376	1.448	3.716	1.107
FRB135	0.481	0.463	0.454	0.374	1.427	3.663	1.172
PHN 1917	0.486	0.466	0.481	0.401	1.444	3.710	1.152
FRB 131	0.484	0.463	0.450	0.368	1.438	3.690	1.168
FRB 1033	0.450	0.435	0.380	0.310	1.422	3.638	1.185
PHN 1611	0.469	0.438	0.598	0.520	1.435	3.661	1.074
PHN 5549	0.487	0.459	0.440	0.366	1.442	3.714	1.132
PHN 1925	0.456	0.440	0.470	0.400	1.442	3.698	1.133
PHN 5267	0.449	0.430	0.445	0.369	1.442	3.703	1.155
PHN 1503C	0.453	0.425	0.403	0.357	1.443	3.701	1.062
BD 2501	0.462	0.443	0.505	0.421	1.439	3.693	1.150
FRB 76	0.465	0.437	0.547	0.466	1.445	3.693	1.105
FRB 140	0.477	0.444	0.533	0.459	1.433	3.664	1.081
PHN 5635B	0.501	0.476	0.304	0.270	1.409	3.614	1.070
PHN 5635	0.511	0.475	0.546	0.500	1.422	3.641	1.016
Mo4500-24	0.507	0.477	0.406	0.359	1.441	3.708	1.068
Vi313-3	0.512	0.482	0.658	0.586	1.415	3.618	1.057
Vi313-4	0.494	0.478	0.357	0.310	1.427	3.669	1.117
Vi313-5	0.496	0.481	0.477	0.418	1.416	3.640	1.107
Vi313-6	0.501	0.484	0.565	0.497	1.415	3.627	1.099
Vi313-8	0.502	0.478	0.536	0.467	1.416	3.636	1.094

Luth *et al.*, 1990								
^{57}Fe Mössbauer data for garnet samples at 77 K								
	Fe^{3+}							
Sample	LW	IS	QS	A	x^2	M $x10^2$	ΔM $x10^2$	Yo $x10^{-6}$
9883	0.393	0.602	0.337	0.024	454	9.62	1.56	1.33
HRV 247A	0.411	0.598	0.255	0.015	643	16.58	1.81	1.24
FRB 838	0.376	0.503	0.250	0.033	392	7.86	1.61	1.24

FRB135	0.545	0.476	0.255	0.057	439	13.97	2.37	1.14
PHN 1917	0.481	0.455	0.255	0.048	474	21.55	3.29	1.19
FRB 131	0.450	0.443	0.255	0.054	300	10.17	4.58	1.55
FRB 1033	0.414	0.448	0.284	0.116	392	13.30	2.72	1.46
PHN 1611	0.514	0.493	0.216	0.094	614	39.26	4.49	1.28
PHN 5549	0.478	0.481	0.238	0.054	478	10.72	1.62	1.06
PHN 1925	0.471	0.455	0.242	0.105	512	15.11	2.10	1.40
PHN 5267	0.431	0.462	0.284	0.121	329	6.30	1.93	1.07
PHN 1503C	0.421	0.467	0.253	0.122	794	15.24	1.38	1.40
BD 2501	0.410	0.477	0.272	0.095	508	16.49	2.29	1.12
FRB 76	0.507	0.479	0.211	0.098	601	19.01	2.22	1.08
FRB 140	0.437	0.473	0.281	0.079	499	20.29	2.89	1.09
PHN 5635B	0.310	0.391	0.255	0.023	361	5.86	1.42	1.43
PHN 5635	0.500	0.459	0.255	0.014	795	56.86	5.18	1.09
Mo4500-24	0.359	0.493	0.255	0.016	592	11.11	1.32	1.16
Vi313-3	0.586	0.516	0.260	0.005	514	35.41	4.89	1.08
Vi313-4	0.439	0.507	0.255	0.028	418	9.86	1.81	1.37
Vi313-5	0.418	0.455	0.260	0.023	404	20.32	3.95	1.05
Vi313-6	0.497	0.583	0.260	0.015	433	33.66	5.84	1.03
Vi313-8	0.467	0.569	0.260	0.020	527	32.30	4.34	1.40

Woodland, A.B. and O'Neill, H.S.C. 1993

Hyperfine parameters and Fe^{3+}/Fe_{tot} ratios for almandine-skiagite garnet

	Fe^{2+}		FWHM	Fe^{3+}		FWHM		Fe^{3+}/Fe_{tot}
Sample	QS	IS	(mm/s)	QS	IS	(mm/s)	x^2	area ratio
aw18(ski02)	3.52	1.29	0.25	0.25	0.32	0.46	1.52	0.045
aw14(ski03)	3.51	1.30	0.25	0.22	0.31	0.36	1.19	0.030
aw5(ski07)	3.54	1.30	0.24	0.18	0.34	0.34	1.42	0.072
aw25(ski08)	3.51	1.30	0.25	0.21	0.33	0.29	1.41	0.074
aw26(ski08)	3.54	1.30	0.27	0.21	0.34	0.32	1.54	0.061
aw30(ski09)	3.53	1.30	0.25	0.22	0.35	0.30	1.13	0.077
aw37(ski15)	3.52	1.30	0.25	0.21	0.34	0.29	1.05	0.141
aw37(ski21)	3.51	1.30	0.25	0.23	0.35	0.25	1.17	0.156
aw47(ski30)	3.50	1.30	0.24	0.23	0.33	0.29	1.99	0.218
uhp458(ski31)	3.51	1.29	0.28	0.23	0.35	0.28	2.04	0.191
uhp541(ski42)	3.52	1.30	0.25	0.25	0.34	0.28	1.34	0.271
Uhp627(ski50)	3.48	1.30	0.29	0.24	0.35	0.30	1.25	0.299
uhp487(ski79)	3.47	1.29	0.23	0.25	0.35	0.24	1.26	0.404
uhp598(ski90)	3.50	1.30	0.24	0.24	0.36	0.25	1.24	0.429
uhp636(ski100)	3.46	1.31	0.23	0.24	0.35	0.26	2.11	0.459

uhp702(ski100)	3.46	1.31	0.23	0.24	0.36	0.25	1.88	0.462

Note: measurements made at 298 K and 1 atm.

*Millimeters per second measured relative to α Fe metal at 298 K. Uncertainties are about ±0.01 mm/s for both QS and IS and ±0.01 for Fe^{3+}/Fe_{tot}. The area ratio assumes the same recoil-free fraction for Fe^{2+} and Fe^{3+} on the different sites.

Appendix B: Mössbauer Spectra

alm

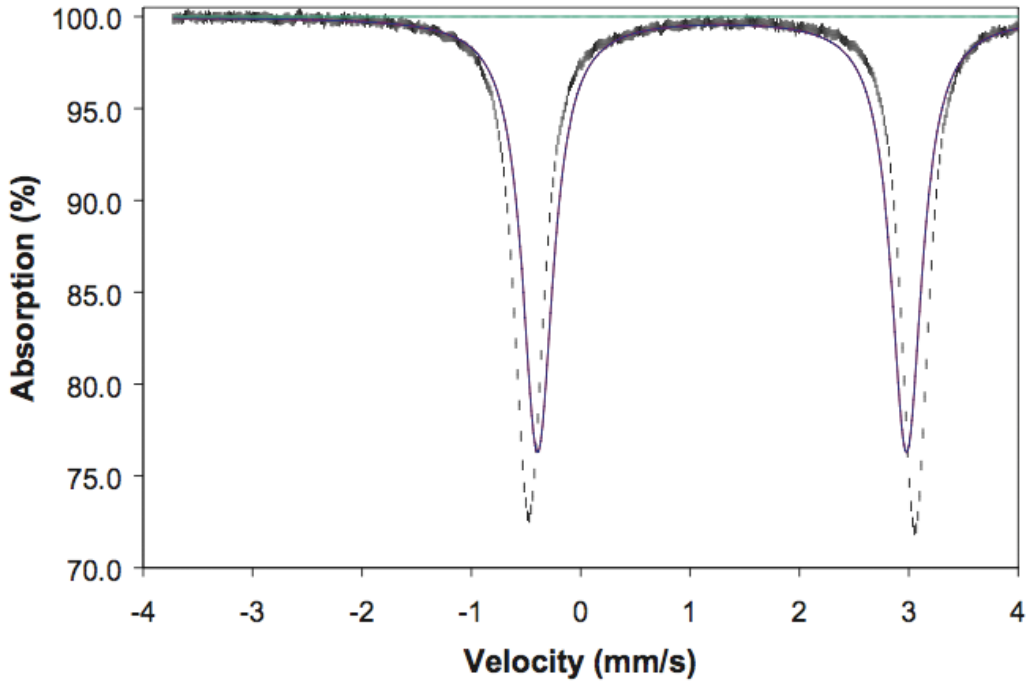

ak9729

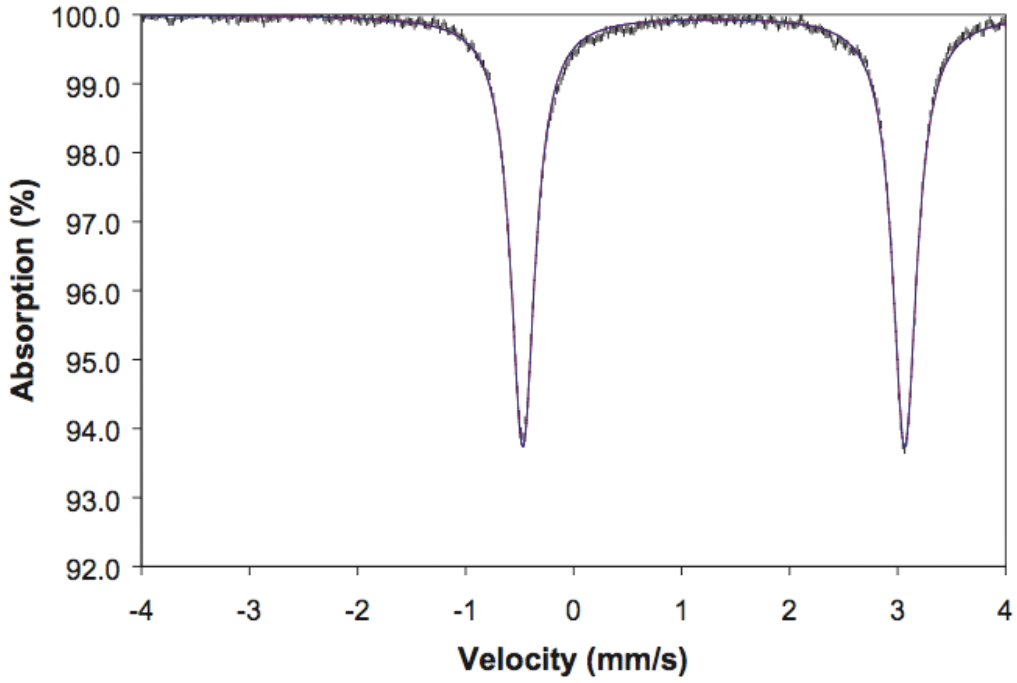

ak972a

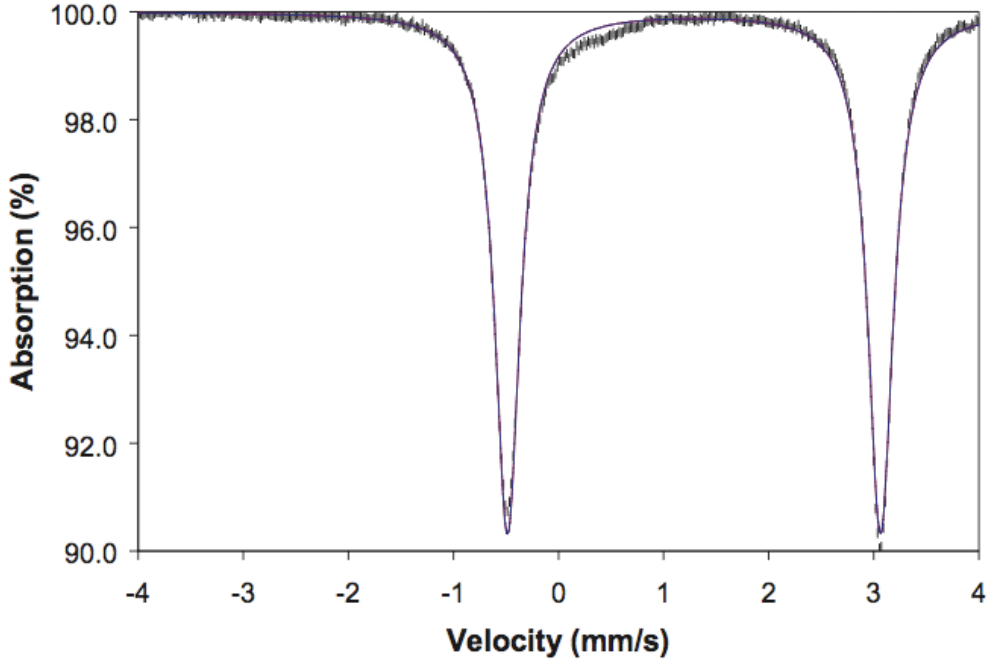

ak978a

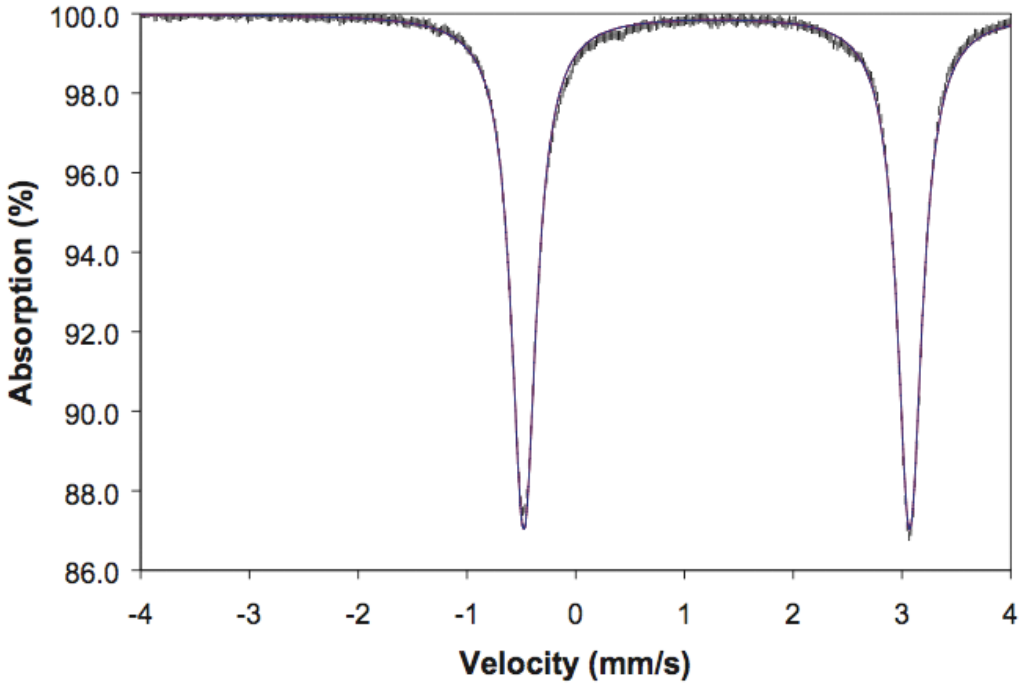

he1

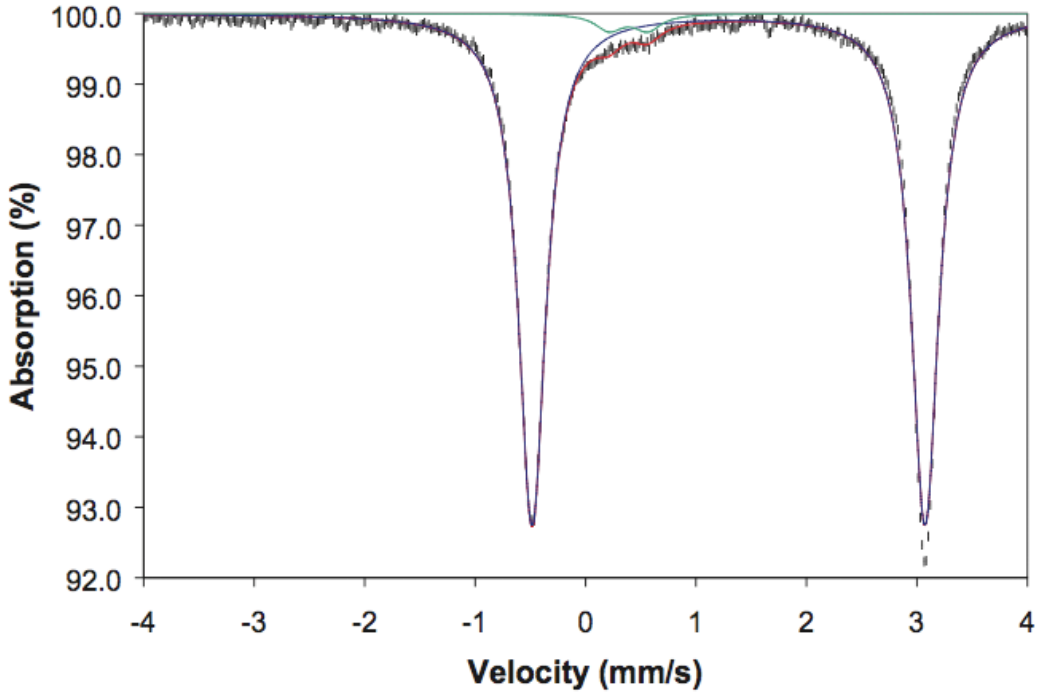
100.0
99.0
98.0
97.0
96.0
95.0
94.0
93.0
92.0
Absorption (%)
-4
-3
-2
-1
0
1
2
3
4
Velocity (mm/s)

Kb-12-9

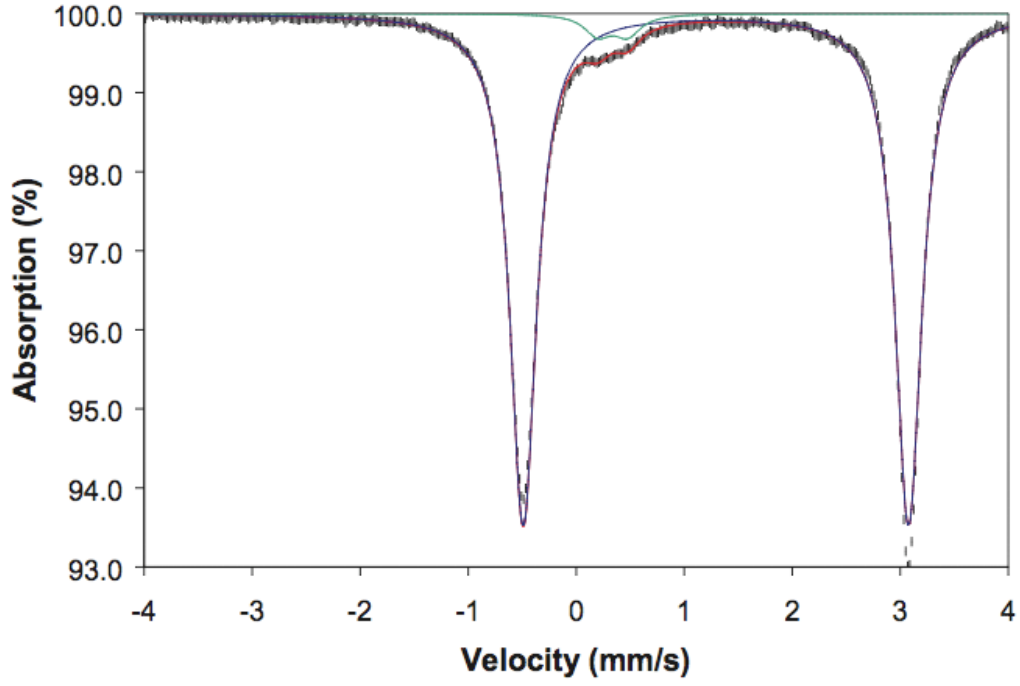
100.0
99.0
98.0
97.0
96.0
95.0
94.0
93.0
Absorption (%)
-4
-3
-2
-1
0
1
2
3
4
Velocity (mm/s)

Kb-12-51

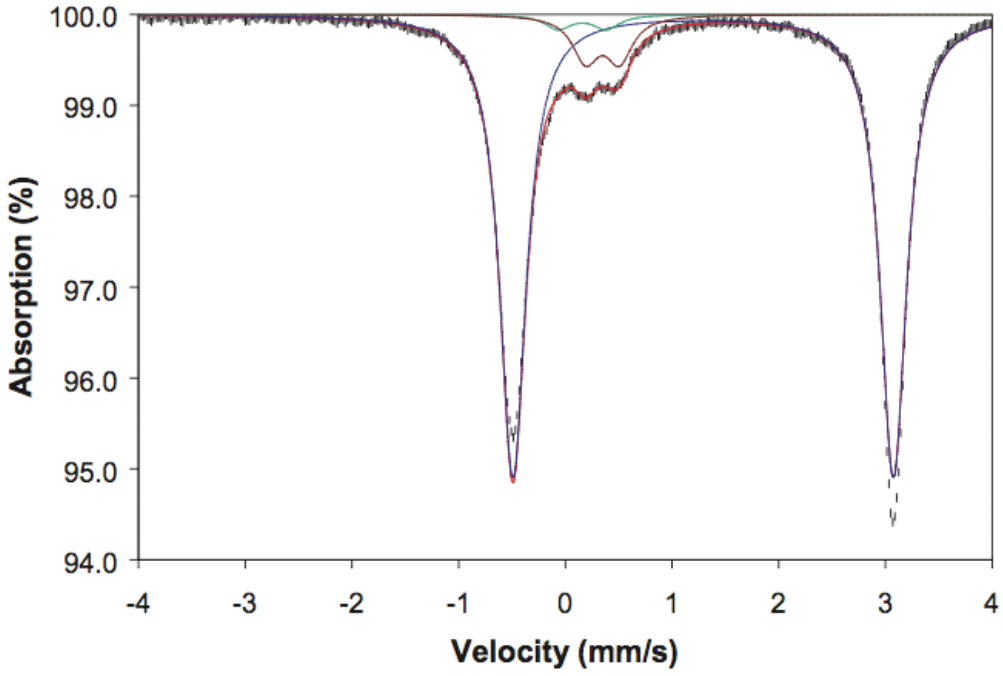

Garnet Standard Mix

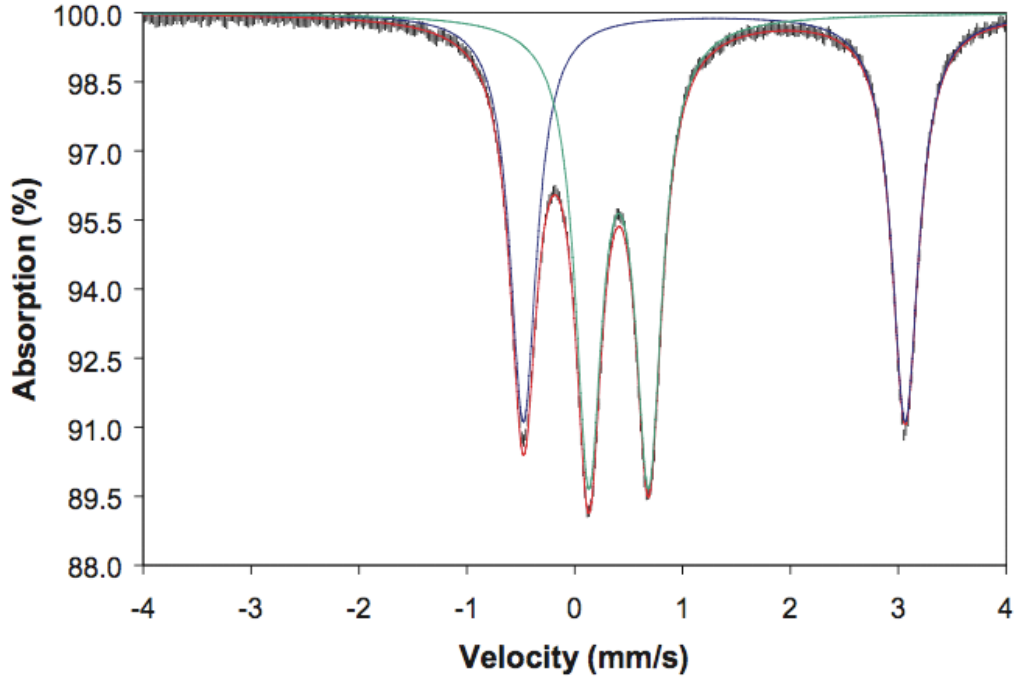

ak979b

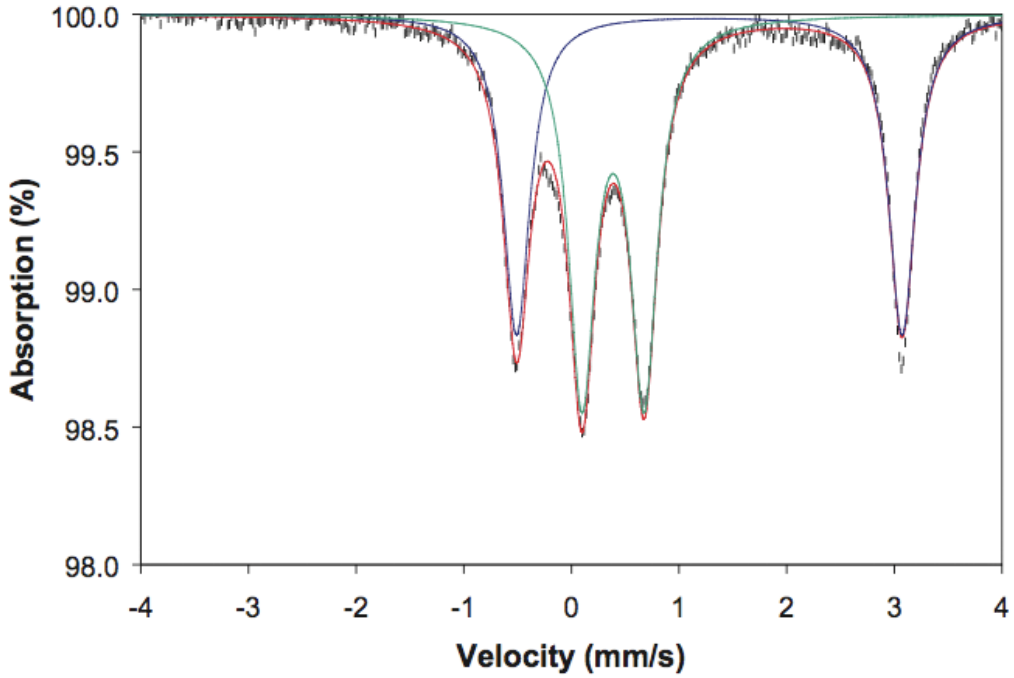

ak9723

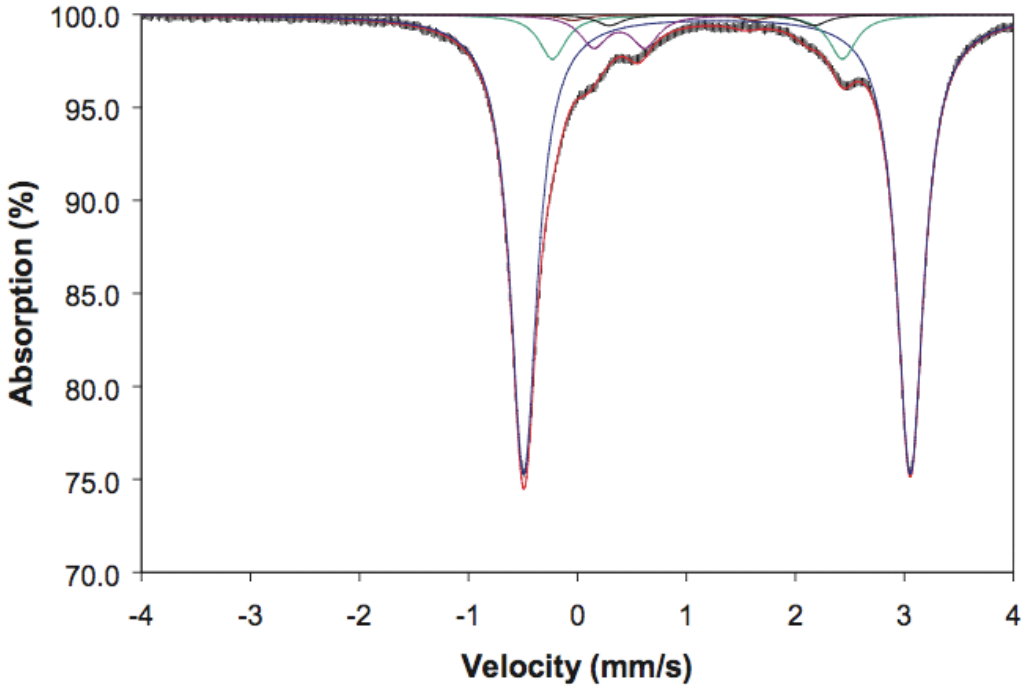

ak972b

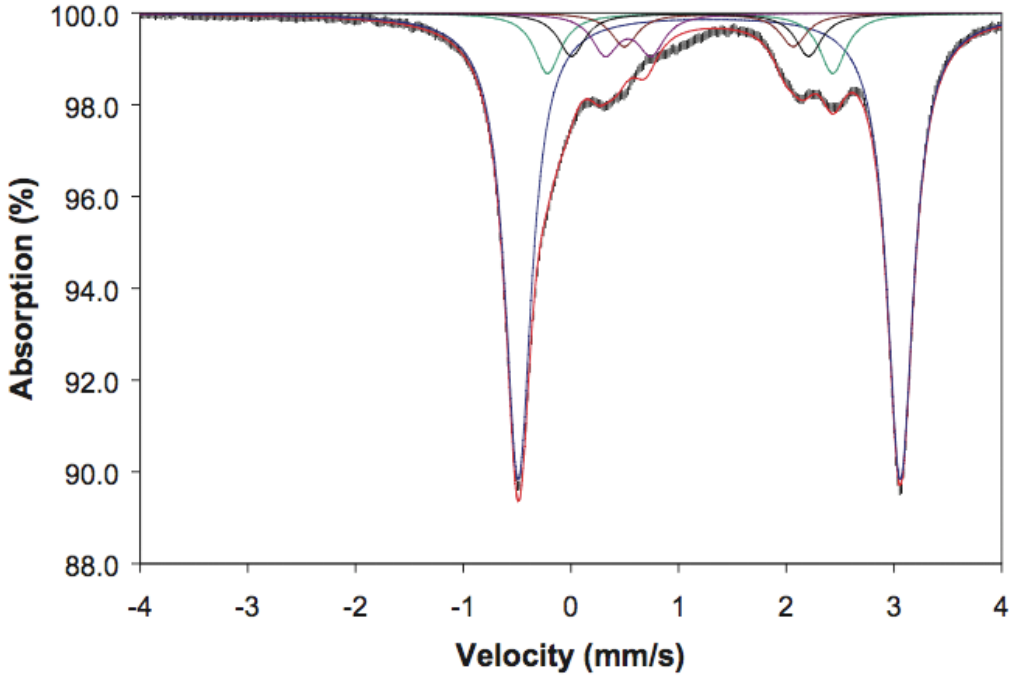
100.0
98.0
96.0
94.0
92.0
90.0
88.0
Absorption (%)
-4
-3
-2
-1
0
1
2
3
4
Velocity (mm/s)

10c

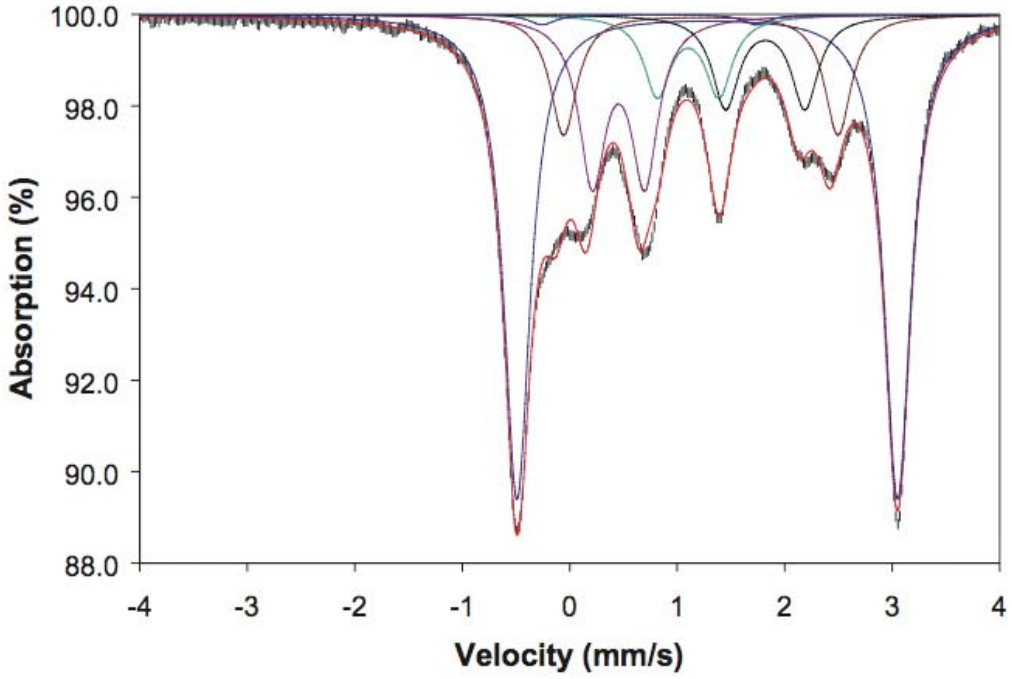
100.0
98.0
96.0
94.0
92.0
90.0
88.0
Absorption (%)
-4
-3
-2
-1
0
1
2
3
4
Velocity (mm/s)

g17

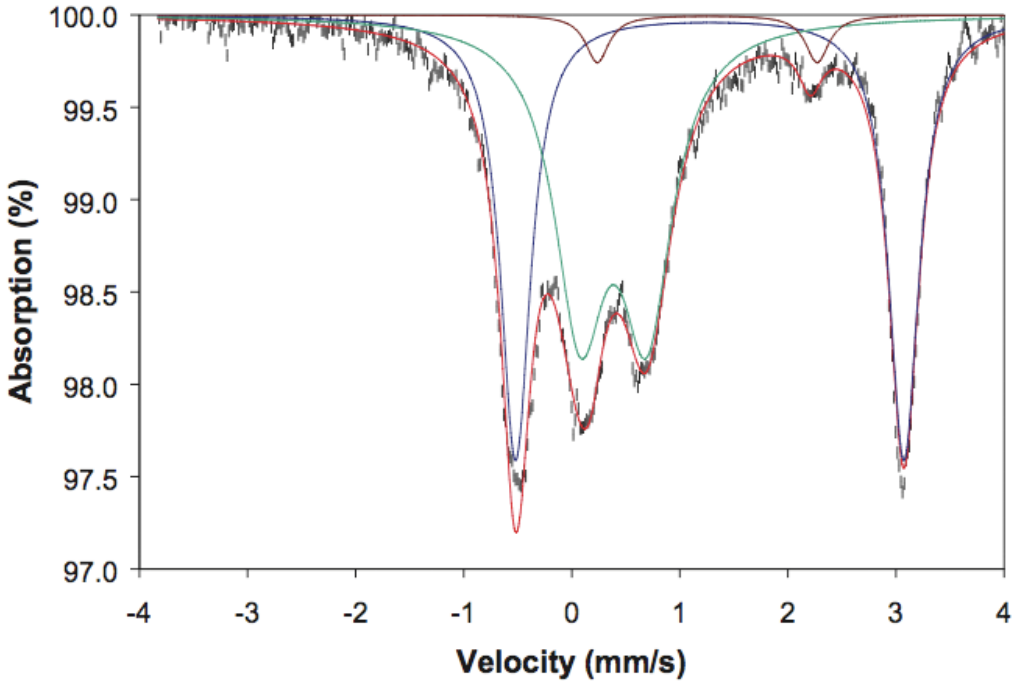
100.0
99.5
99.0
98.5
98.0
97.5
97.0
Absorption (%)
-4
-3
-2
-1
0
1
2
3
4
Velocity (mm/s)

g89

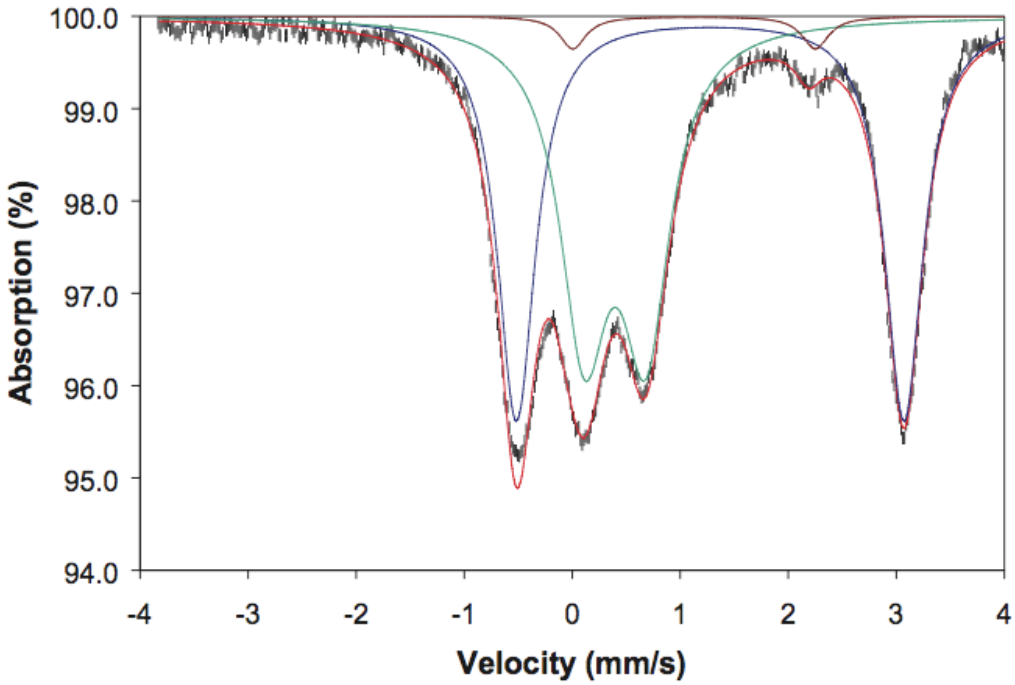
100.0
99.0
98.0
97.0
96.0
95.0
94.0
Absorption (%)
-4
-3
-2
-1
0
1
2
3
4
Velocity (mm/s)

bbkg

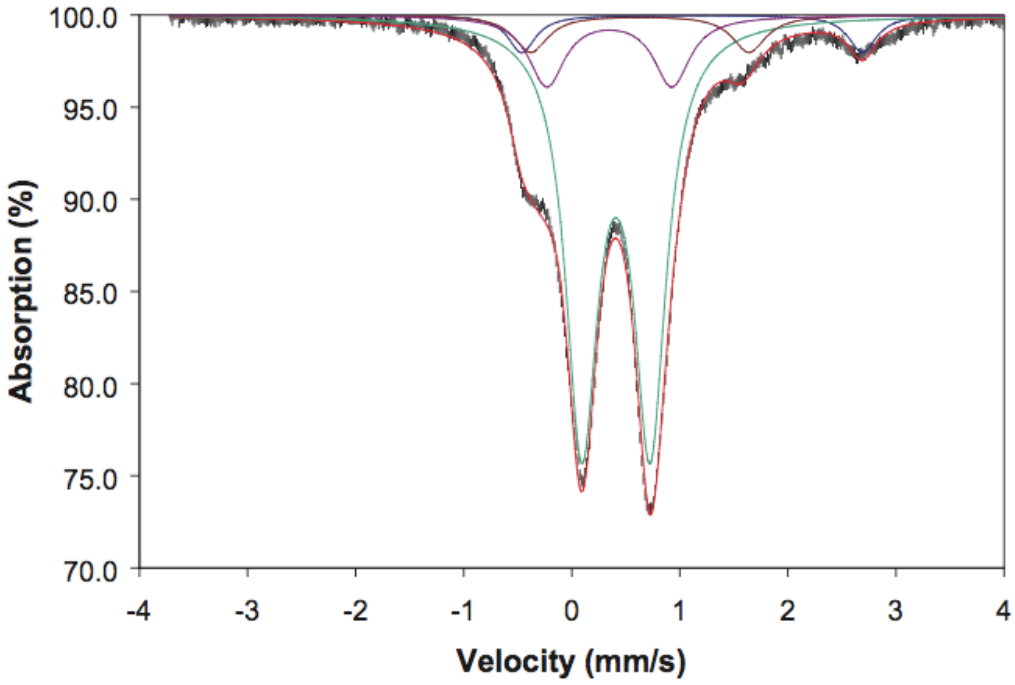
100.0
95.0
90.0
85.0
80.0
75.0
70.0
Absorption (%)
-4
-3
-2
-1
0
1
2
3
4
Velocity (mm/s)

g5183

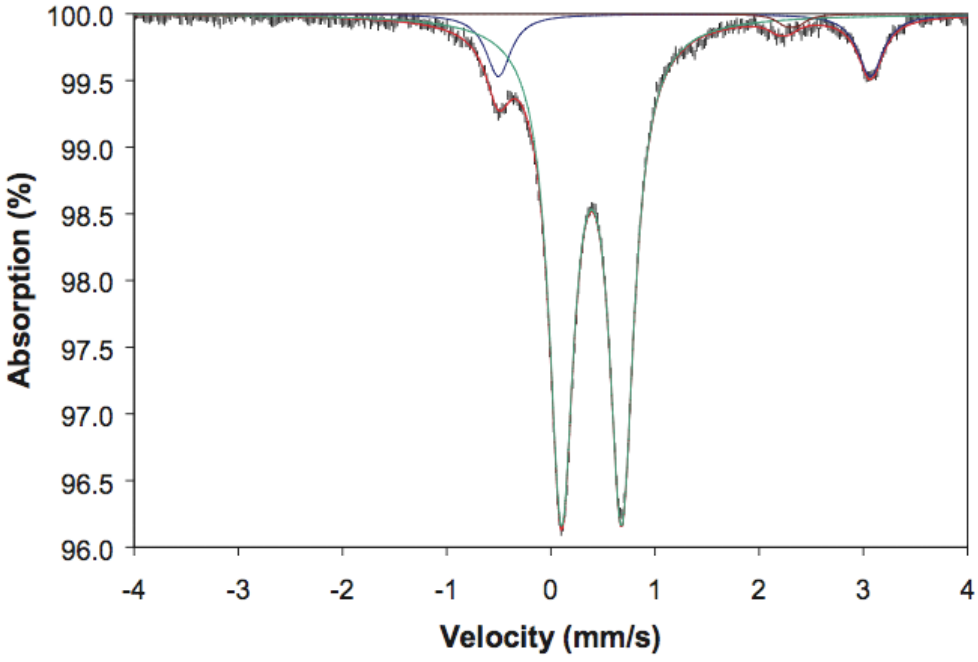
100.0
99.5
99.0
98.5
98.0
97.5
97.0
96.5
96.0
Absorption (%)
-4
-3
-2
-1
0
1
2
3
4
Velocity (mm/s)

ak32w

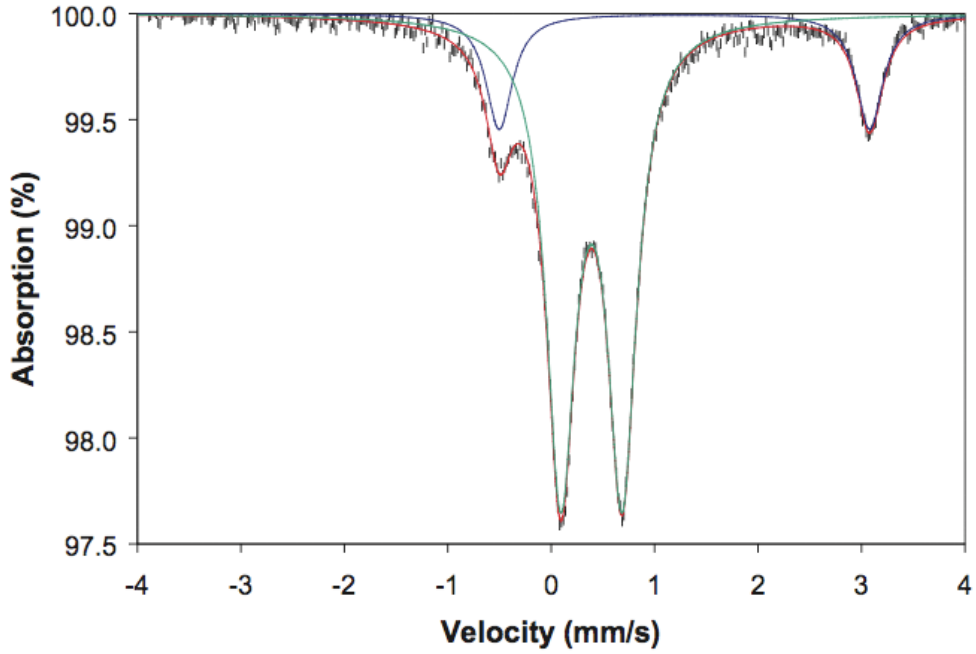
100.0
99.5
99.0
98.5
98.0
97.5
Absorption (%)
-4
-3
-2
-1
0
1
2
3
4
Velocity (mm/s)

ahun

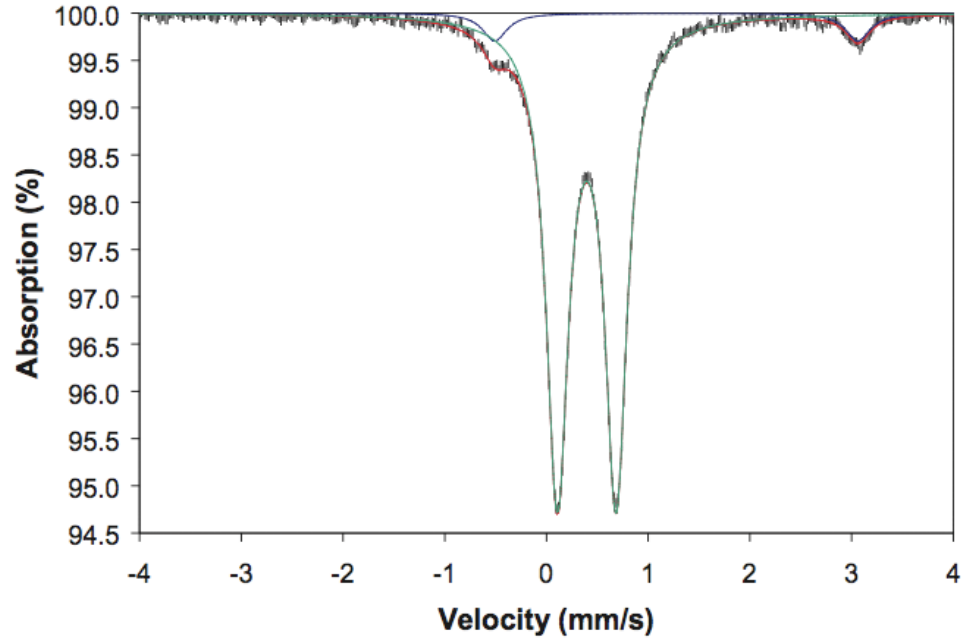
100.0
99.5
99.0
98.5
98.0
97.5
97.0
96.5
96.0
95.5
95.0
94.5
Absorption (%)
-4
-3
-2
-1
0
1
2
3
4
Velocity (mm/s)

hrm1

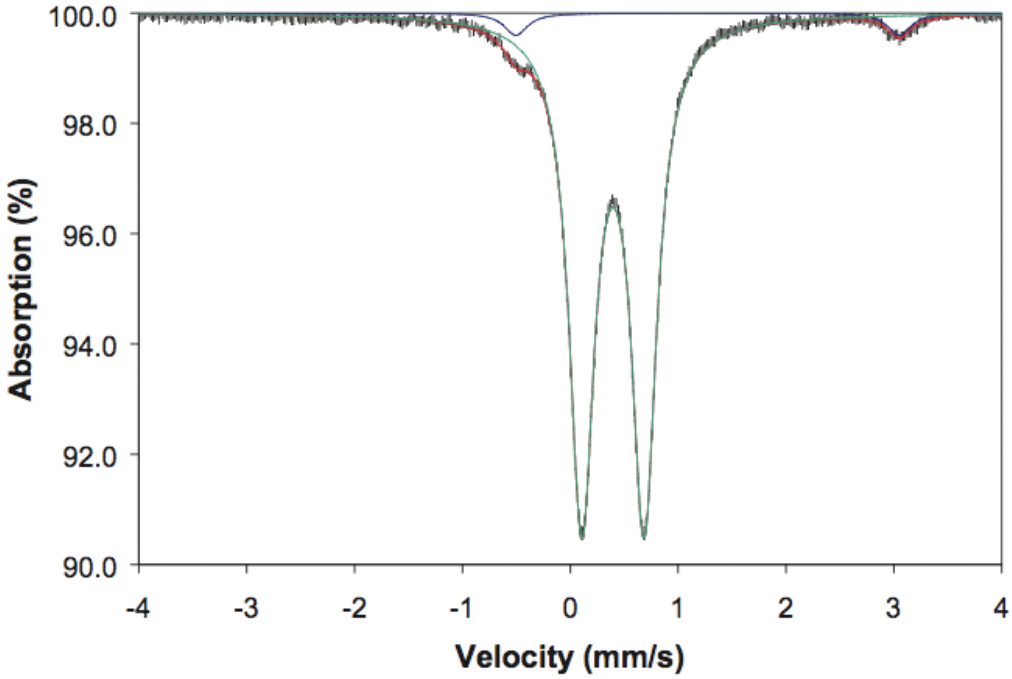
100.0
98.0
96.0
94.0
92.0
90.0
Absorption (%)
-4
-3
-2
-1
0
1
2
3
4
Velocity (mm/s)

and

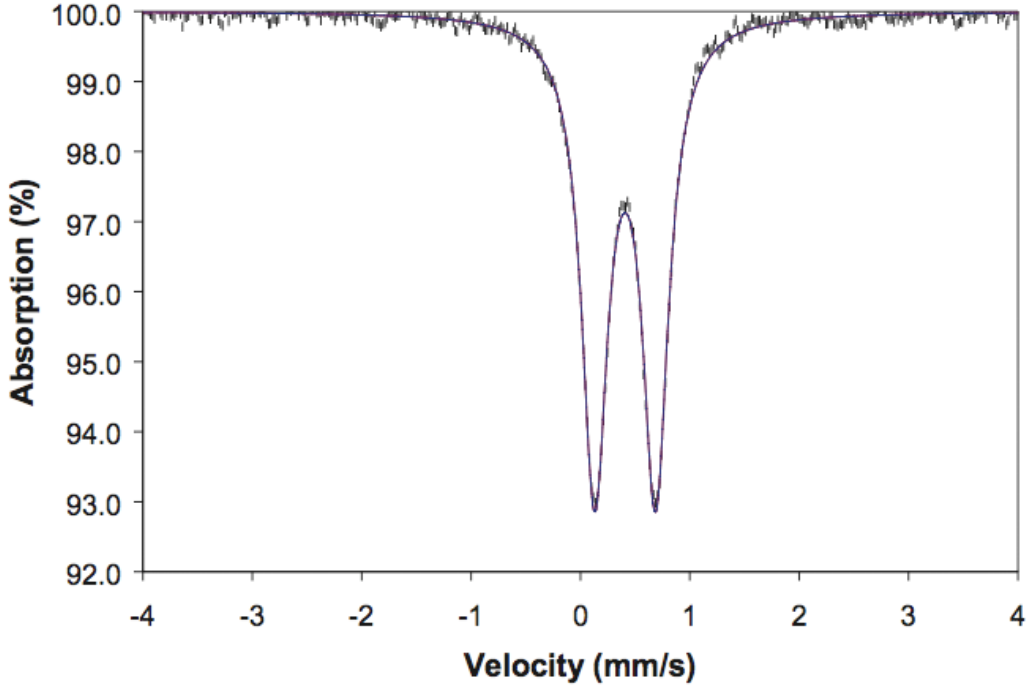
100.0
99.0
98.0
97.0
96.0
95.0
94.0
93.0
92.0
Absorption (%)
-4
-3
-2
-1
0
1
2
3
4
Velocity (mm/s)

Appendix C: XANES Results

alm1.017

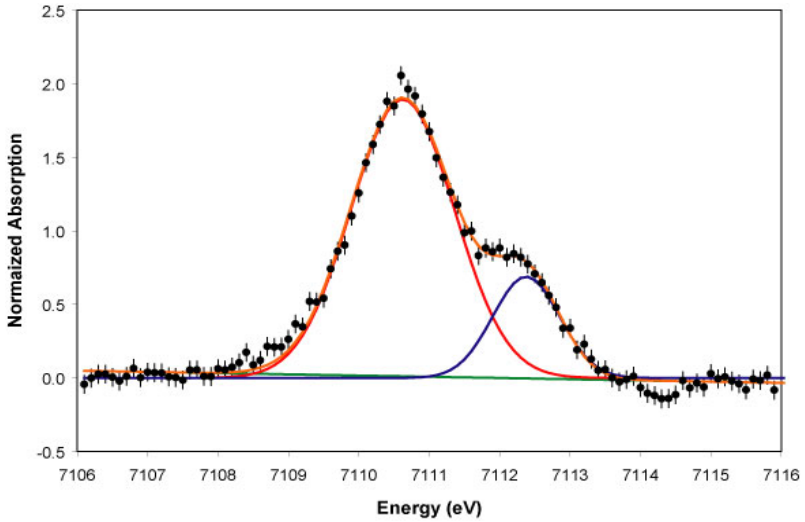

alm1b.087

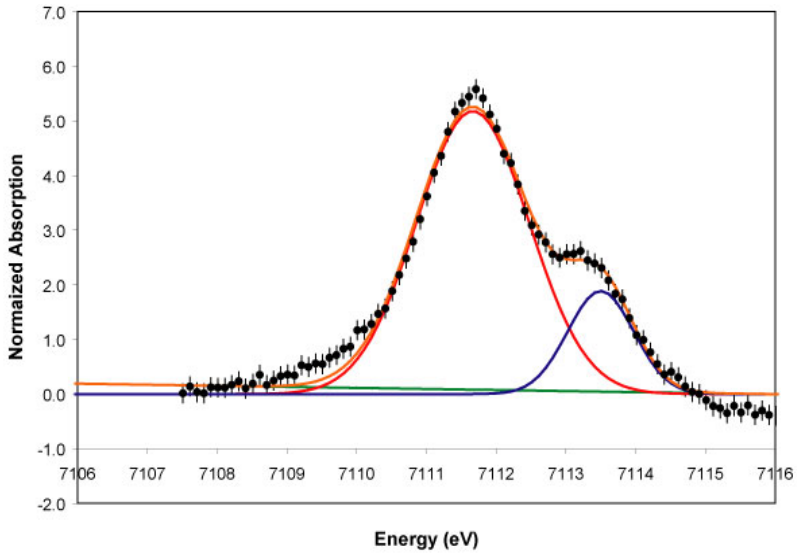

alm3.008

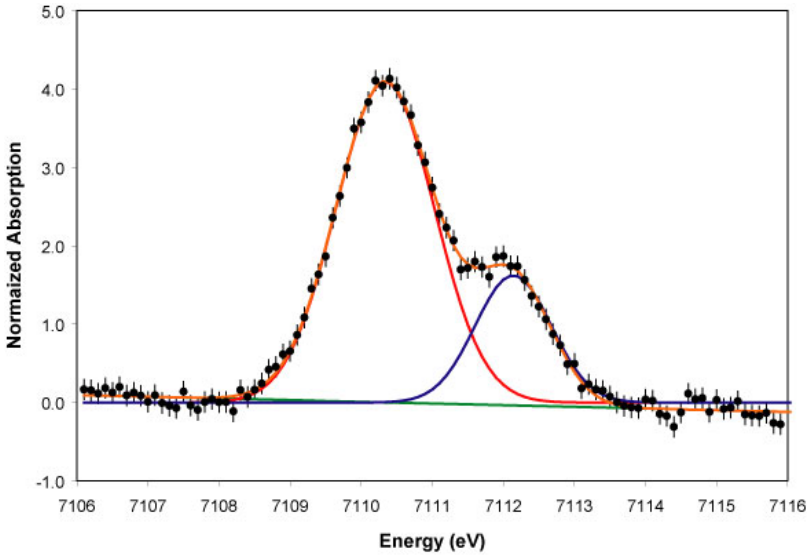

ak9729.011

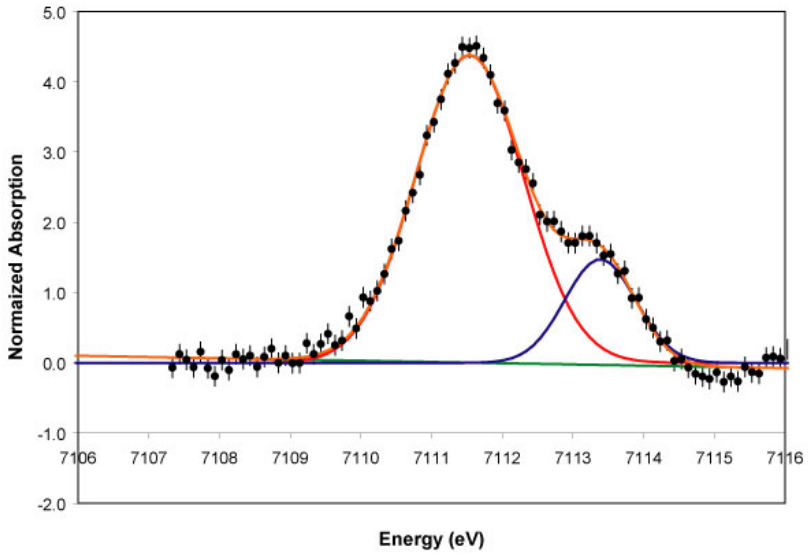

ak9729b.108

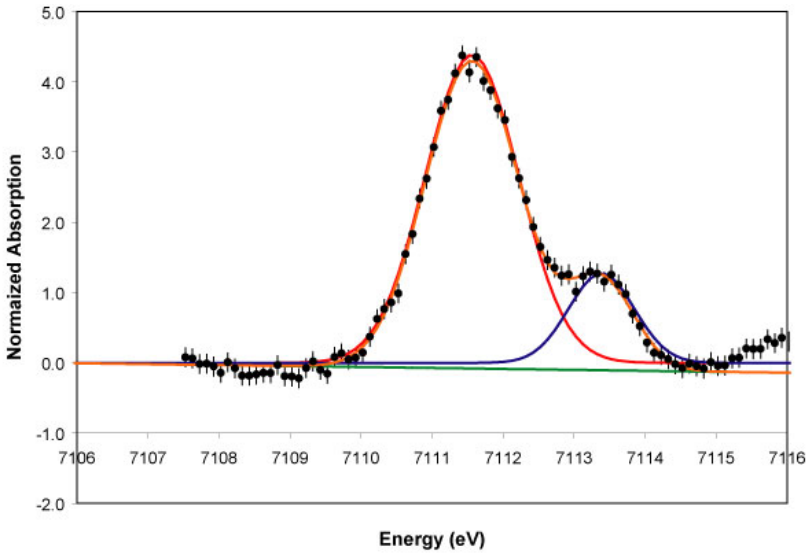

2a.030

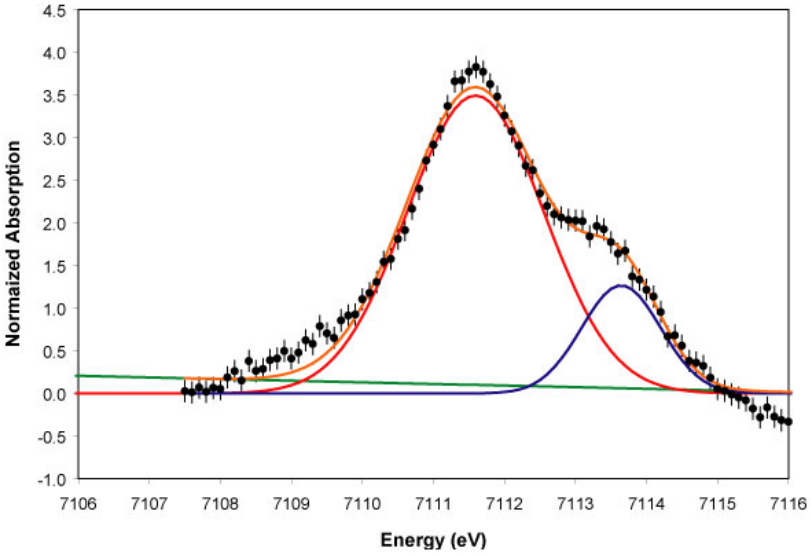

2ab.103

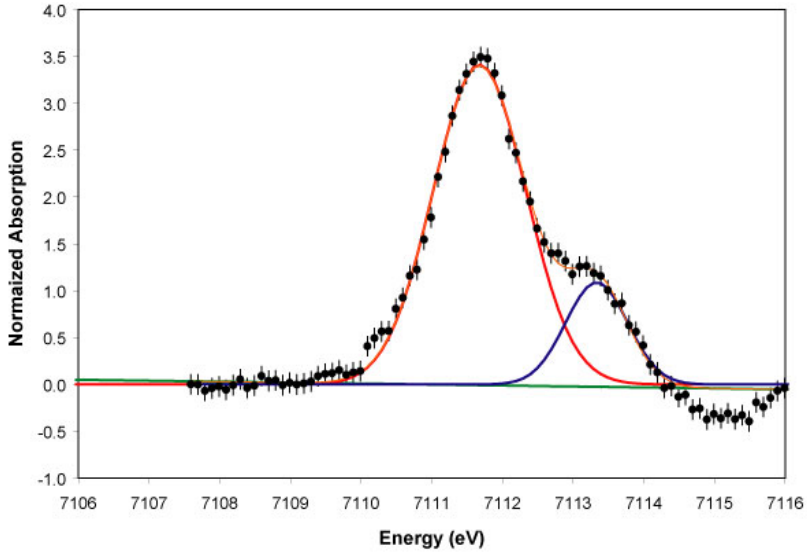

8a.010

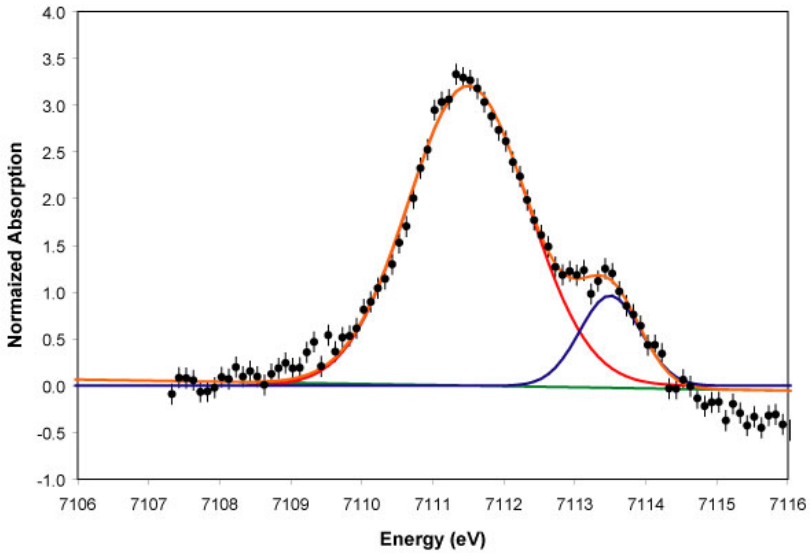

8ab.106

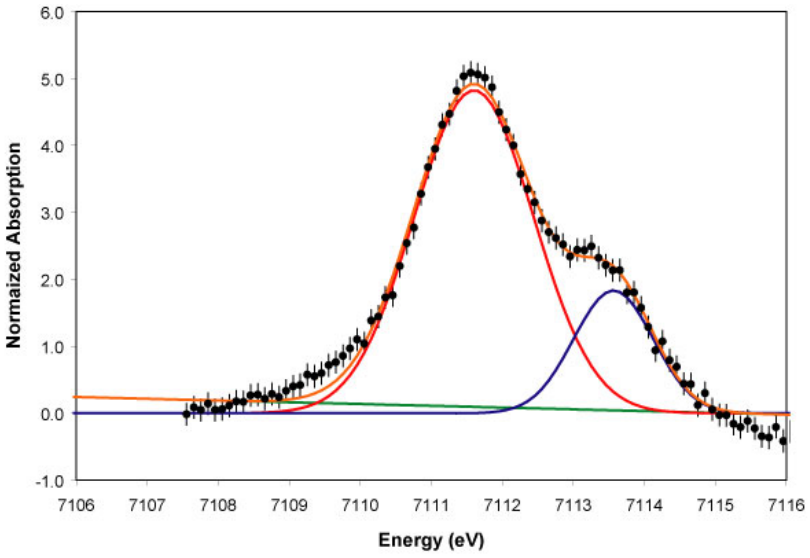

he1.083

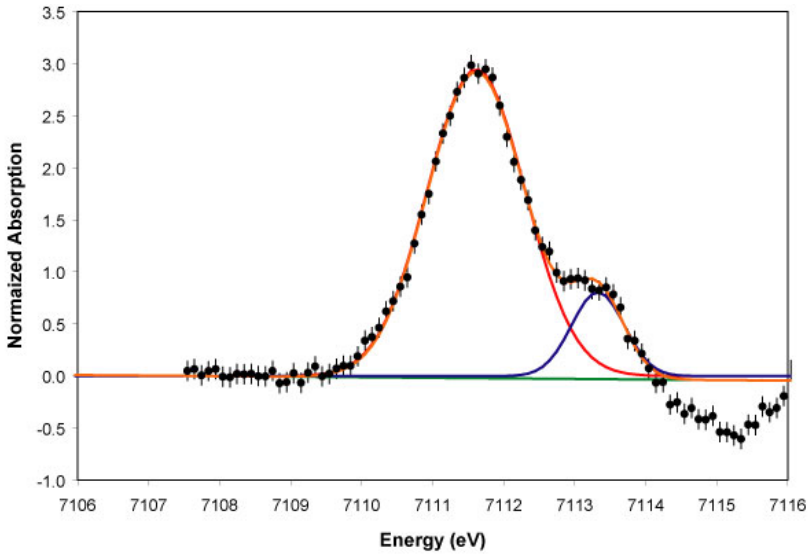

he1b.107

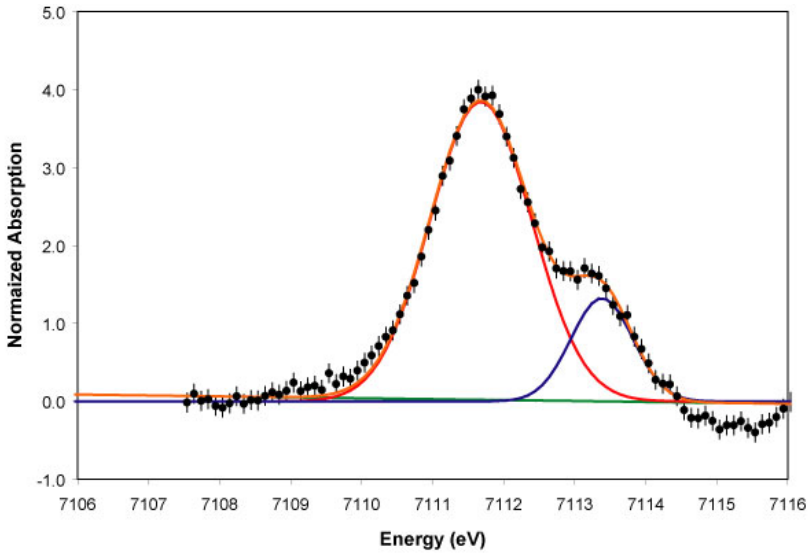

129b.102

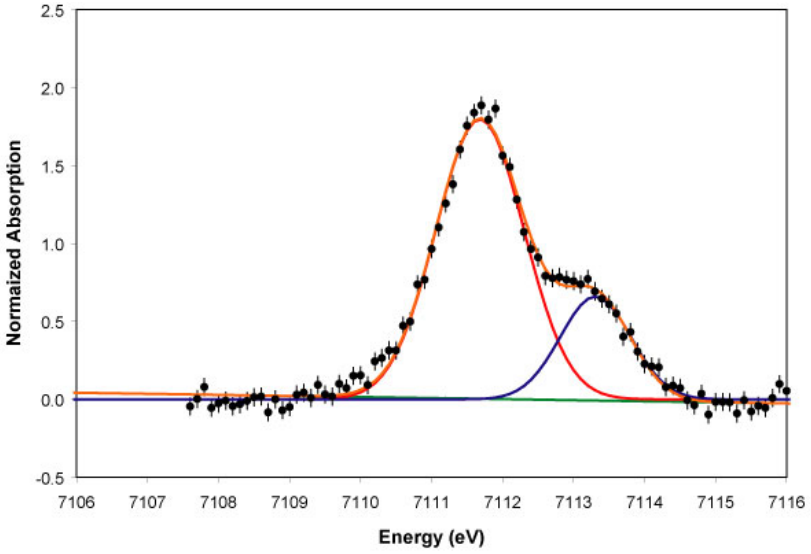

ak9723.079

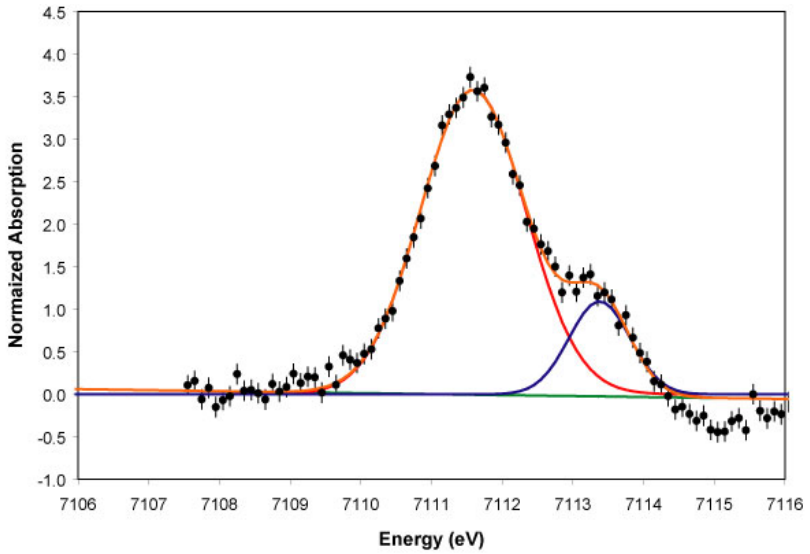

ak9723b.104

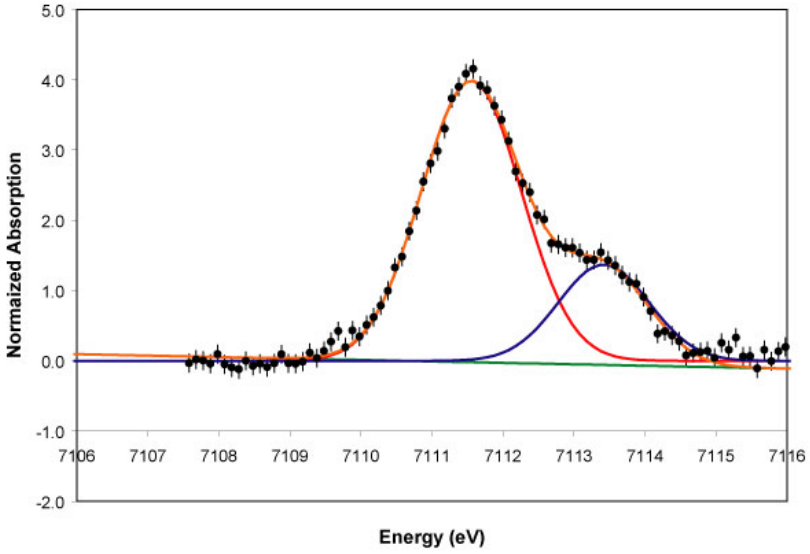

2b.031

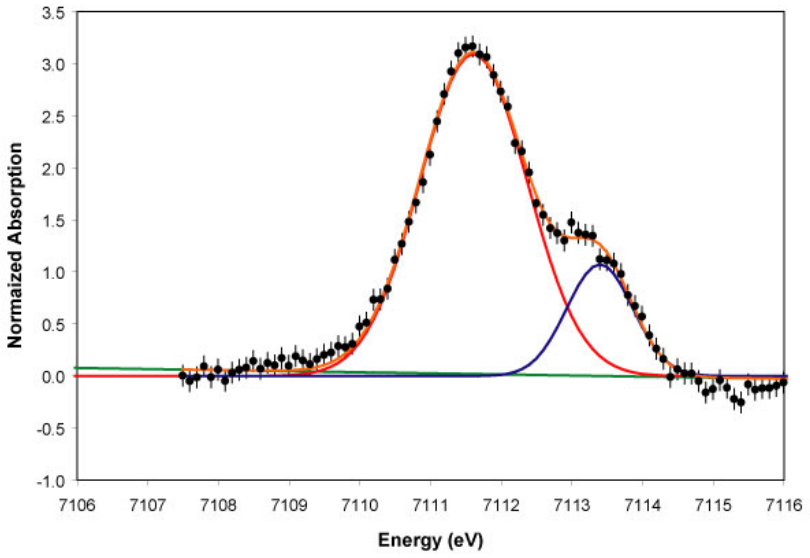

2bb.095

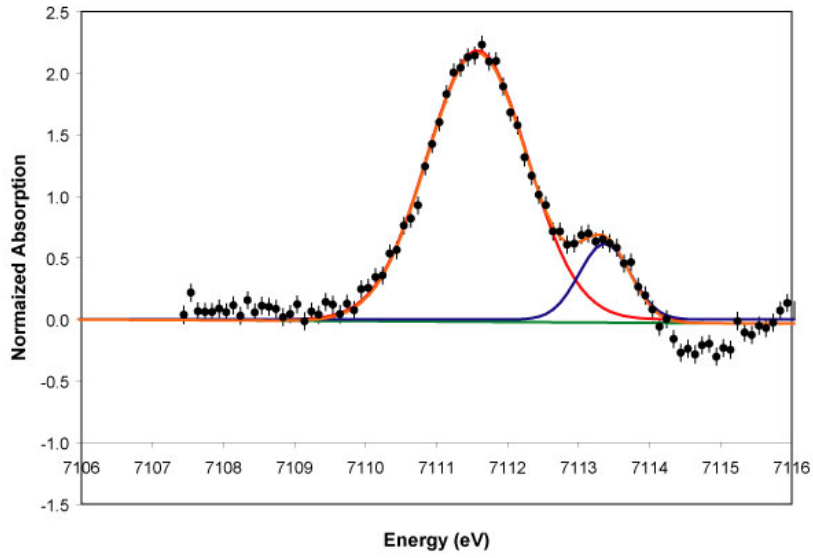

ak972b.082

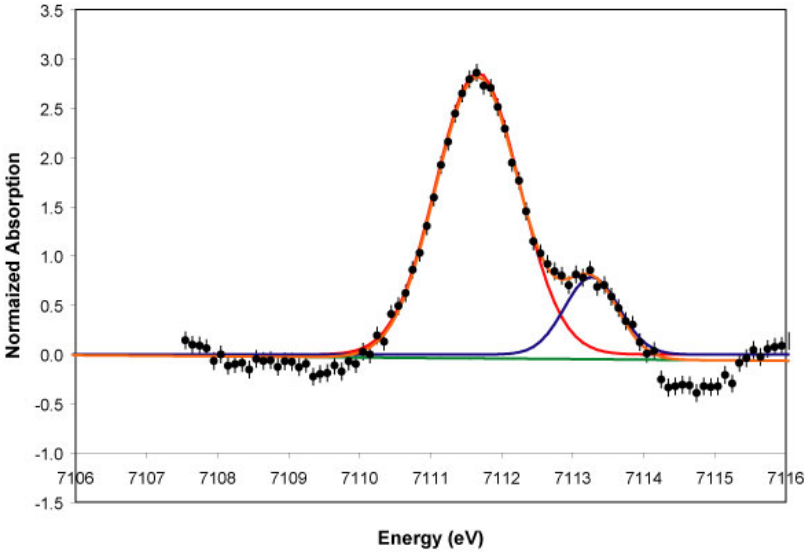

10c.028

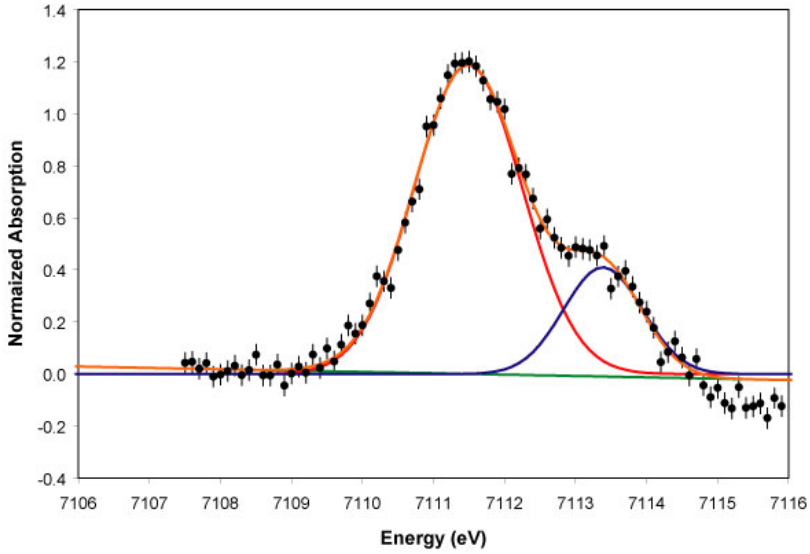

10cb.094

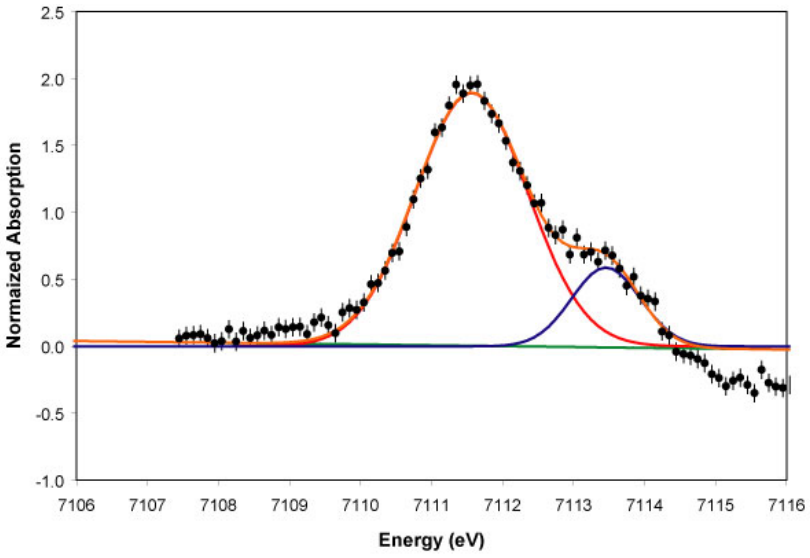

1251.032

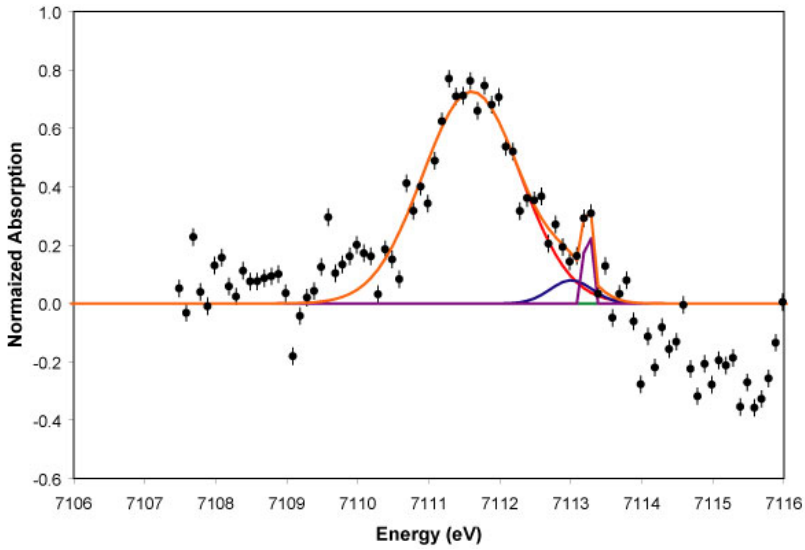

1251b.096

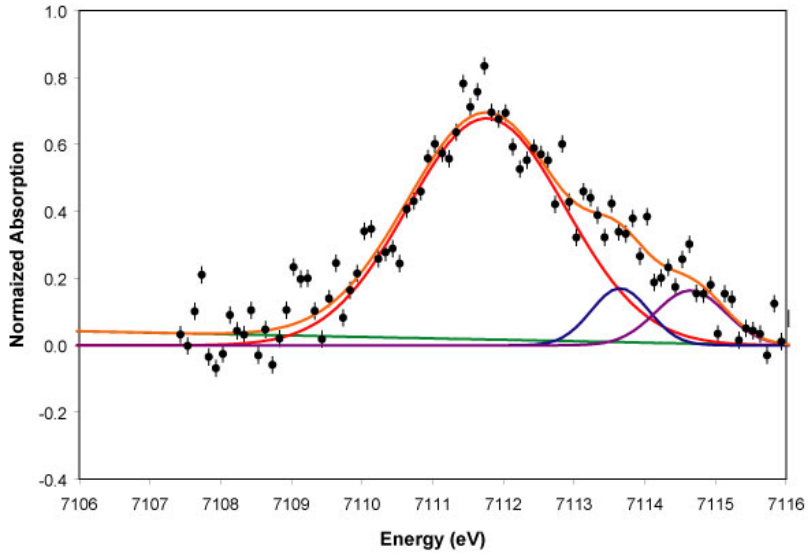

9b.080

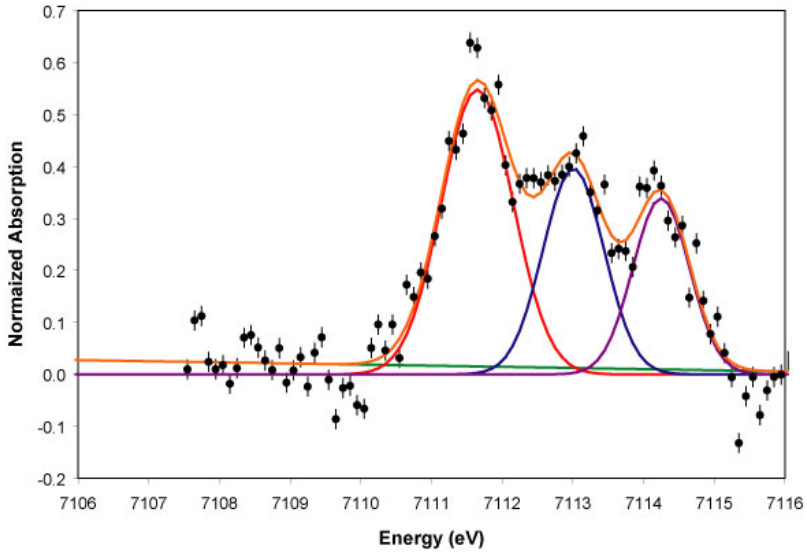

9bb.081

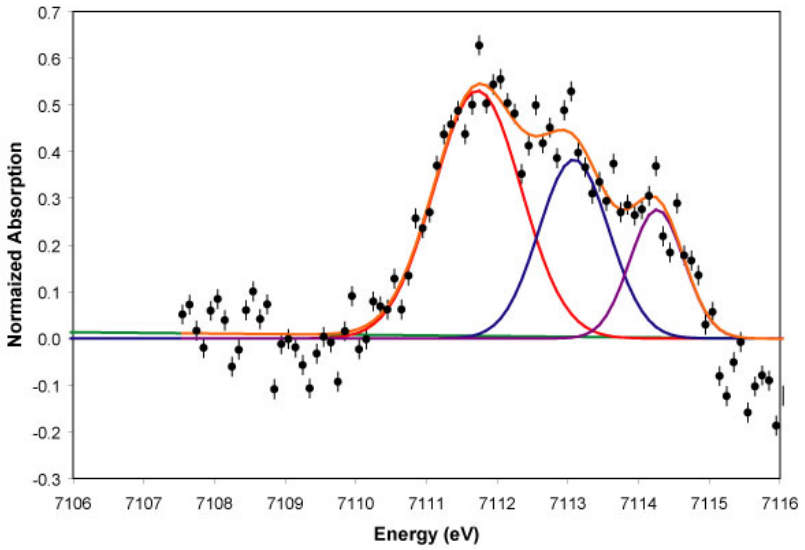

g17.019

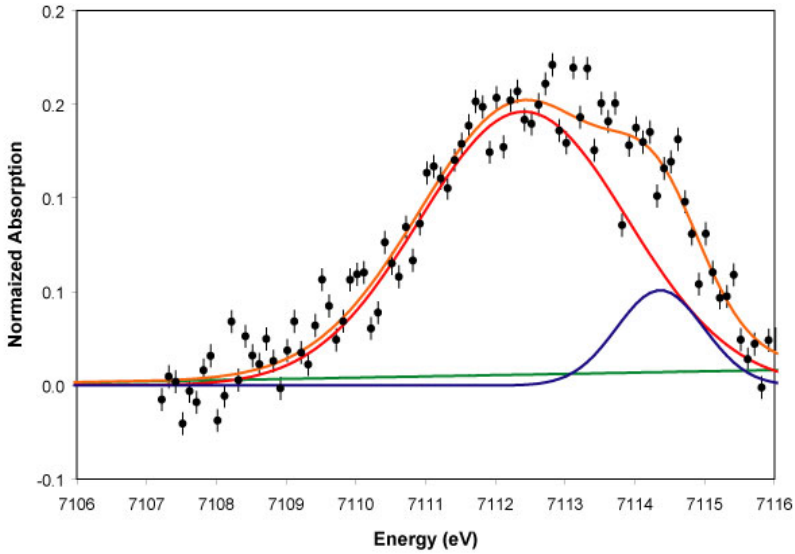

g17b.089

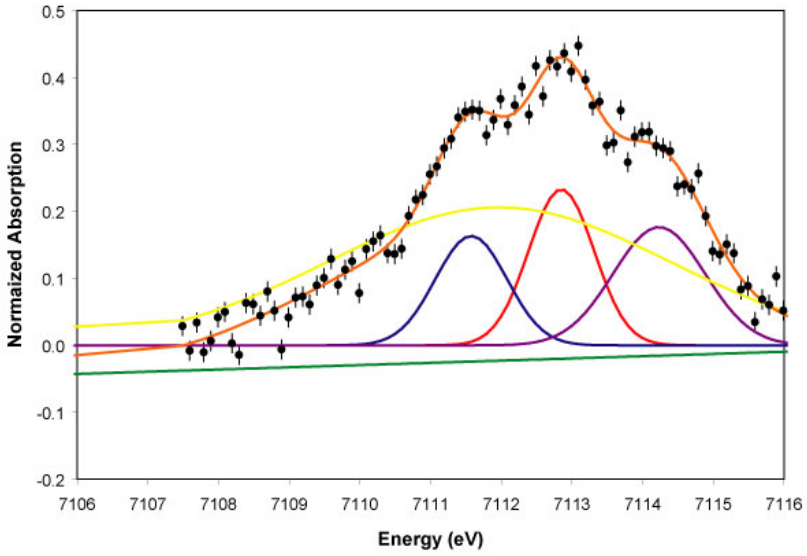

g89.020

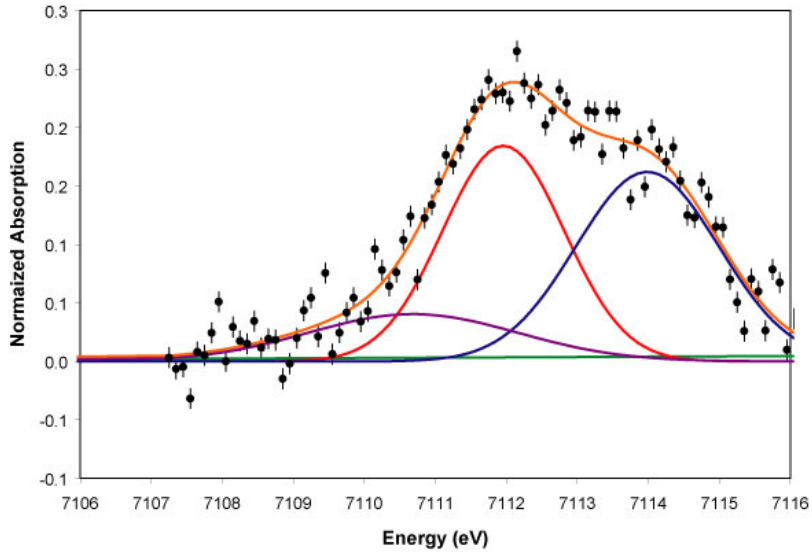

g89b.090

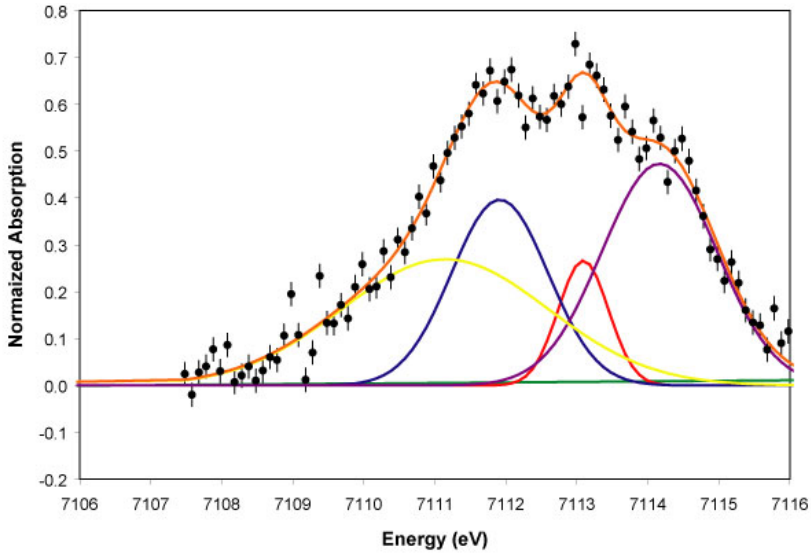

bbkg.026

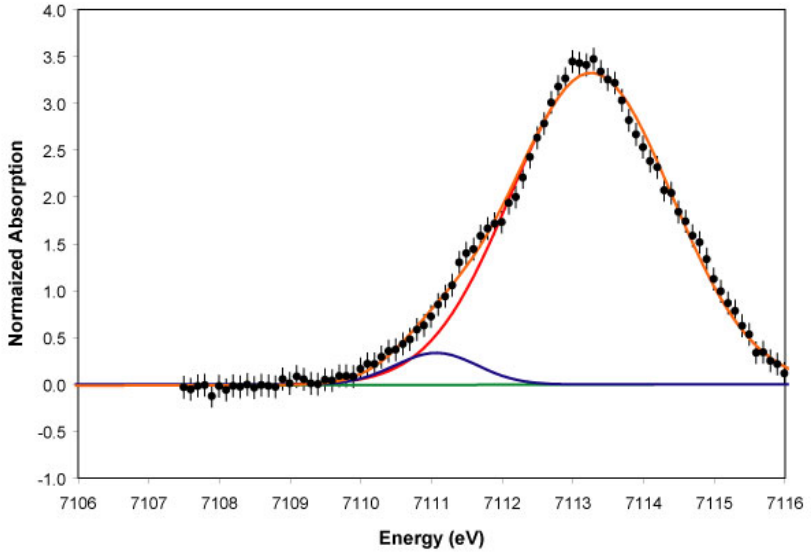

bbkgb.093

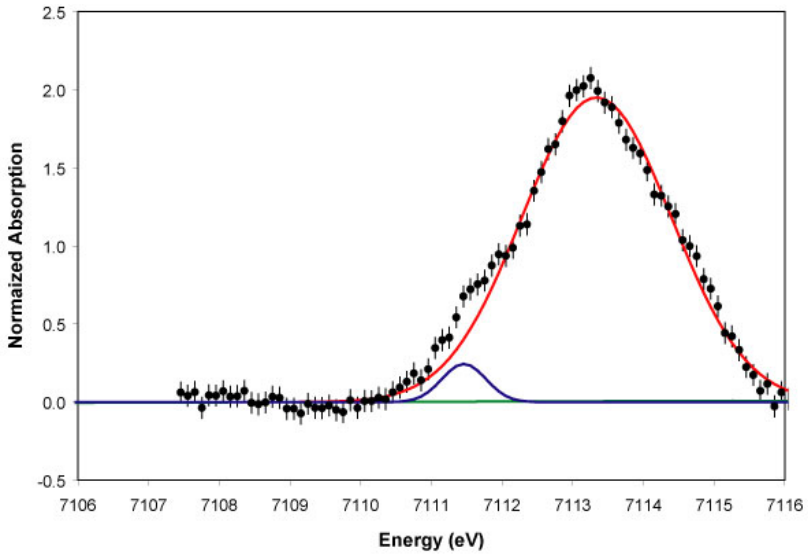

g5183.025

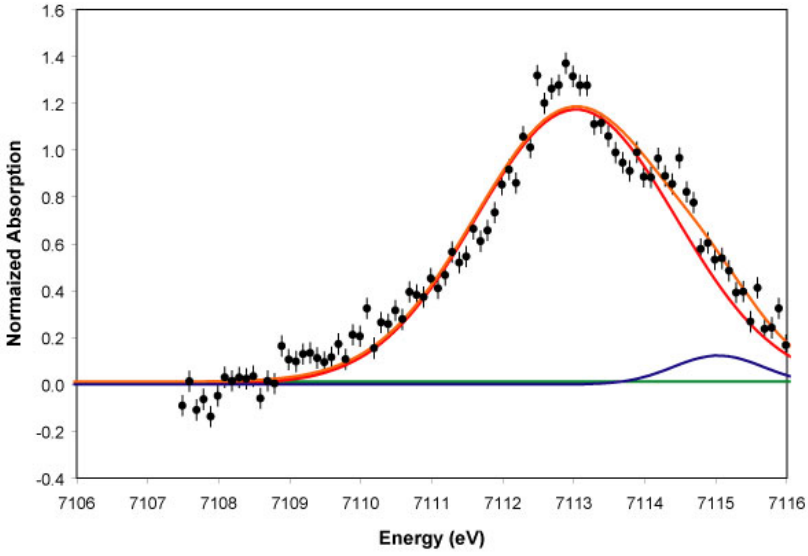

g5183b.101

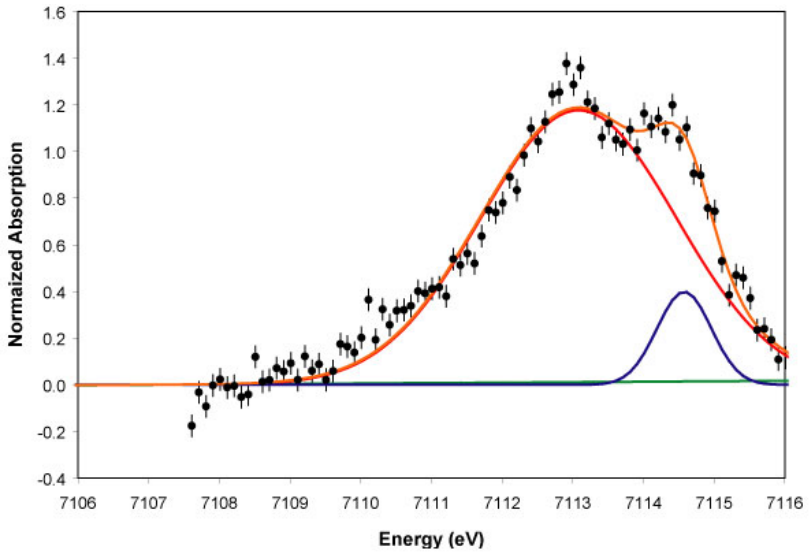

a32w.085

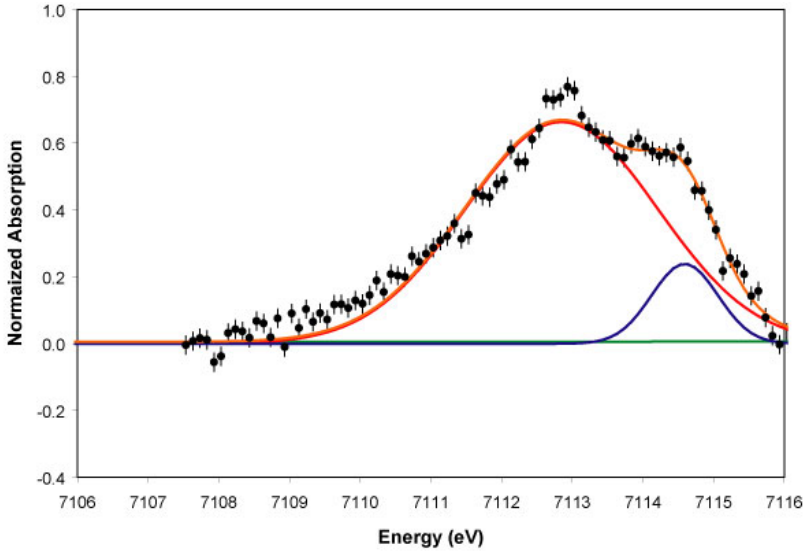

a32wb.109

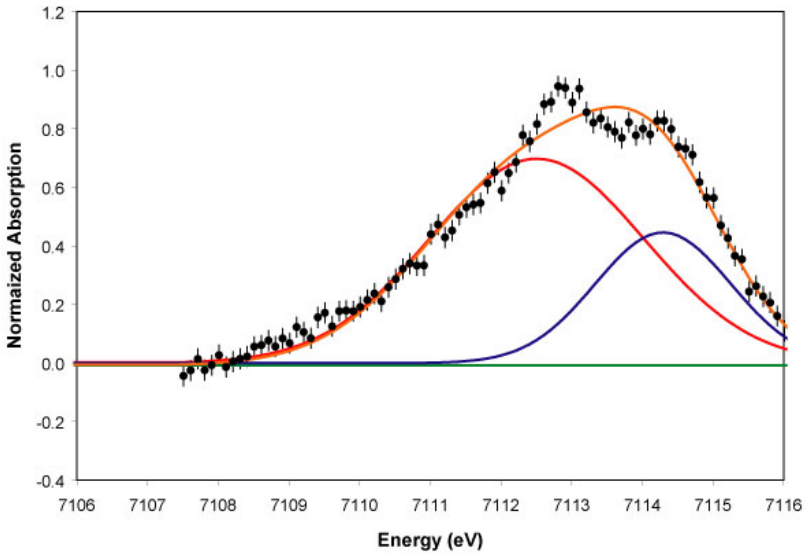

ahun.018

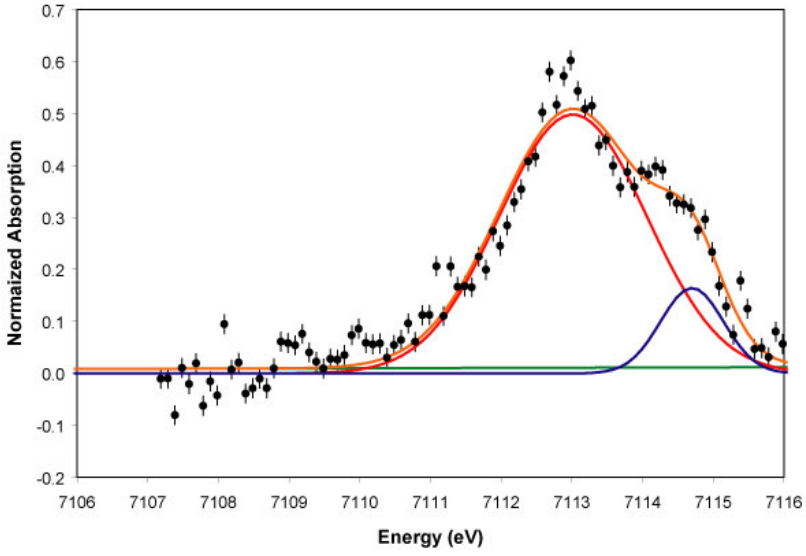

ahunb.088

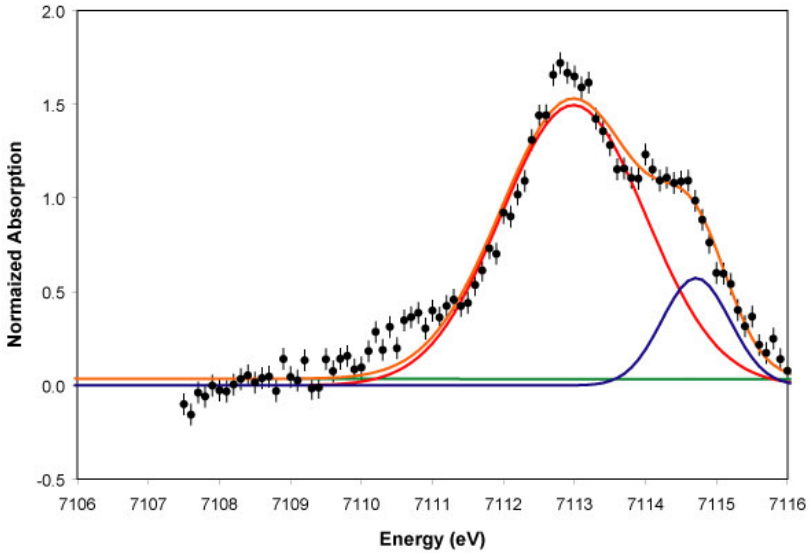

hrm1.086

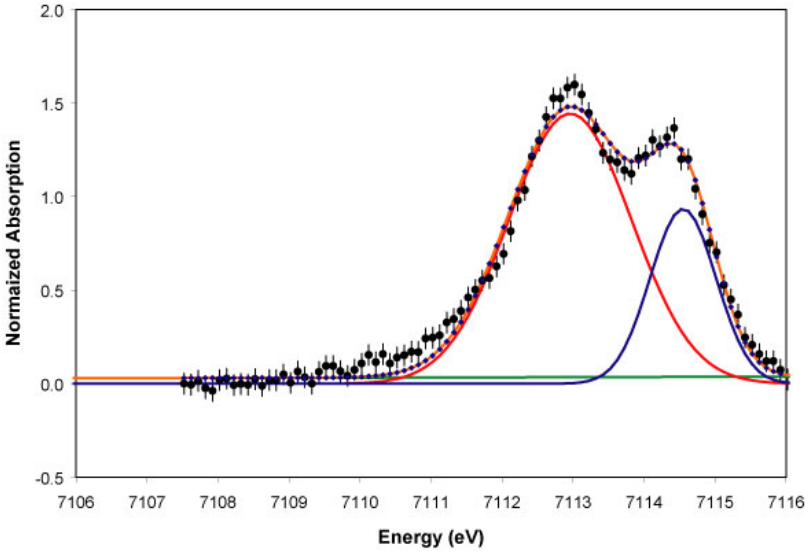

hrm1b.110

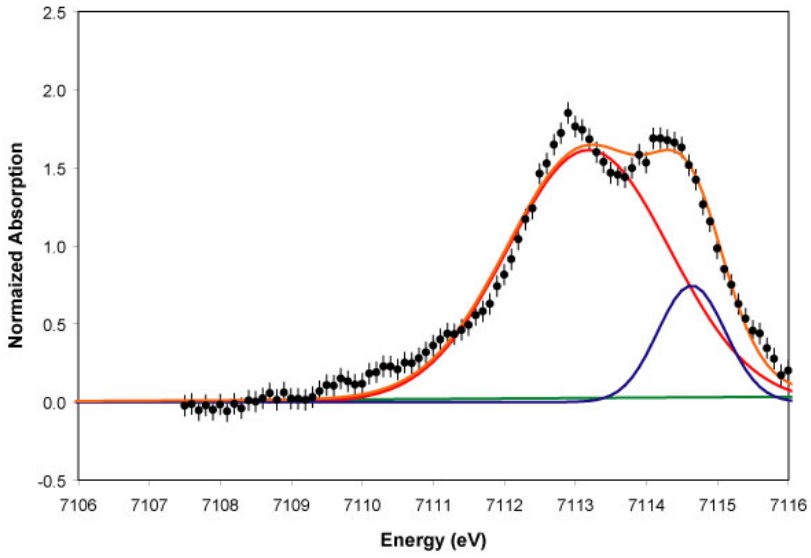

and1.021

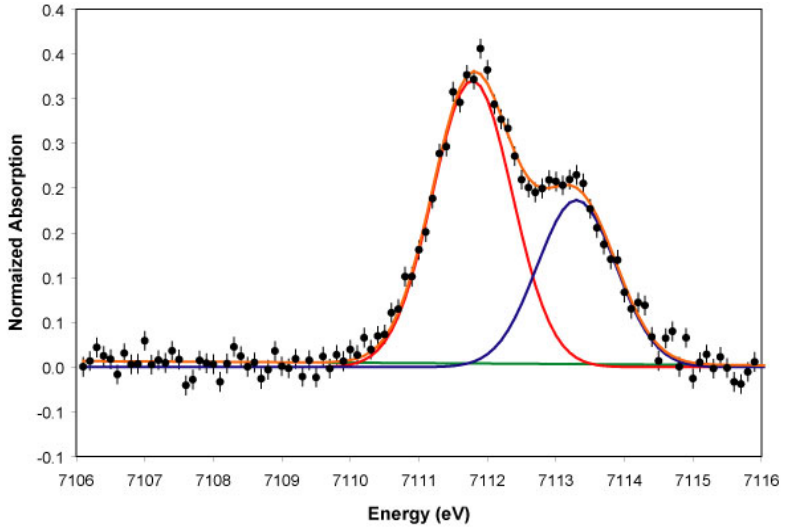

and1.092

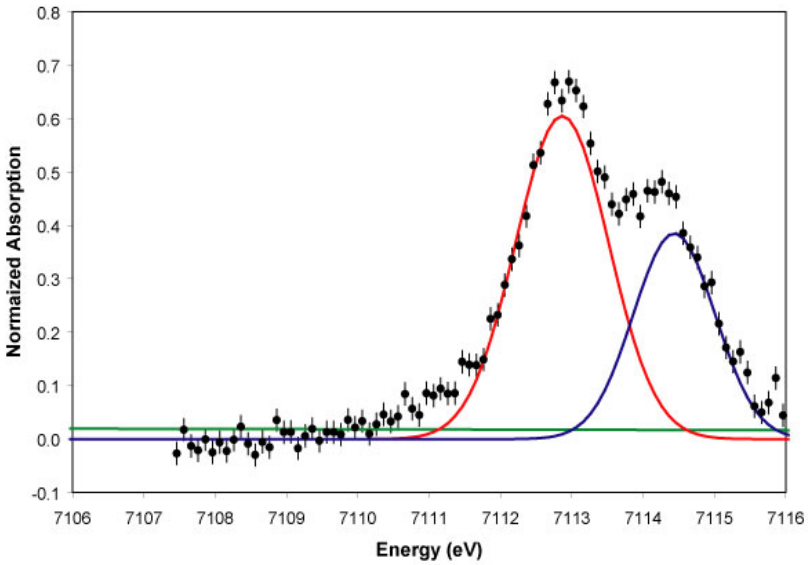

and3.009

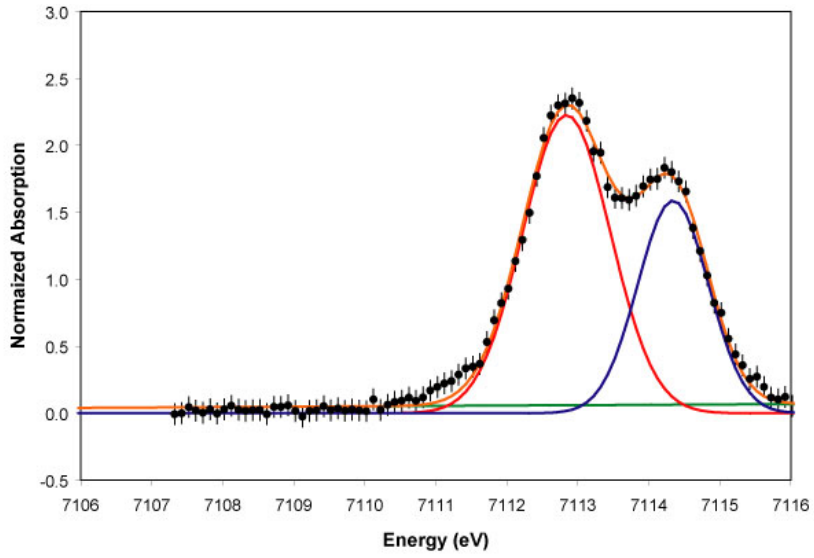

Works Cited

Amthauer, G., Annersten, H., Hafner, S.S. (1977). The Mössbauer Spectrum of ^{57}Fe in Titanium-Bearing Andradites. *Phys. Chem. Minerals 1*,399-413.

Bajt, S.; Sutton, S.R.; Delaney, J.S., (1994) X-ray microprobe analysis of iron oxidation states in silicates and oxides using X-ray absorption near edge structure (XANES). *Geochimica et Cosmochimica Acta.* 58:23, 5209-5214.

Barcova, K., Mashlan, M. and Martinec, P. (2002) Mössbauer Study of the Thermal Behaviour of Garnets Used in High-Energy Water Jet Technologies. *Hyperfine Interactions.* 139/140. 463-469.

Bartolomé, P. (1960) Genesis of the Gore Mountain Garnet Deposit, New York. *Economic Geology*. Vol. 55. 255-277.

Belozerskii, G.N., Gittzovich, V.N., Murin, A.N., Marshak, L.A., Shapiro, A.I., Yakovlev, YU.M. (1969). Investigation of Garnet Single Crystals by Mössbauer Spectroscopy. *Proceedings of the Conference on the Application of the Mössbauer Effect (Tihany, 1969).*

Berry, F.J., Dávalos, J.Z., Gancedo, J.R., Greaves, C., Marco, J.F., Slater, P., Vithal, J.F., (1996). Cation Distribution and Magnetic Interactions in Substituted Iron-Containing Garnets: Characterization by Iron-57 Mössbauer Spectroscopy. *Journal of Solid State Chemistry.* 122. 118-129.

Bianconi, A. "Surface X-ray Absorption Spectroscopy: Surface EXAFS and

Surface XANES" Appl. Surf. Sci. Vol. 6 pag. 392-418 (1980)

Blackwell, M. (2000) Temperature Dependence of Grunerite Mössbauer. Undergraduate Thesis, Mount Holyoke College.

Brown, Jr., G.E.; Calas, G.; Waychunas, G.A.; Petiau, J. X-ray absorption spectroscopy and its applications in mineralogy and geochemistry. Chp. 11, 432-512

Calas, G.; Brown, Jr., G.E.; Waychunas, G.A.; Petiau, J. (1987) X-ray Absorption Spectroscopic Studies of Silicate Glasses and Minerals. *Physics and Chemistry of Minerals* 15:19-29.

De Grave, E.; van Alboom, A. (1991). Evaluation of ferrous and ferric Mössbauer fractions. *Physics and Chemistry of Minerals.* 18: 337-342.

Delaney, J.S.; Dyar, M.D.; Sutton, S.R.; Bajt, S.; (1998) Redox ratios with relevant resolution: Solving an old problem by using the synchrotron microXANES probe. *Geology.* 26;2, 139-142.

Dyar, M.D. (1984).Precision and interlaboratory reproducibility of measurements of the Miissbauer effect in minerals. *American Mineralogist.* Vol. 69, 1127-1144.

Dyar, M.D.; Gunter, M.E.; Delaney, J.S.; Lanzarotti, A.; Sutton, S.R.; (2002) Systematics in the structure and XANES spectra of pyroxenes, amphiboles, and micas as derived from oriented single crystals. *The Canadian Mineralogist.* 40, 1375-1393.

Dyar, M.D.; Lowe, E.W.; Guidotti, C.V.; Delaney, J.S. (2002). Fe^{3+} and Fe^{2+}

partitioning among silicates in metapelites: A synchrotron micro-XANES study. *American Mineralogist.* Vol. 87, 514-522.

Dyar, M.D.; Klima, R.L., Lindsley, D.; Pieters, C.M. (2007). Effects of differential recoil-free fraction on ordering and site occupancies in Mössbauer spectroscopy of orthopyroxenes. *American Mineralogist.* Vol. 92, 424-428.

Eeckhout, S.G.; De Grave, E. (2003). Evaluation of ferrous and ferric Mössbauer fractions. Part II. *Phys Chem Minerals.*30: 142-146.

Geiger, C.A., Armbruster, Th., Lager, G.A., Jiang, K., Lottermoser, W., Amthauer, G. (1992). A Combined Temperature Dependent ^{57}Fe Mössbauer and Single Crystal X-ray Diffraction Study of Synthetic Almandine: Evidence for the Gol'danskii-Karyagin Effect. *Phys Chem Minerals.* 19:121-126.

Geiger, C.A., Grodzicki, M., Amthauer, G. (2003). The crystal chemistry and Fe^{II}-site properties of aluminosilicate garnet solid solutions as revealed by Mössbauer spectroscopy and electronic structure calculations.

Grant, C. (1995) Sources of Experimental and Analytical Error in Measurements of the Mössbauer Effect in Amphibole. Graduate Thesis, University of Oregon.

Lustig, H. (1961). The Mössbauer Effect. *American Journal of Physics*, 29 (1), 1-18.

Luth, R.W., virgo, D., Boyd, F.R. and Wood, B.J. (1990). Ferric Iron in mantale-

derived garnets. *Contributions to Mineral Petrology.* 104: 56-72.

Sklute, E. (2006) Undergraduate Thesis, Mount Holyoke College.

Stowell, H. H., Geology of Southeast Alaska: Rock and ice in motion. Fairbanks: University of Alaska Press, 2006. ISBN-13: 978-1-889963-81-5. xii + 140 pp.98-102

Whipple, E. R. (1973). Quantitative Mössbauer Spectra and Chemistry of Iron. Earth and Atmospheric Science, Graduate Thesis, Massachusetts Institute of Technology, Cambridge, MA.

Woodland, A.B. and O'Neill, H.S.C. (1993). Synthesis and Stability of $Fe^{2+}_3 Fe^{3+}_2 Si_3O_{12}$ Garnet and Phase Relations with $Fe_3Al_2Si_3O_{12}$-$Fe_3^{2+}Fe_2^{3+}Si_3O_{12}$ Solutions. *American Mineralogist*. Vol. 78. No. 9-10.1002-1015.

Garnet structure source

http://cache.eb.com/eb/image?id=2670&rendTypeId=4

Planetary Science Research Discoveries. (2008) Definition of oxygen fugacity

http://www.psrd.hawaii.edu/Aug02/oxidation.html

Recoil figure source

http://www.cmp.liv.ac.uk/frink/thesis/thesis/node10.html

USGS. An Overview of Production of Specific U.S. Gemstones. U.S. Bureau of Mines Special Publication 14-95 (2002)

http://minerals.usgs.gov/minerals/pubs/commodity/gemstones/sp14-95/garnet.html

I give permission for public access to my thesis and for any copying to be done at the discretion of the archives librarian and/or the college librarian.

Erica A. Emerson